Functionalised nanodiamond as a platform for skeletal tissue engineering

Despoina Paschou

A dissertation submitted in partial fulfillment

of the requirements for the degree of

Doctor of Philosophy

of

University College London.

Department of Electrical and Electronic Engineering

University College London

August 31, 2021

I, Despoina Paschou, confirm that the work presented in this thesis is my own. Where information has been derived from other sources, I confirm that this has been indicated in the work.

"The only true wisdom is in
knowing you know nothing."

Socrates

Abstract

Diamond has come of age, as a material for technology and life science applications. Despite its reputation as a gemstone, high grade single crystal diamond can be grown in the laboratory at modest cost. Other forms of diamond, such particulate nanodiamonds (typically 5nm in size) can be formed. Its superior mechanical and functionalisation properties make diamond a great candidate for skeletal tissue engineering material. In this thesis, the potential of functionalised diamond as a nanomaterial for the chondrogenic and osteogenic differentiation of Mesenchymal Stem Cells (MSCs) has been investigated.

Results in chapter 4 describe the biocompatibility of human Adipose Derived Stem Cells (hADSCs) with oxygen–functionalised BBD-PPy scaffolds and oxygen–terminated nanodiamonds (NDs) and the ability of the cells to form uniform monolayers on ND substrates. Chapter 5 verifies the ability of hydrogen and oxygen terminated NDs to sustain hADSC proliferation and chondrogenic differentiation. In the same chapter, the ability of another type of mesenchymal stem cells (MSCs), chondrogenic precursor/ stem cells (CSPCs) to differentiate on H–NDs and O–NDs into three key skeletal precursors (chondrocytes, osteocytes and adipocytes) is demonstrated through staining and colorimetric quantification assays.

In Chapter 6, a novel 3D scaffold made out of fibrin that incorporated H–NDs is characterised. CSPCs underwent chondrogenic and osteogenic differentiation in this novel structure. Differentiation outcomes were qualitatively demonstrated through section staining and were subsequently quantified using quantitative real time Polymerase Chain Reaction (qRT-PCR). Results indicate chondrogenic differ-

entiation and potential endochondral ossification was promoted by increasing concentrations of H–NDs in the scaffolds, without enhancing the Young's modulus of the constructs.

Impact Statement

The results presented on this thesis highlight how oxygen and hydrogen terminated nanodiamonds can be utilised as powerful tools for skeletal tissue engineering.

Parts of this thesis have been accepted and presented in various international conferences, resulting in 3 invited presentations in prestigious nanoscience conferences, as well as a poster presentation in the biggest tissue engineering conference in the world. Each chapter of this thesis presents novel results, with hADSCs and CSPCs cultured and differentiated for the first time on H– and O–NDs.

A highlight of this thesis in the fabrication of novel 3D scaffolds for tissue engineering that combine fibrin and H–NDs and were shown to upregulate chondrogenic differentiation in CSPCs. For the purposes of these experiments, 3D scaffolds containing fibrin and various concentrations of H–NDs were compared in order to understand the link between H–ND concentration and upregulation of skeletal differentiation. The key result is the upregulation in expression of key chondrogenic differentiation indicators such as Sox9, ColX, Aggrecan, in scaffolds that include the highest concentration of H–NDs. This result demonstrated a clear link between presence of H–NDs in the scaffolds and chondrogenic differentiation. This promising result paves the way for a whole new class of biomaterials that can promote formation of cartilage.

Another exciting result was the detection of upregulated levels Osterix and Runx2 gene markers in 3D fibrin samples containing H–NDs and undergoing chondrogenic differentiation. This result highlights the possibility of the formation of

bone by means of endochondral ossification with the utilisation of nanodiamonds.

The results on the effect of H–ND concentration on CSPC differentiation in relation to the stiffness of fibrin scaffolds is also unexpected. One of the use cases for NDs in skeletal tissue engineering is the enhancement of the mechanical properties of the scaffold as a means to increase their stiffness and thus promote tissue formation. In this thesis we demonstrate that the presence of NDs indeed upregulates key factors in chondrogenic differentiation without enhancing the stiffness of the scaffold, therefore paving the way for new research that examines the potential electrochemical and biochemical effects of the presence of H–NDs in 3D chondrogenic differentiation. As such, the results of this thesis are relevant both for academic and clinical purposes.

The interdisciplinarity of this project is also of particular significance and demonstrates the significance of collaboration between different departments within UCL. All results generated have been produced by the author, who mastered both engineering and life sciences techniques in order achieve the results demonstrated in this thesis.

Acknowledgements

It took a village of support and guidance that made this PhD happen and so I struggled fitting this in one page. Prof Richard Jackman and Prof Patrizia Ferretti, thank you for being such great supervisors, for always believing in me and encouraging me to put my work out there. You are not only great scientists, but amazing people. Your patience, motivation, empathy and enthusiasm never cease to humble me.

To the DEG and Ferretti groups, thank you for helping me navigate my journey through the amazing world of diamond and stem cells. Special thanks to Dr Alice Taylor and Terry Kang, who supported me during the early days. Dr Oliver Gardner, thank you for all your guidance in going 3D. Dr Eleonora Zucchelli, thank you for kick starting my long affair with tissue culture. Dr Jenny Lange, thank you for all your support. To Max, for all your help. To Joe, for always being there to resolve any crisis. To the rest, thank you for your support through the past few years.

Special thanks to Dr Dale Moulding for being the best imaging teacher there is, Dr Mehran Moazen for his support with the bioindentation experiments and Dr Emmanuele Scorsone for providing samples utilised in this thesis.

Thank you to my family and friends. To my husband Niko, for being a huge source of strength and support. To my parents, Takis and Patra, none of this would have been possible without you. To my sister Angeliki, your tenacity and work ethic inspire me. To my fan club, my friends and my in laws, I am lucky to have you.

And finally, Cesar, for being a hell of a Chief Motivational Officer.

Contents

List of Figures

List of Tables

List of Abbreviations

β-Gly	β - glycerophosphate
2D	2–dimensional
3D	3–dimensional
AFM	Atomic Force Microscopy
Agg	Aggrecan
ANOVA	Analysis of variance
BDD	Boron doped diamond
BM–MSCs	Bone Marrow Stem Cells
cDNA	Complementary DNA
CFD	Craniofacial birth defects
ColII	Collagen type 2
ColX	Collagen type 10
CSPCs	Cartilage Precursor/ Stem Cells
CSPs	Cortico–spongeous progenitor cells
CVD	Chemical Vapour Deposition
dH_2O	distilled water
Dex	Dexamethasone

DLC	Diamond Like Carbon
DMEM	Dubecco's Modified Eagle Medium
DMSO	Dimethyl sulfoxide
DNDs	Detonation Nanodiamonds
dNTPs	Deoxynucleotide triphospahtes
DPBS	Dulbecco's Phosphate Buffered Saline
DPEC	diethylpyrocarbonate
ECM	Extracellular Matrix
EDTA	Ethylenediaminetetraacetic acid
ES–FBS	Embryonic Stem Cell Fetal Bovine Serum
FGF	Fibroblast Growth Factors
FNDs	Fluorescent nanodiamonds
GAGs	Glycosaminoglycans
GAPDH	Glyceraldehyde 3-phosphate dehydrogenase
GFP	Green Fluorescent Protein
H–NDs	Hydrogen functionalised nanodiamonds
hADSCs	human Adipose Derived Stem Cells
HMDS	Hexamethyldisilazane
hNSCs	Human Neural Stem Cells
HPHT	High Pressure High Temperature
HSD	Honestly Significant Difference
IBMX	3-isobutyl-1-methylxanthine
IP	Inner Perichondrium

IPA	Isopropanol
ITS	insulin-transferrin-selenium supplement
MPECVD	Microwave Plasma Enhanced Chemical Vapour Deposition
MSCs	Mesenchymal Stem Cells
NBF	Neutral Buffered Formalin
NCDs	Nanocrystalline diamond
NDs	Nanodiamonds
O–NDs	Oxygen functionalised nanodiamonds
OP	Outer perichondrium
Osx	Osterix
pADSCs	pediatric Adipose Derived Stem Cells
PCD	Polycrystalline Diamond
PCL	polycaprolactone
PDDAC	poly-diallyldimethylammonium
PEG	Polyethylene glycol
PFA	Paraformaldehyde
PGa	Proteoglycans
PLA	Poly(lactic acid)
PLGA	Poly(lactic-co-glycolic-acid)
PLM	Polarised Light Microscope
PPAR γ	Peroxisome proliferator-activated receptor gamma
PPy	Polypyrrole
PU	Polyurethane

qRT–PCR	quantitative real–time Polymerase Chain Reaction
RIE	Reactive Ion Etching
RNA	Ribonucleic acid
RoI	Region of Interest
RPL19	60s ribosomal protein L19
RT	Reverse transcriptase
Runx2	Runt-related transcription factor 2
SCD	Single Crystal Diamond
SEM	Scanning Electron Microscopy
Sox9	sex-determining region Y-box 9
TCPS	Tissue Culture Polystyrene
TF	Transcription Factors
TGF–β	Transforming Growth Factor β

Chapter 1

Introduction

Craniofacial birth defects (CFD) are a type of congenital defects, observed in the structure of the cranium and the facial skeleton. The prevalence of craniofacial malformations are 1/3 of all congenital defects, affecting 2-3% of all live births. Across all phenotypes and physical manifestations of CFD there are present high deficiencies in bone and cartilage. These are both types of tissue that can arise from the differentiation of Mesenchymal Stem Cells (MSCs) . The significance of correcting CFD lies in two main factors: The health risks associated with the various phenotypes, such as respiration and nutrition issues, hearing and speech impediments; and the psychosocial factors, such as peer relationships, self-esteem issues and delayed social skills development that may arise by factors such as speech impediments [7]. Therefore, intervention at young ages is advised, in order to ensure that the patients experience a happy, healthy childhood and fulfilling social lives.

Autologous tissue which stems from the patient's own body is the golden standard for avoiding compatibility issues and rejection. While certain autografts provide good volume and tissue compatibility, morbidity associated with the donor site creates the demand for less invasive techniques, particularly for young, developing bodies. For example, chostochondral rib grafts make for an excellent autograft for facial cartilage reconstruction, however, they are associated with morbidities at the donor site. Alveolar bone grafts are a popular way of correcting cleft lip palette, a common CFD. The most common autograft stems from the iliac crest. Surgery on

this donor site is associated with drawbacks such as scarring and long term pain. Creating autografts is one of the cornerstones of tissue engineering.

Research for the utilisation of nanodiamonds (NDs) in skeletal tissue engineering is an emerging area. Although research in NDs as a drug delivery system and a potential cell labelling mechanism has advanced, the study of NDs as a material for tissue engineering has started to be explored only in the past decade. This thesis provides and insight in the use of functionalised NDs as a potential material for the engineering of cartilage and bone tissue using human Adipose Derived Stem Cells (hADSCs) and Cartilage Precursor/ Stem Cells (CSPCs) .

Chapter 2 introduces the concept of tissue engineering and its key components. Cartilage as a tissue is introduced and the key characteristics of mesenchymal stem cells are explored. Chapter 2 also introduces diamond as a scientific material. It's properties are examined, as well as methods of creating synthetic diamond. Nanodiamond and its functionalisation properties are introduced, detailing the manufacturing and purification of NDs, as well as its functionalisation abilities. NDs as a biomaterial and its applications on tissue engineering are also discussed. Chapter 3 introduces the experimental methods utilised throughout the thesis.

Chapter 4 is the first results chapter, which describes the investigation of oxygen functionalised boron doped diamond (BDD) and NDs as potential materials where mesenchymal stem cells (MSCs) can proliferate. Through SEM and stereoscopic imaging, the biocompatibility of BBD substrates with human adipose derived (hADSCs) stem cells is demonstrated, as well as the growth patterns of human adipose derived stem cells (hADSCs) on porous BBD coated substrates. The utilisation of different techniques for the seeding of NDs on glass substrates is examined through AFM topology. Furthermore, the biocompatibility of oxygen functionalised diamond in 2–dimensional hADSC culture is demonstrated through fluorescence microscopy and quantification of GFP^{+} cells.

In Chapter 5 the ability of H–NDs and O–ND two–dimensional substrates to sustain chondrogenic differentiation of hADSCs and trilineage differentiation of

cartilage stem/ precursor cells is demonstrated. After 21 days in culture, the differentiation outcomes on hADSCs and CSPCs are demonstrated through brightfield microscopy and colorimetric assays.

The final results chapter, Chapter 6 examines the incorporation of H–NDs in 3–dimensional culture and its effect on chondrogenic and osteogenic differentiation of CSPCs in H–ND–fibrin composites. The effects of different concentrations of H–NDs in the polymerisation of fibrin are shown. Polymerised H–ND–fibrin scaffolds with different concentrations of H–ND were investigated using a bioindenter in order to better understand the effects of H–ND incorporation upon the Young's modulus of the scaffolds. CSPCs were incorporated in scaffolds containing 3 different concentrations of H–NDs, as well as control fibrin-only scaffolds. The outcome of induced chondrocyte and osteocyte differentiation on these scaffolds after 21 days was examined using histology and quantitative real time polymerase chain reaction (qRT-PCR) techniques.

Chapter 7 summarises the results attained in this thesis, and comments on the impact and potential applications of those results. Chapter 8 details potential future work stemming from this thesis.

Conference papers

Oral Presentations

Towards active neural-diamond networks: Adipose-derived stem cells interacting with nanodiamonds
E-MRS Fall meeting an exhibit, Poland, 2016

Adipose (fat tissue)-derived stem cell-nanodiamond interactions for the development of differing cell types
E-MRS Spring meeting and exhibit, France, 2017

Nanodiamonds as a platform for skeletal tissue regeneration
The 29th International Conference on Diamond and Carbon Materials, Croatia, 2018

Poster Presentations

3D nanocrystalline and nanodiamond structures as a platform for the spontaneous differentiation of adipose derived stem cells
SBDD XXII, Hasselt Diamond Workshop, Belgium, 2017

Nanodiamonds as a platform for skeletal tissue regeneration
5th TERMIS World Congress, Japan, 2018

Chapter 2

Background

2.1 Tissue Engineering

Tissue engineering is a prominent example of interdisciplinary science. It is a field that employs scientists of different backgrounds in order to help and replace, repair and boost the function of damaged organs and tissues [8]. In order to achieve this, tissue engineering requires three major components:

1. A source of cells that will become specialised to make up and carry out the tissue's functions, and will tether the cells to each other and give the tissue its shape and mechanical properties. This source is usually precursor cells known as stem cells [9].

2. A scaffold, which will give the cells the initial support, mechanical and chemical cues that will aid the cells to create the new organ or tissue. These scaffolds can be naturally derived or artificial [10].

3. Chemical and physical cues that will lead the stem cells seeded to the scaffolds towards the desirable differentiation fate [11].

These three components when put together create a robust system that provides cells with mechanical and chemical cues. Eventually, this system will develop into a functional tissue that can be integrated with the patient's body. There are many types of tissues and organs that tissue engineering is aiming to restore. It is important for

scientists to have a good understanding of the tissues they are reconstructing from a biological, structural and mechanical perspective [12], [13]. Hence, this thesis will describe two tissues that are of paramount importance in tissue engineering and will therefore be closely examined throughout.

2.2 Cartilage in tissue engineering

Cartilage is one of the most investigated tissues in tissue engineering [14] [15] [16]. As it is present in many of the human body's vital organs and joints, it is susceptible to both damage and developmental anomalies.

Common developmental anomalies affect both the proteins and the extracellular matrix [17]. Common protein anomalies are achondroplasia and several forms of chondrodysplasias, causes of dwarfism and developmental defects affecting, amongst others the development of the respiratory tract [18], [19], [20]. These affect both cartilage formation and bone growth. Other defects affect extracellular matrix components and also result in abnormal growth; they include type II collagenopathies, resulting from mutations in the Col2A1 gene [21].

Common cartilage injuries include knee sports injuries, including deep lesions that can result in early onset degenerative knee arthritis [22].

2.2.1 Cartilage biology and its mechanical properties

Cartilage is a dense connective tissue that is an important structural component in all vertebrate bodies . During development, cartilage forms the template of long bones [23]. In adults, it functions as a connective tissue that is found in the weight-bearing ends of articular (joint) bones [24], [25], as well as the nose, the bronchi, the ears, the rib cage and the inter vertebral discs [26]. Cartilage is tough, yet flexible. It is able to withstand large forces and can protect the bone it surrounds from large impact. Its primary cell type is the chondrocyte, a type of cell that deposits cartilage's extracellular matrix (ECM) . The ECM is composed of large numbers of collagen fibres, proteoglycans (PGa) and elastin fibres [27], [28]. The

ECM is a firm and gelatinous substance that is also rich in glycosaminoglycans (GAGs) [29], [30] . The ability of cartilage to withstand strong forces is derived from its biological composition. The polysaccharide gel resists compressive forces, while the collagen fibres make the matrix tough [31]. Finally, the elastin fibres give cartilage bending abilities and provide resilience [32]. For example, the shear modulus of hyaline cartilage has been measured to be 800 kPa [33], while articular cartilage shear modulus is 740 kPa [34]. In contrast, the shear modulus of some common materials measure at 450 GPa for polycrystalline CVD diamond [35], 77 GPa for stainless steel [36], and 670 MPa for cortical bone [37]. Cartilage is not a vascularised tissue. Rather, the cells in cartilage receive nutrients and oxygen through diffusion [38], [39]. Cartilage is not a vascularised tissue. Rather, the cells in cartilage receive nutrients and oxygen through diffusion [38], [39].

2.2.1.1 Glycosaminoglycans (GAGs)

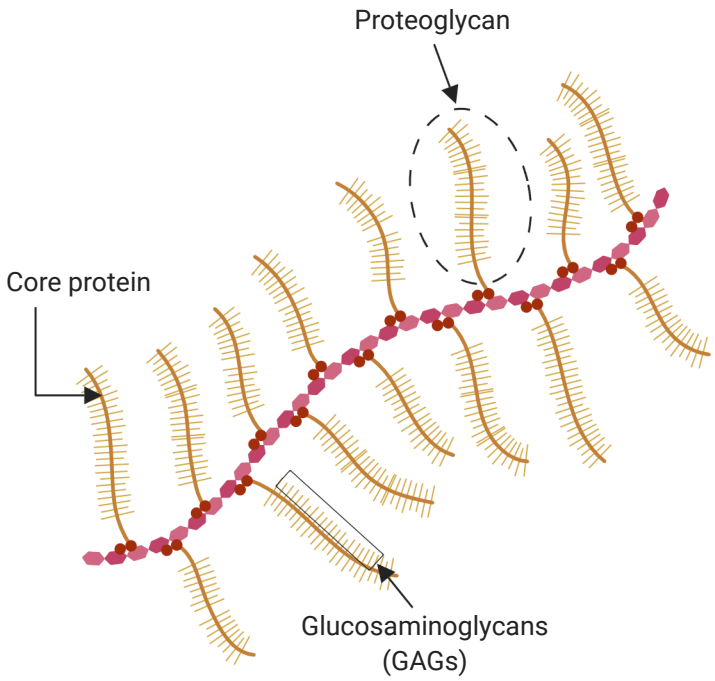

Figure 2.1: The structure of a molecule of a proteoglycan aggregate, a major component of the cartilage ECM. Each proteoglycan unit is composed by a core protein, which has GAGs linked to it. The backbone is composed by hyaluronic acid.

2.2.2 Types of cartilage

There are multiple types of cartilage found in the human body, each with different ratios of its main organisational components and structural organisation [40]. As a result, each different type of cartilage has different mechanical properties and characteristics. Some types of cartilage are also surrounded by the perichondrium, a dense piece of connective tissue that can be divided in two parts: the outer perichondrium (OP) , which is composed of fibres and vessels and supplies the underlying tissue with oxygen and nutrients, and the inner perichondrium (IP), which contains

fibroblasts and cortico–spongeous progenitor cells (CSPs) of a spindle like morphology [41]. There are three main types of cartilage.

2.2.2.1 Hyaline cartilage

Hyaline cartilage is divided in two subcategories: articular cartilage, which is found at the ends of free-moving joints, and costal cartilage, which is found at the ends of the ribs, nose, larynx and bronchi. The ECM composition of hyaline cartilage is mainly collagen fibres, specifically, collagen type II, which accounts for 85 -– 90% of the collagens in hyaline cartilage. Aggrecan is also largely present in this type of cartilage, and forms a hydrated gel in the tissue. The chondrocytes are evenly dispersed in lacunae across the tissue [42]. Lacunae are small cavities in the ECM [43]. These structural components make hyaline cartilage a strong, yet load bearing tissue, which is also very uniform. Hyaline cartilage uniformity arises from the uniform distribution of its collagen fibrils throughout the structure [44]. On top of its solid phase, hyaline cartilage is also fluid permeable [45]. As the cartilage is compressed under load, the pores of the ECM shrink, and as a result its permeability decreases. This results in an increase in the drag movements of the fluid. Ultimately, this results in a self-protective feedback mechanism, whereby the cartilage stiffens as increasing load is applied to it [28]. Due to these properties, hyaline cartilage is a stiff, yet flexible tissue that provides structural support.

2.2.2.2 Fibrocartilage

This type of cartilage is predominantly found in the intervertebral disks, the pubic symphysis, and the intersections of ligaments and tendons [46]. It is the densest of all forms of cartilage due to its packed fibre formation. The main component of fibrocartilage ECM is collagen type I, which is only present in this type of cartilage [47]. It also contains fibroblasts alongside its chondroblasts and chondrocytes. Therefore, it is a mixture of fibrous and cartilaginous tissue, which are present in different ratios in different parts of the tissue [48]. Fibrocartilage composition makes it tough and resilient. It is utilised by the body in order to resist

compression, mitigate bone-on-bone friction and limit relative moment [46].

2.2.2.3 Elastic cartilage

This type of cartilage is mainly found in the cranium and the neck. It is present in the auricle, the external auditory meatus, the middle part of the ear canal, the Eustachian tube, the epiglottis and the larynx [49]. As indicated by its name, it is the most flexible type of cartilage, due to its composition. Its ECM is made mainly out of elastin fibres, as well as collagen type II and PGas. Because of its properties, it can provide support, while resisting deformation without damage [50].

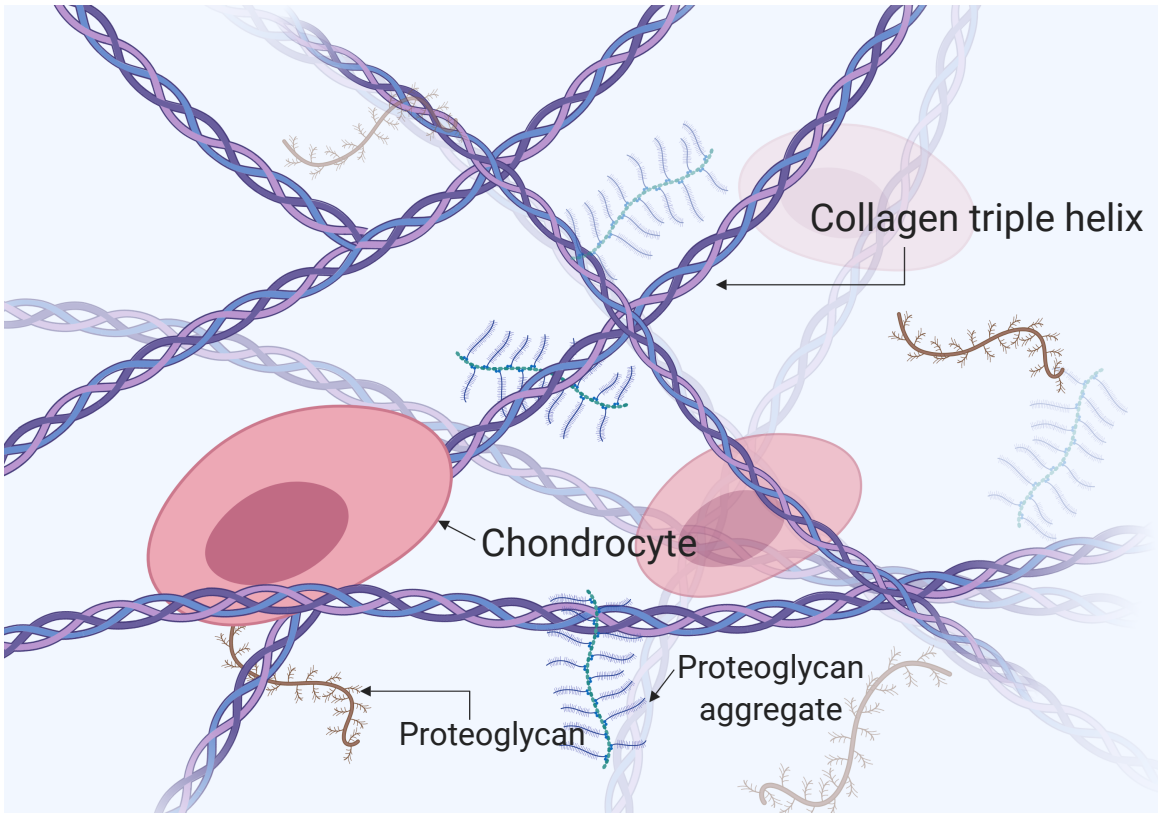

Figure 2.2: Simplified schematic of the collagen ECM with its key components. Collagen triple helix composes the majority of the extracellular matrix, where chondrocytes can be found. Proteoglycans and proteoglycan aggregates are also embedded in the collagen fibrils.

2.2.3 Cartilage development: Chondrogenesis

Ectoderm, mesoderm and endoderm are the three germ layers that occur early in embryonic development and are the origin of all specialised and non-specialised

cells in the body. Different germ layers result in different tissues. [51]. Chondrogenesis is the multi-step differentiation process of undifferentiated multipotent mesenchymal /stromal stem cells (MSCs) into chondrocytes. This process gives rise to cartilage [52]. During embryonic development, different germ layers give rise to cartilage in different parts of the body. Craniofacial cartilage is of ectodermal origin [53], while the cartilage found in other parts of the body is of mesodermal origin [54].

During development, chondrogenesis plays a significant role in body growth, since cartilage acts as the bone structural template and predecessor [52]. The cartilage that results from chondrogenesis can undergo two different fates during development: either remain as cartilage, where the chondrocytes remain as resting cells and form the different types of cartilage tissue (hyaline cartilage, fibrocartilage and elastic cartilage) or undergo proliferation and subsequent hypertrophy and eventually undergo a process called endochondral ossification, which results in bone formation [55], [56].

The underlying molecular mechanisms of chondrogenesis are still under investigation [57]. However, some of the main transcription factors have been uncovered, and it is now possible to harness their abilities for the purpose of modern tissue engineering.

One of the key transcription factors (TF) in chondrogenesis is Sox9 (Sex-determining region Y-box 9), which is believed to be the master regulator gene of chondrogenesis [58] [59]. As the Sox family of transcription factors regulates the initiation of MSC differentiation, other factors from the family, such as (L)-Sox5 and Sox6 play an important role in early chondrogenesis [60].

The Sonic Hedgehog (Shh) protein, as well as Bone Morphogenic Proteins (BMPs) have been shown to play a crucial role in the induction of Sox9 expression and somatic chondrogenesis in general [61], [57]. Shh plays an important role in vertebrate patterning, whereas some studies in chicks have shown that BMP signals are necessary and sufficient to promote chondrogenic differentiation during

development [61]. Other types of signalling involved in chondrogenesis and cartilage maintenance include Wnt, which promotes chondrogenesis via hypertrophy and Sox9 upregulation [62] , Fibroblast growth factors (FGF) by increasing cell proliferation and augmenting ECM production [63], and transforming growth factor β (TGF-β), via the fine tuning of Sox9 expression.

TGF-β plays an additional role in chondrogenesis, by stimulating chondrogenic differentiation [64]. In vitro studies have shown that the TGF-β pathway promotes condensations, while the TGF-β 1 and 3 proteins enhance Sox9 expression [65].

After chondrogenesis, Sox9 plays a fundamental role in the maintainance of cartilage. It has been shown that Sox9 prevents premature chondrocyte hypertrophy, therefore preventing endochondral ossification when not needed [66].

2.2.4 Cartilage cells

There are two major cell types participating in cartilage formation and maintenance: **chondroblasts** and **chondrocytes**. Chondroblasts are immature cells that deposit the majority of the ECM. As they produce and secrete the matrix, they become entrapped in it and eventually mature into chondrocytes [67]. Chondrocytes are fully differentiated and deposit around 1-5% of the ECM [68]. They reside in small cavities in the ECM called lacunae. Lacunae can contain either one cell (primary lacunae) or two/ three cells (secondary lacunae) [43].

Cartilage growth is divided in two categories, according to the type of cell that deposits the matrix: Interstitial growth refers to the deposition of the matrix by mature chondrocytes. It forms by enlargement of the internal mass, when cells that already exist within the cartilage matrix divide by mitosis and deposit ECM. On the other hand, we have appositional growth, which refers to matrix added by the differentiation of cartilage precursor cells [69].

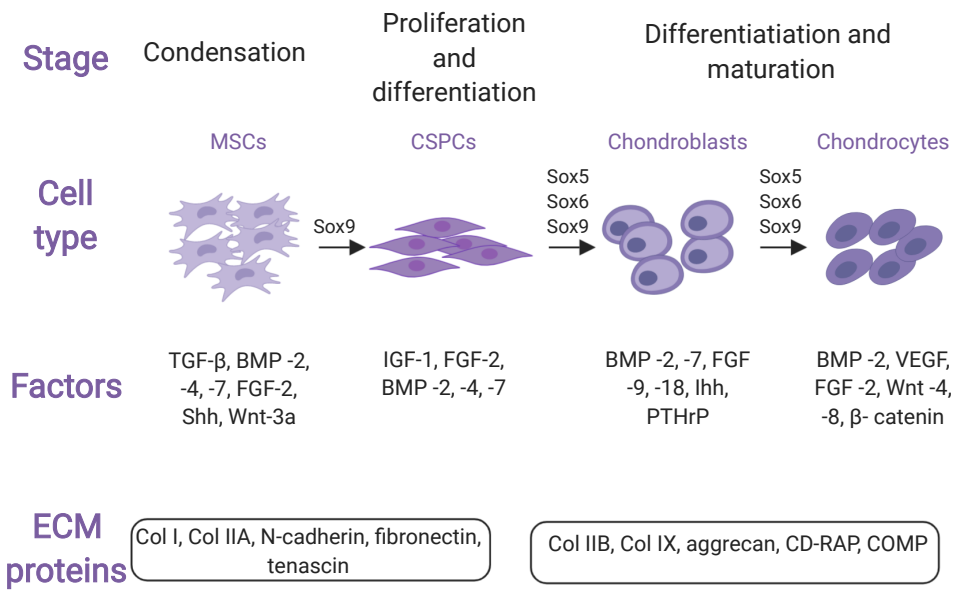

Figure 2.3: Process of chondrogenesis with the relevant growth factors and ECM proteins associated with each stage of differentiation. Adapted from [1]

Since cartilage is not a vascularised tissue, chondrocytes receive nutrients and oxygen from the bloodstream via diffusion. Therefore, such cells have a low metabolic rate and the processes described above happen in a low oxygen environment [39].

2.3 Cells in tissue engineering

2.3.1 Cell adhesion and proliferation

In order to understand their environment and respond to relevant cues, all cells rely on cell signalling. Cell signalling does not only facilitate proper function of individual cells, but also promotes correct function of tissues, which are organised communities of cells. Through signalling, cells are able to communicate with each other and carry out functions collectively [70].

Part of cell signalling involves mechanotransduction, which requires cells to be connected to each other and to the ECM [71]. Adhesion of cells within tissues is facilitated by a range of adhesive molecules. A special class of these molecules is called integrins. Integrins are transmembrane proteins that do not only establish mechanical links between cells and the ECM, but also facilitate signalling [72].

The characteristics of number and types of cells differ from tissue to tissue. Another key differentiator of tissues is their geometry. Cell spacing is tightly regulated, in order to ensure proper tissue function. For tissue architecture to be maintained, adhesive molecules help maintain contact between cells and structures within a tissue [73]. Additionally, tight junctions ensure the passage of nutrients and ions to the cells [74]. Meanwhile, cell signalling relies on signalling molecules that ensure messages are passed between cells, as well as the cells and the ECM.

2.3.1.1 Cell adhesion in vitro

While inside the human body cells utilise molecules in order to stabilise their tissues and communicate with each other, but in artificial environments they need to rely on different adhesion methods. It is a passive cell adhesion process, when cells are situated in a static medium, for example tissue culture flasks and tissue culture plates [75]. Since the cells are now proliferating in an almost 2-dimensional environment, they undergo structural and morphological transformations in order to adapt to their surroundings. There are three stages to this type of adhesion: (a) attachment of the cell body to its substrate (initial stage), (b) flattening and spreading of the cell body, and (c) the organisation of the actin skeleton with the formation of focal adhesion between the cell and its substrate. Over time, the cell spreads further in its surrounding area, increasing the contact area between itself and its substrate. This is result in the formation of new focal adhesion and the strengthening of the existing ones. Therefore, the longer a cell stays in a static substrate, the stronger it attaches to it [76], [77].

The mechanism of attachment and the formation of the focal adhesion involves the action of integrin and it starts with single receptor–ligand pairs. This initiates

a cascade of additional receptor–ligand bonds, which increase quickly in number, thus making the connection stronger over time. The adhesion properties of cells can be studied by looking into their adhesion on substrates over time [78].

2.3.1.2 Cell proliferation

Cells are capable of replication in a process called cell division. In healthy tissues, the total number of cells is the sum of cells resulting from division, minus cells that have either died or differentiated. This process is called cell proliferation [79].

There are different categories of adult human cells. A few types of differentiated cells, like cardiac cells, have lost their capacity for further divisions, being results of stem cell differentiation during embryonic development. Upon injury, these cells are unable to heal the tissue [80].

The majority of human tissues, however, are made up of cells that have the capacity of proliferation and differentiation. These cells include fibroblasts, epithelial cells and cells of most of our internal organs, such as the liver and pancreas. These cells are able to repair tissues upon injury and also have a limited life [81].

Adult tissues also contain several groups of stem cells, responsible for its maintenance and homeostasis. Certain tissues, such as the outer skin layer, the digestive tract and blood cells, contain cells with short life spans that need to continuously be replaced by means of proliferation. These short-lived cells do not have the capacity for cell division. Instead, they need to rely on the proliferation of less differentiated cells called stem cells. Stem cells divide to produce daughter cells, which can then either differentiate into specialised tissue cells or remain in the stem cell state. This makes them a source of production of differentiated cells through time [82].

2.3.2 Stem cells

One of the most important components in tissue engineering are stem cells. Stem cells are the source of specialised cells that will make up the new tissue and

will secrete the extracellular matrix that will tether the cells together and give the tissue its shape [83], [84].

Stem cells are defined as undifferentiated and unspecialized cells that are capable of self- replication and self-renewal. During embryonic development, they give rise to all the different types of tissue in the human body. In adults, stem cells are responsible for tissue homeostasis and maintenance. There are many different types of stem cells, with many different ways of categorisation. One of the main methods is categorizing according to their plasticity. The four main categories are [82], [85]:

1. **Totipotent stem cells.** These are the stem cells found in the very early stages of the zygote. They are able to differentiate into any type of human cell, including the placenta.

2. **Pluripotent stem cells** [12]. These cells are extremely plastic and possess the ability to differentiate into any type of cell found in the adult human body (except for the placenta). Embryonic stem cells (ESCs) and cells found on the umbilical cord after birth are classified as pluripotent [86].

3. **Multipotent stem cells.** This type of cells has the ability to differentiate into a specified range of specialized cells. Essentially, pluripotent stem cells specialize further down to multipotent stem cells. These cells still have a certain plasticity range, but can only give rise to a certain group of tissues, usually associated with each other. For example, mesenchymal stem cells are able to give rise to osteocytes, chondrocytes, adipocytes and myocytes [87], [86].

4. **Adult stem cells.** These are multipotent stem cells present in adult organs, residing among differentiated cells. Their role is to maintain the tissue homeostasis and replace cells that have lost their function. They are able to differentiate into cells specific to the organ in which they reside. In the case of adult stem cells, their stem cell fate is dictated in big part by their microenvironment. Adult stem cells reside in stem cell niches. These structures ensure stem cells are maintened in a quiescent state, but when influenced by external

stimuli (such as tissue injury), they send signals of either self-renewal or differentiation to its resident stem cells. Consequently, stem cells differentiate either symmetrically (self-renewal) or asymmetrically (differentiation into a specific cell type) [86].

2.3.2.1 Cells with chondrogenic and osteogenic potential

There are many different types of adult stem cells. Mesenchymal stem cells (MSCs) possess the ability of differentiating into an array of mesenchymal lineages, such as adipocyte, cadiomyocyte, endothelial, chondrocyte, myocyte, neuronal-like, osteoblast and marrow stroma. It has been shown that these cells, initially derived from the bone marrow, are able to proliferate in colonies and differentiate into their different lineages under controlled conditions in vitro. Due to their abilities they are a very good candidate for use in stem cell therapy and tissue regeneration [87].

MSCs are mostly found in the bone marrow (BM-MSCs), the umbilical cord and the adipose tissue (ADSCs). Initially, BM-MSCs were the primary source of stem cells for stem cell therapies and tissue regeneration projects. Their major limited factor though is the invasive nature of their harvesting. Furthermore, BM-MSCs are found to decline with age of the patient. ADSCs on the other hand, thanks to the accessibility and abundance of fat tissue, seem like an ideal source for further differentiating cells. It has been shown that the differentiation potential of ADSCs is as good as the one of BM-MSCs, especially regarding mesenchymal lineages [88]
.

Adipose-derived stem cells (ADSCs) are a highly-plastic category of stem cells that have the ability to self- renew and to differentiate into a range of cell types. Initially, ADSCs were thought to be able to differentiate into mesodermal tissue, though it has been shown that ADSCs are capable of both ectodermal and endodermal differentiation, despite their mesodermal origin [89].

Studies have been performed in order to assess the efficiency of ADSCs versus BM-MSCs [90]. Samples of both types of cells derived from the same patient

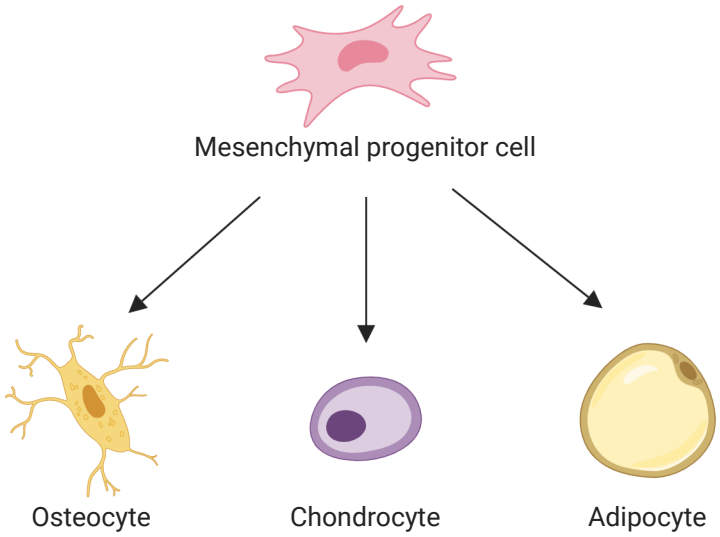

Figure 2.4: Trilineage differentiation of mesenchymal progenitor cells

were tested, with the results indicating no significant difference in terms of yield of adherent cells, multi-lineage differentiation potential, growth kinetics and other significant indicators [91].

In terms of location, ADSCs are found both in white fat and in brown fat deposits. The highest concentration of ADSCs is found in the subcutaneous white adipose tissue versus the visceral type. Nowadays, most of the ADSCs used are derived from adipose tissue derived via lipoaspiration [91], [92]. This minimally invasive technique draws fat directly from under the skin in areas with high fat concentration, such as the belly and the thighs, without the need for major surgery and recovery in patients. Techniques have also been developed that allow easy isolation of the stem cells from the surrounding fat explant. This accessibility of the ADSCs make them a very attractive stem cell type for tissue regeneration [93], especially

for patients that cannot endure multiple invasive surgeries and long recovery times, such as young children.

There is a lot of potential for the use of ADSCs in regenerative medicine. ADSCs are capable of paracrine secretion, producing a signal that can alter the behaviour of nearby cells, and thus creating a favourable environment for proliferation. For example, ADSCs secrete most of the factors needed for wound healing. Once ADSCs are transported to the wound, they are able to respond to environmental cues and, by releasing these factors in a regulated manner, mimic the normal process of wound healing. Furthermore, the vascular endothelial growth factor (VEGF) secretion from ADSCs promotes vascularisation, another major contributor to successful wound healing. Myoskeletal tissue experiments carried out in the Ferretti lab and focusing on paediatric ADSCs (pADSCs) have indicated high levels of plasticity in the cells with multilinear potential. Specifically, the cells appear to be able to differentiate particularly well into bone tissue and under controlled conditions into tissues such as cartilage [94]. These results build on the previous Guasti et al, 2012 study, which showcases the vast plasticity of ADSCs especially when in comparison with chondroblasts. These findings are of paramount importance regarding tissue regeneration in children, as autologous tissue ensures that the implant does not get rejected, but instead it integrates with the system of the young patient and grows with them. Engineering is also possible using ADSCs, *in vitro* studies have highlighted the big differentiation potential of ADSCs into skeletal and smooth muscle, as well as osteoids. In terms of skeletal repair, the combination of ADSCs with biomaterials has been successfully used for bone damage repair [93]. Finally, research into the construction of a hADSCs/ polymer bionanoscaffold, which was pre-seeded with stem cells led into positive integration with the patients' tissue, together with quick vascularization [95].

As a tissue, cartilage lacks regenerative capacity upon injury [96]. However, certain stem cells, called cartilage stem/ precursor cells (CSPCs) are thought to be involved in tissue maintenance and homeostasis [97]. These cells have a spindle-like form and large numbers of them can be found in hyaline cartilage, such as

ear cartilage. Although a clear marker that identifies CSPCs has not been reported yet, and the *in vivo* origin, function and identity of these cells is unclear, there have been definitive studies that indicate that CSPCs respond to tissue damage [98], [99]. While further investigation is required, these cells demonstrate great potential for cartilage tissue engineering. Although they tend to de-differentiate in *in vitro* monolayers, under specific culture conditions with media including ITS, cortisol and TGF-β they are able to maintain their cartilage phenotype *in vitro* [100], [101].

They have been demonstrated to have trilineage differentiation ability (chondrogenic, adipogenic and osteogenic) up to 35 passages [102].

CSPCs can be easily isolated from ear cartilage samples [103] and were easily accessible to our lab from children undergoing surgeries on 'bat ear' (normal tissue cartilage) and microtic ear. For the purposes of this thesis, CSPCs derived from normal ear cartilage were used.

2.4 Biomaterials

The interface between cells and solid materials has been well studied and utilized in recent years. Biomaterials are an essential part of tissue engineering, as they can provide both morphological and physiological cues for cells to proliferate and develop into the desired type of tissue. Furthermore, biomaterials can promote better integration between cells and an organism [104], [105].

Humanity has understood the importance of using materials interfaced to the body as solutions to various disabilities from the ancient times. References to prosthetics are found even in ancient Greek texts. Pelops, whose namesake is the Peloponnesian peninsula in southern Greece, is certainly one of the most famous implant bearers recorded in mythology, reflecting the actual experiences of Greeks at the time. According to legend, upon being slaughtered by his father, Pelops' body was reassembled by the gods of Mount Olympus, save for his left shoulder. In order to rectify this, Hephestus, the god of Fire, modelled him a prosthetic shoulder made out of ivory ([106]).

Across the Mediterranean, in Egypt, prosthetic toes have been found, estimated to have been used around 1000 BC. Those toes were made out of wood and leather, making them the original biomaterials, alongside animal sinew, which the Egyptians used for sutures ([107]).

It is therefore evident that humanity identified the importance of restoring skeletal function from the earliest ages and was inspired to do so by turning into early biomaterials. In the early 20th century humanity started moving from natural to synthetic materials [108]. This gave the ability for people to have better control over the mechanical properties, the reproducibility and the durability of the new materials and their interaction with the human body. Such materials are typically ceramics, metal alloys and synthetic polymers. They are employed for functions such as hip replacements, vascular stents, dental implants and contact lenses and have led to changes to the lives of people forever [107].

In order to avoid rejection from the human body that would potentially inhibit

the function of the medical device they were composing, biomaterials developed during that era were labelled as 'inert' [106]. This meant that they would not interact with the host organism. However, with advances in molecular biology, proteomics and genomics between the 1970s and the 2000s, molecules that play significant roles in tissue regeneration and remodelling were discovered. These were incorporated into materials, giving rise to bioactive materials that promoted interaction between host and prosthetic [109]. Scientists were encouraged to study the ways the body heals and grows and try and find ways of coming up with better materials and techniques that can mimic this processes and in turn create better materials and hence more useful devices.

In vivo, it is the extracellular matrix (ECM) that provides cells with the morphological, chemical and mechanical cues that helps them organize themselves in tissue [110]. Therefore, we seek to create materials that can mimic this sort of environment. Such materials compose porous three dimensional structures similar to the *in vivo* structure and also are made from biodegradable materials. Biodegradability is an important property in biomaterials. Material biodegradability is meant to match the rate of tissue remodelling and deposition of newly formatted tissue [111].

The most important properties of the materials chosen are, biodegradability rate aside, biocompatibility [112] and stiffness [113], [114]. These properties can aide greatly with the integration of cells onto biomaterials and promote cell adhesion, proliferation and differentiation [113], [114].

Usually, scaffolds in tissue engineering are polymer-derived. The polymer can be either naturally derived or synthetic. Naturally derived polymers carry the advantage of biological recognition which in turn can promote cell development [111]. An important naturally-derived polymer is collagen. Collagen is a naturally occurring scaffold material used in tissue engineering. Collagen is the main component present in the extracellular matrix, and can therefore promote processes such as differentiation and cell proliferation [115]. On the other hand, because it is derived

from other mammalian organisms, issues with biocompatibility may arise. Furthermore, collagen on its own presents poor mechanical properties and biodegradability [116], [117].

These limitations have prompted scientists to look further afield and create synthetic biomaterials that offer more of the properties desired for an ideal tissue engineering scaffold. Poly (α-hydroxyacids), such as poly(lactic-co-glycolic-acid) (PLGA) and poly(lactic acid) (PLA) have been widely used in scaffold fabrication [118]. They possess the property of autocatalytic degradation, eventually breaking down into oligomers that can enter metabolic pathways for safe disposal from within the body. Such materials can be tailored in order to control their actual degradation rates. On the other hand, materials such as polyurethane (PU) provide better mechanical properties in spite of very slow degradation rates [119]. Polyethers such as polyethylene glycol (PEG) are used as hydrogels in stem cell encapsulation and drug delivery [120].

Finally, nanofibrous nanomaterials can be incorporated into scaffolds that can mimic some of the collagen properties without the associated dangers with biocompatibility [121]. But, there is yet to be found a material that is biodegradable, biocompatible and matches the tissue material properties, as well as being robust. Recently, scientists have turned to alternative materials that, despite being used in other fields for a long time, have not been employed as biomaterials. An interesting example is diamond.

2.4.1 Fibrin

Fibrin (also known as Factor Ia) is a protein involved in blood clotting and is a major factor in wound healing [122], [123]. The precursor to fibrin are fibrinogen molecules, elongated 45 nm structures that consist of two outer D-domains, each consisting of a β and a γ subdomain [123]. The formation of fibrin follows the cleavage of fibrinogen A α chains into fibrinopeptide A (FpA) by thrombin, a naturally occurring enzyme. Through this process, the polymerisation site E_A is exposed. Each E_A site is then combined with a complementary-binding pocket in

the D domain. This binding results in a double-stranded fibril conformation. The resulting structure is a branched network with a tight matrix conformation [124].

Further thrombin activity releases the fibrinopeptide B (FpB) which in turn exposes the independent polymerisation site E_B. This site then enables cross linking between fibrin I protofibrils [125].

2.4.1.1 Fibrin use in skeletal tissue engineering

Fibrin has shown promise as a hydrogel for skeletal tissue engineering. It promotes cell adhesion [126]. Commercial availability of both human derived fibrinogen and thrombin enables creation of 3-dimensional models in the lab [127].

Figure 2.5 demonstrates the process described above.

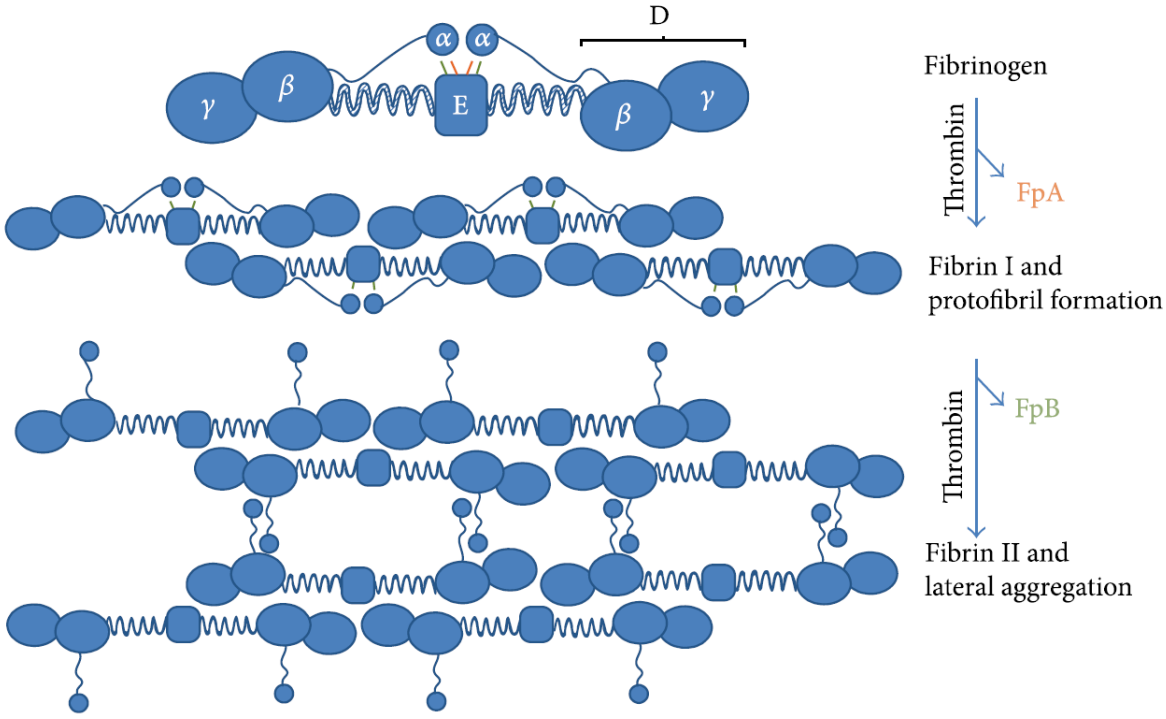

Figure 2.5: Schematic representing the assembly of fibrin from fibrinogen as a result of the action of thrombin in two stages: the formation of protofibril formation as a result of the action of FpA and the lateral aggregation as the result of the action of FpB. Adapted from [2].

2.4.2 Diamond as a biomaterial

Carbon allografts have been an attractive biomaterial proposition for a long time, thanks to the fact that all living organisms are made out of carbon compounds [128] [129]. Pyrolytic carbon's excellent compatibility with blood was discovered in the late 1960s and ushered in the first age of carbon based biomaterials for artificial heart valves [130]. With the advance of materials and prosthetic research, a range of materials, such as metals, ceramics and polymers, were utilised. However, these materials do not provide optimal performance and can interfere with the integration of a medical device and a biological organism. The most common effect is inflammation, which can lead to formation of scar tissue around bone implants and subsequent problems with stability and integration, as well as long term inflammation and subsequent implant rejection. In order to address this important issue, scientists turned to surface coatings [131] [132].

Of particular recent interest is the novel use of diamond both as a single crystal and nanocrystalline biocompatible substrate [133] [134] [135]. Further, individual nanodiamonds (NDs) have shown great promise in this context [136] [137] [138] . This will be discussed further later in this chapter.

2.5 Diamond

Diamond, apart from being one of the most famous and desirable gemstones, is one of the greatest materials for scientific application. This is due to its great mechanical properties, being the hardest known material, its extreme stiffness and minimal compressibility [139], in addition to its superlative electronic [140] and optical properties [141].

Diamond it is known to have been naturally generated between 140 km and 200 km below the Earth surface under extreme conditions (900 – 1400^{o}C temperatures and 4.5 to 6 GPa pressure) during the initial geological stages of the Earth's development. Under these physical conditions diamond is thermodynamically favoured over other possible allotropes of carbon [142]. In recent years, technology advancement has allowed for the creation of synthetic diamonds, that is diamond materials whose origin is not from deep within the Earth. This enables the wider use of diamond for scientific purposes by overcoming the obstacle of limited supply of natural diamond in nature. Further limitations associated with naturally occurring diamonds, such as high costs, are the range of impurities and inhomogeneity [143].

But what is that makes diamond so special? This section will discuss diamond's properties, where it derives them from, and synthetic growth methods currently in use.

2.5.1 Carbon

2.5.1.1 Bonding in carbon - the importance of hybridisation

Carbon is one of the most abundant elements in nature. It is the cornerstone of organic chemistry and the building block of life as we know it. This should come as no surprise, as carbon is one of the elements with the highest bonding versatility. Having 4 electrons in its outer shell, carbon is able to both donate and receive electrons, as well as forming single, double as well as triple covalent bonds. Looking at its electronic structure, we can get a better idea of the abilities of carbon

bonding. The model of orbital hybridization is a good place to start. Proposed by Linus Pauling in 1931, it shows that carbon is able to use its higher energy orbitals in order to bond with a variety of molecules [144].

One of the molecules that stand out from Pauling's research is that of methane (CH_4). In methane, the 4 outer electrons of carbon form covalent bonds with the single electrons of 4 different hydrogen atoms.

Orbital hybridisation describes the ability of the 2s and 2p wavefunctions to hybridise with one another. This is made possible by the promotion of the 2s orbital electrons to higher energy orbitals, while 2p electrons are demoted to lower energy orbitals [144]. In carbon, there are 3 types of hybridisation: sp^3, sp^2 and sp. sp^3 hybridisation gives rise to 4 sp^3 orbitals. Each orbital contains a single valance electron. Their formation is a result of equal hybridisation of 2s and 2p orbitals, which provides the ability to form four identical σ covalent bonds. These bonds are configured at a 109.5^{o} angle from each other and can be observed in methane and diamond.

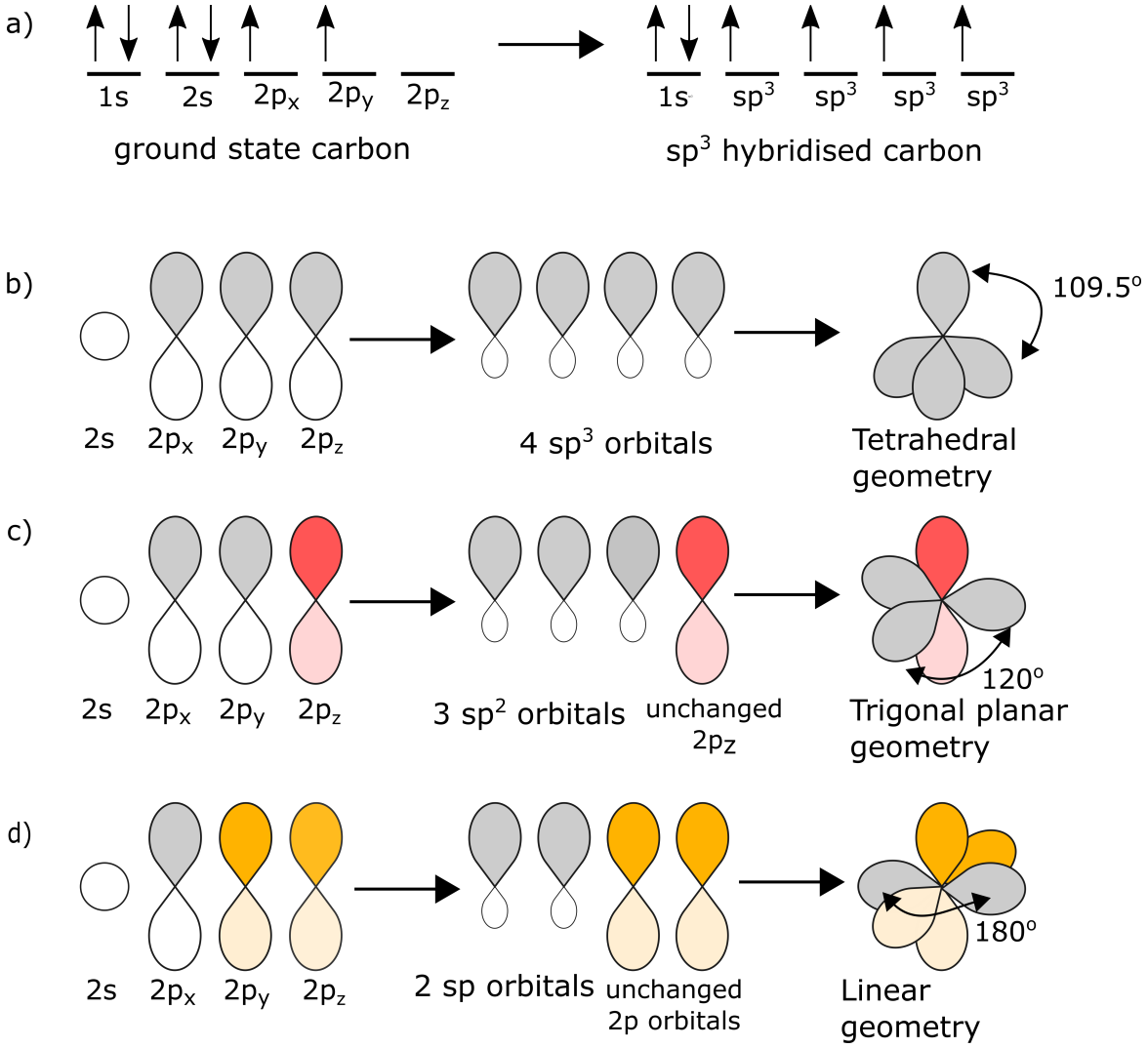

Figure 2.6: (a) Difference of electron distribution between ground state and sp^3 hybridised carbon (b) s and p molecular orbital hybridisation into sp^3 hybrid orbitals, (c) s and p molecular orbital hybridisation into sp^2 hybrid orbitals, (d) s and p molecular orbital hybridisation into sp hybrid orbitals.

Other types of covalent bonding in carbon include unsaturated bonding, such as double bond which results from sp^2 hybridisation. The simplest molecule that contains a double bond is ethene (CH_2=CH_2). 3 sp^2 orbitals are formed by the hybridisaton and the empty $2p_z$ orbital is excluded from this process. The sp^2 orbitals are then able to form 3 σ bonds, while the empty $2p_z$ orbital, which is perpendicular to the plane, is able to form a π double bond with the p_z orbital from another carbon in the same plane.

Essentially, this means that the π bond occurs between the carbon atoms, while

the sp^2 orbitals are formed between the carbon and hydrogen atoms. This results in the sp^2 bonds having an 120^o angle of separation. Finally, sp bonding is the third type of covalent bonding in carbon. This simply refers to the ability of carbon to form a triple covalent bond. Ethyne is the simplest example of this (CH≡CH). sp hybridization results in the formation of two sp orbitals, leaving the $2p_y$ and the empty $2p_z$ orbitals unchanged. These unchanged orbitals then make 2 parallel π bonds, resulting in a linear π triple bond.

2.5.1.2 Carbon in biology

Carbon is important both as a building block, as well as a part of fueling organisms. This is particularly demonstrated when looking into some key structures of molecules involved in biology.

Glucose, one of the the simplest of the carbohydrate family of compounds, is one of the most abundant sugars in nature. It is used as the primary fuel of all organisms, including humans and has a molecular formula of $C_6H_{12}O_6$. It is mainly made by plants and algae during photosynthesis, using CO_2 and water [145].

As a fuel in all living organisms, it is used in the glycolysis pathway, where it is degraded into carbon dioxide and water. The energy released by breaking down the covalent bonds formed within the glucose molecule, is the energy used to fuel organisms.

As a building block, glucose is abundant in the cell walls of plants, as well as in glycogen, a polysaccharide that is used as a form of energy storage for mammals, fungi and bacteria. In humans, it is primarily found in the liver and the skeletal muscles [146].

One of the most important classes of molecule for organism proliferation are lipids. Lipids are not only used as the main type of energy storage in animals, but also as signalling molecules and cell building blocks. Lipids are made of saturated and unsaturated carbon chains. The breaking up of these chains results in the release of energy. An important subcategory of lipids are the triglycerides, which are the

main constituents of body fat. Body fat resides in the adipose tissue and is the main form of energy stores in animals [147].

In vertebrates, carbon is also one of the key components of bones. Bones are composite material made out of minerals and collagen. Carbon is found in both the collagen and the mineral component of bones [148].

Another important structure for vertebrates is cartilage. Cartilage is an important tissue in the body, which provides support, structural integrity and resistance to body damage. Cartilage is comprised by specialized cells called chondrocytes, which in turn deposit extracellular matrix, proteoglycans and elastin fibres. Proteoglycans are made up mainly of glucosaminoglycans (GAGs) which are long polysaccarides, comprised by long carbohydrate chains. Both elastin fibres and extracellular matrix also contain carbon atoms, in the form of both carbohydrate chains and other carbon-containing molecules [30], [32].

2.5.1.3 Carbon allotropes

The different types of hybridization found in carbon give rise to a range of allotropes. The most well-known ones are diamond and graphite. In recent times as both science and technology advance, other natural and synthetic carbon allotropes have been discovered, with tremendous potential of applications in science, medicine and industry. A non-exhaustive list of such allotropes in demonstrated in figure 2.7.

2.5.1.4 Carbon and its structure

Diamond is a giant covalent structure, composed entirely of carbon. Its structure is face-centred cubic, with 8 carbon atoms per cube. The system is composed of carbon atoms on the centre of each face of the cube, as well as 4 carbons at each corner of the lattice [149]. Each cubic unit lattice side is equal to 3.567 Åat room temperature ($26^{o}C$ or 300K) [150]. In order to express the location of each of the additional carbon atoms of the lattice, we utilize this length as the carbon constant a_0 (3.566986 Å$\pm$ 2.6×10^{-6}). According to this formula, the location of each addi-

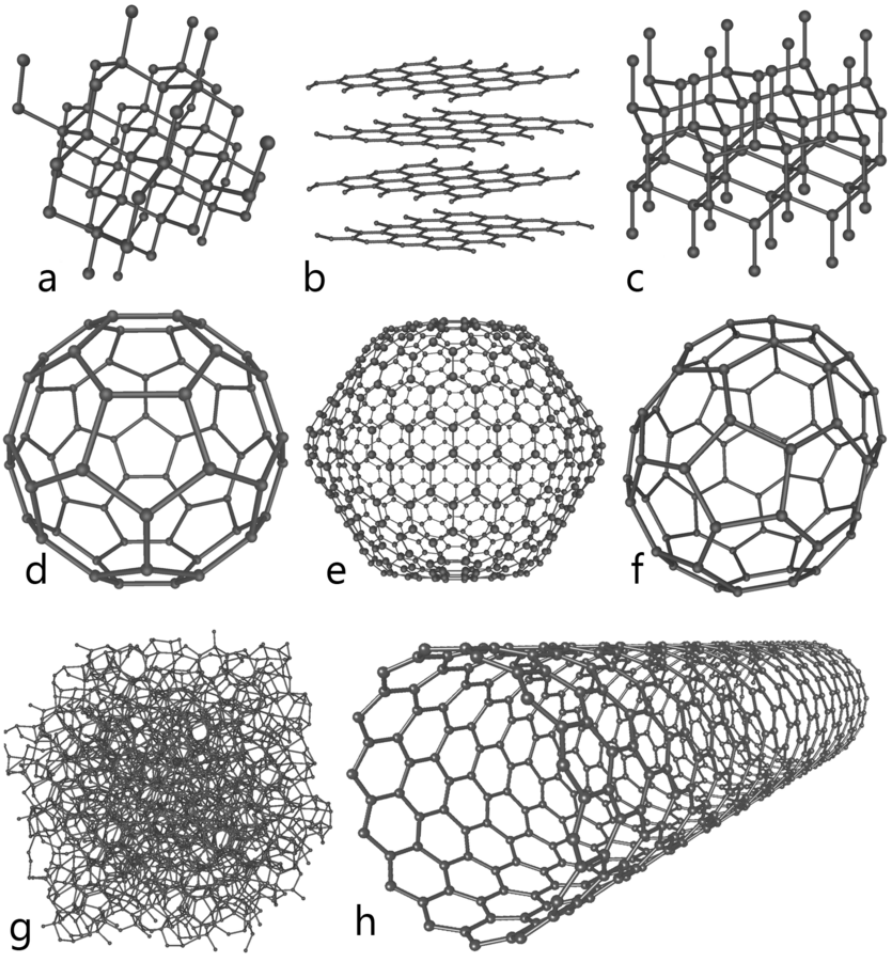

Figure 2.7: Eight allotropes of carbon: (a) Diamond, (b) graphite, (c) Londsdaleite, (d) C_{60} (buckminster)fullerine, (e) C_{540} fullerine, (f) C_{70} fullerine, (g) amorphous carbon, (h) single walled carbon nanotube (Picture taken from Wikimedia Commons).

tional carbon atom is at a_0 (1/4,1/4,1/4), a_0 (3/4,3/4,1/4) and a_0 (1/4,3/4,3/4) [151]. The length of the C-C bond between the atoms of the lattice is measured at ¼ of the cubic body diagonal, which is at $d = \sqrt{\frac{3}{4}a_0} = 1.53$ Å[152].

The structure of diamond can be also discussed using crystallography. The three crystallographic Miller planes within the diamond lattice are (100), (110) and (111) and they can be used to describe both the diamond structure, as well as its surface.

This tightly bonded cubic lattice structure also results in diamond's high density at 1.76×10^{23} atoms/ cm^3. This is the highest material density known and

explains diamond's superlative mechanical properties, which give rise to its many industrial applications.

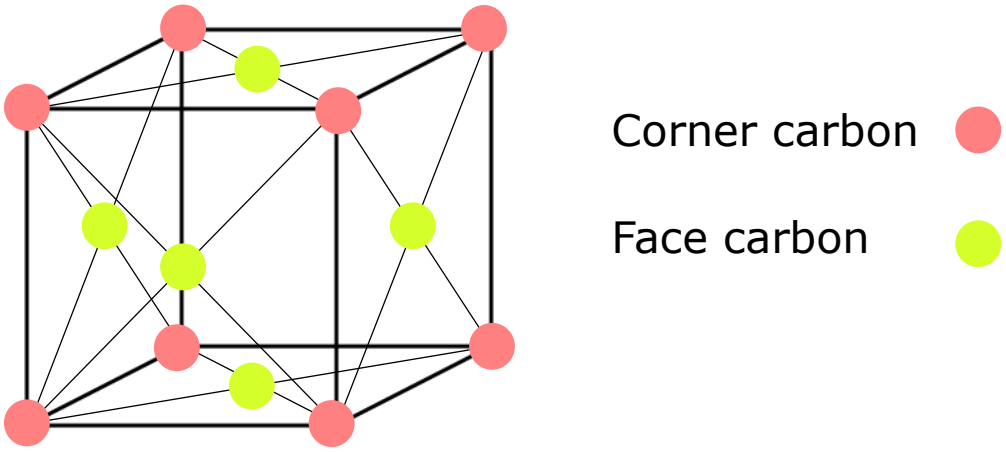

(a) Face Centered Cubic (FCC) structure of diamond.

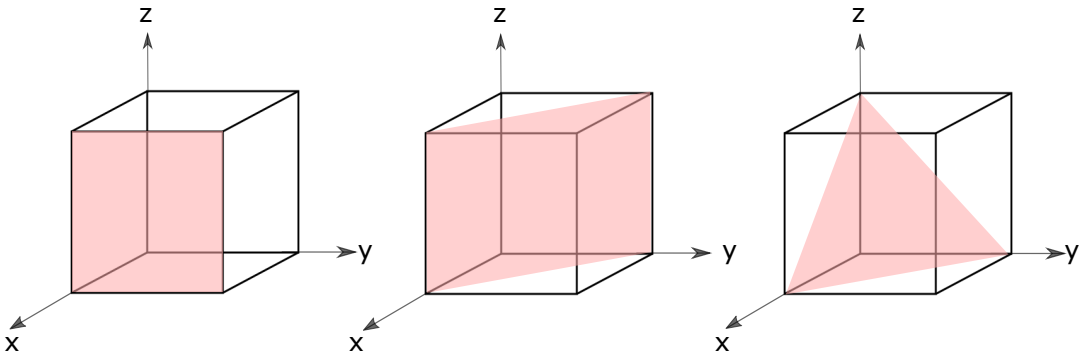

(b) The (100, (110) and (111) Miller planes.

Figure 2.8: The distribution of carbon in cubic diamond models

2.6 The formation of diamond

A material as dense as diamond can only be made naturally under conditions of extreme pressure and temperature, in conjunction with rapid cooling. In nature, these temperatures range from 900 to 1400°C and pressures from 4.5 to 6 GPa. Diamonds are formed between 140 and 200 km below the Earth's surface, and are brought to the surface through volcanic activity [153]. As mined diamonds can be used as gem stones, their quality is assessed using visual criteria. Those visual characteristics are determined by defects such as the inclusion of foreign atoms, like boron, nitrogen and hydrogen [154].

All bonds in diamond are sp^3 σ bonds, with carbon atoms bound together by 4 covalent bonds. On the other hand, graphite is made up of carbon atoms bound together by sp^2 π bonds. Diamond is metastable, meaning that once formed it cannot revert back to graphite as the barrier is too high. The transformation rate of diamond to other carbon phases at room temperature and pressure is almost zero, therefore for all intents and purposes we can assume that diamond is an absolutely stable material in normal environmental conditions.

2.7 Diamond growth

Given diamond's excellent properties, but lack of abundance in nature, from the 19th century onward, attempts were made in order to create artificial diamond. Reportedly, the first such attempt was made by James Ballantyne Hannay in 1879, which involved heating charcoal above 3000°C [155]. Since then, more sophisticated techniques were established. Diamond synthesis was achieved in the 1950's and since then synthetic diamond has been widely used in areas where natural diamond had limited uses. These limitations were due to the high price of naturally occurring diamond, as well as its inhomogeneity and various impurities.

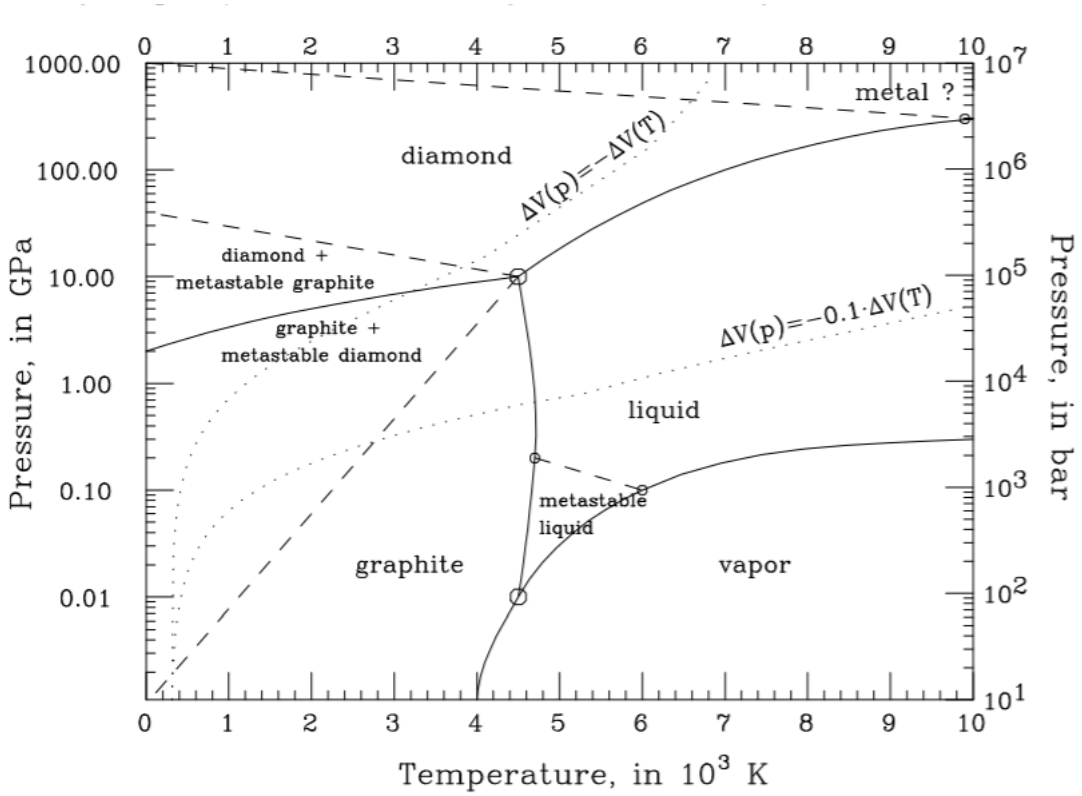

Figure 2.9: Phases of diamond. Taken from [3]

2.7.1 Artificial diamond

Artificial diamond is classified under two main categories: single crystal and polycrystalline diamond, abbreviated as SCD and PCD respectively. PCD is formed when grains of SCD are bonded together, and it can be further classified, according to the diameter of the resulting crystals (insert table). SCD is a single piece of diamond, where all the carbons are connected covalently with sp^3 σ bonds in one structure. This gives SCD excellent properties, which match the properties of naturally occurring diamond, such as its very high Young's modulus and its stiffness.

Table 2.1: Degree of crystallinity and corresponding size of grains, adapted from [6].

Degree of crystallinity	Size of grains
Microcrystalline	100 nm - several μm
Nanocrystalline	5 - 100 nm
Ultrananocrystalline	$\leq$ 5 nm

2.7.1.1 High Pressure High Temperature (HPHT)

The basic principle of making diamond using the HPHT method is the same as for the formation of naturally occurring diamond. Carbon is subjected to high temperature and high pressure conditions in the presence of a metal catalyst. The first verified successful HPHP diamond synthesis was achieved in 1954. Pressure conditions in the range of 10 GPa and 2000^{o}C were reportedly achieved [156]. However, it was not until 1970 that GE was able to produce an artificial diamond of gem-level quality. The HPHP method includes the use of a metal-solvent catalyst, which is usually nickel, iron or platinum. The carbon is then dissolved in the catalyst and then transferred to the growth substrate where it crystallizes in diamond form under favourable thermodynamic conditions. The inclusion of the catalyst ensures that these conditions are met at lower pressure and temperatures. Namely, the diamond-graphite transition pressure drops from 13 GPa to 5.5 GPa and from 3000^{o}C to 1300^{o}C) [157], [158].

In terms of quality, HPHP diamond contains fewer lattice dislocations than naturally occurring diamond, making it comparatively harder and denser. This makes it a useful component for grinding and cutting tools. On the other hand, it contains higher concentrations of impurities than natural diamond, mainly nitrogen [159]. This makes HPHT diamond less desirable for optical applications.

2.7.1.2 Chemical Vapour Deposition (CVD)

A technique that requires less extreme conditions for the creation of diamond is the CVD method. Under this technique, which was developed in 1962 by William Eversole, the conditions required are 900 -1100^{o}C and 7-14 MPa, as well as a carbon-containing precursor gas being used [160].

This method makes diamond with better optical properties and higher purity levels than HPTP diamond. However, the technique originally developed was deemed too slow for industrial uses. It wasn't until 1982, when a novel technique was established and rates of diamond growth become enough for commercial ap-

plication [161]. This method of CVD, dubbed as 'hot filament' (HFCVD), uses relatively low pressures (25 – 40 mbar) and temperatures (700 – 1100^{o}C) and produces diamond films on substrates made out of materials such as Si, Mo or silica at relatively high deposition rates (0.3 to 20 μmh^{-1}), achieving coating areas as high as 20×20 cm^2 [162]. However, due to corrosion of the hot filament, the technique did not yield high quality films, especially at high growth rates [163]. In 1983, the same group announced yet another technique for CVD diamond growth, this time using a Microwave Plasma Enhanced CVD (MPECVD) reactor for the production of diamond thin films [164]. In 1985, a technique that uses RF glow discharges was developed. These two techniques enable the deposition of CVD diamond due to radicals that are created while using the MW and RF power [162].

These techniques produce higher quality diamond compared to the original filament method. Because the filament is eliminated from the chamber, less impurities are being introduced and thus higher optical quality diamond is being made.

2.7.2 Nanodiamonds

Nanodiamond (ND) is defined as structure with a diameter of 100 nm or less. In nature, NDs occur thanks to high pressure high temperature (HPHT) shockwaves which are a result of a meteorite impacting Earth. When created artificially, similar conditions are recreated in controlled chambers, with the detonation of explosives containing carbon in an oxygen deficient chamber. The rough material that results from this procedure is clusters of highly aggregated NDs in the form of a powder[165].

The challenge posed by the above process is the deagreggation of the resulting nanodiamond clusters. This can be achieved by taking the rough product of the detonation procedure and putting it through a purification process. It results in a colloidal solution containing ultra-dispersed NDs that can have various scientific applications.

The interest in monodispersed NDs lies not only in their size, but also in their

structure. Like regular diamond, the core of NDs is an sp^3 diamond structure, whereas its surface is composed of sp^2 graphitic carbon. Thanks to the π-bonding ability of sp^2 orbitals, we are able to terminate the surface of NDs with a range of functional groups. The most common ones are hydroxyl groups ($-$OH) due to their prevalence during the de-aggregation process of DNDs. Other functional groups of interest include (carboxyl), $-$C=O (carbonyl), $-$O$-$C=O (lactone) and (ether).

As water or ice are the primary factors used in the cooling process for DNDs, the ND surface is able to react with hydroxyl radicals. In order for the NDs get purified and the graphitic layer removed, oxygen is used. As a result of these two processes, the surface of the NDs is populated by a variety of oxygen containing functional groups. As such, when we discuss 'untreated' NDs, which are NDs that have not been functionalised on purpose, we expect their surface to contain a range of non-homogeneous oxygen containing functional groups [166]. Raman spectra, which were obtained using ultraviolet laser, indicate that diamond cores in detonation soot are completely covered in detonation soot, as their Raman spectrum is dominated by the G-band of graphitic carbon and contains no diamond peak. The diamond peak begins to emerge when nanodiamonds as the graphitic layer becomes thinner. Nanodiamonds that are oxidised in air have their graphitic layer completely removed, and therefore have a even stronger diamond peak [166].

2.7.3 Fluorescent nanodiamonds

Although they are biocompatible and largely non–cytotoxic [137], [138], [167], one of the major disadvantage of NDs in terms of monitoring is their transparency. This is something that is overcome by introducing nitrogen-vacancy defects inside the NDs. These defects are introduced by means of high energy ion beam irradiation with N_+, with subsequent thermal annealing. This type of NDs possess superior qualities as fluorescent markers, such as being significant brighter than their fluorophore counterparts, as well as being resistant to photobleaching [168]. Protocols for live imaging of fluorescent NDs with commercial microscopes has been established both with fixed and live cells, using confocal stimulated emis-

sion depletion (STED) imaging [169]. FNDs have also been used for the labelling and tracking of neuronal differentiation from Embryonic Carcinoma Cells (ECSs) [170].

2.7.4 Nanodiamond functionalisation

Diamond particles have the ability to be functionalised with a range of chemical groups. As mentioned previously, due to the way DNDs are processed after formation, 'untreated' NDs are usually found terminated with -O or -OH groups. However, there are ways to change its functionalisation. The oxidation of H-terminated surfaces can be achieved using thermal, plasma, and electrochemical techniques, as well as functionalisation with singlet oxygen [171], irradiation with vacuum ultraviolet light (VUV) [172] and ozone treatment [173], [174], [175]. So far, there are no distinguishing differences between the effectiveness of any of these techniques, as no attempt has been made to compare them in literature [176].

2.7.4.1 Ozone O_3

Ozone is an inorganic molecule, consisting of 3 oxygen (O) atoms, bound covalently. Ozone is a polar molecule, and a powerful oxidant. Ozone is able to react with carbon and produce CO_2 and O_2 even at room temperature. This property of ozone makes it an ideal candidate for ND termination in two different ways: it can react with allotropic carbon impurities at the surface of NDs and eliminate them, while enriching the same surface with oxygen–containing chemical groups [176].

2.7.4.2 Diamond-Like Carbon (DLC)

Diamond-like carbon (DLC) is a form of amorphous carbon that is metastable and contains significant sp^3 bonding. Its extreme properties, like high mechanical hardness, optical transparency and chemical intertness, are similar to those of diamond. These properties are achieved in an isotropic thin film with no grain boundaries. DLC is cheaper to produce than diamond and it can be prepared with a variety of deposition methods such as ion beam, mass selected ion beam, sputtering,

plasma-enhanced chemical vapour deposition (PECVD), pulsed laser deposition, and cathodic arc [177].

2.7.5 Biological uses of diamond

2.7.5.1 Diamond biocompatibility

Thanks to its chemical and mechanical properties, the medical community has been intrigued by diamond and has made extensive research into the biocompatibility of the material.

When the human body detects an invader, it recruits its first line of response, the neutrophils, cells which then recruit further white blood cells (leucocytes) in order to fight the invader. In conjunction with diamond, neutrophils remain inactive, thus indicating the bionert nature of diamond [178]. Further, cell types, such as macrophages also do not display any adverse effects when they come in contact with diamond. The example of macrophages is an important one, as they internalize the invader in a process called phagocytosis, and then neutralize it [179]. It has been shown that macrophages do internalize diamond, then they are also able to expel it, with no effect on their function and mobility [180].

On a more macroscopic level, diamond also does not promote blood coagulation [181]. Blood coagulation is a non-inflammatory response of the body, which ensures that external blood loss is prevented and also that foreign invaders are blocked. However, when a medical implant is introduced to the body, this property can cause formation of scar tissue around the implant and potential isolation of the introduced object from its surroundings. This eventually leads to implant failure. The bioinert properties of diamond make in an ideal candidate for implant coating, as the tissue will come in direct contact with the coating itself and not promote coagulation [182].

Studies conducted using nanodiamonds (NDs) *in vivo* and *in vitro* have demonstrated that NDs do not facilitate further blood coagulation [183]. Initially, chemical-vapour-deposited diamond (CVD) has demonstrated biocompatibility as

a coating on titanium implants [178]. It has been shown that fibrinogen (the main component of blood clots) and platelets, show low adsorption rates on CVD. When investigated further, it is shown that the low thrombogenic activity of Diamond Like Carbon (DLC) is thanks to the high concentration of sp^3 carbon states (diamond) [184].

One study using crystalline diamond instead of DLC has shown that platelets do not adhere on the crystalline diamond surface, therefore obstructing blood clot formation [185].

In the case of nanodiamond particles (NDs), there was an inhibition of macrophage metabolic activity at concentrations higher than 200 micrograms per ml [180]. High concentration of NDs have been proven as toxic to aquatic life [186], [187]. Interestingly, mammalian cells show tolerance of concentrations of NDs at least one order of magnitude higher than crustaceans [188].

There is interesting category of cells for which NDs prove toxic: Bacteria. Diamond shows excellent antibacterial properties. Studies have demonstrated that bacteria can be particularly sensitive to certain ND sizes. Antibacterial properties have also been demonstrated on diamond thin films, especially on films terminated with hydrogen [189].

2.7.5.2 Diamond in cell culture

Diamond has been studied against other tissue culture friendly materials [190]. When osteoblasts (bone precursor cells) and endothelial cells were cultured on tissue culture plastic (TCP), glass and diamond, they showed high attachment and proliferation rates under all three conditions. However, they show aversion for silicon [191]. Further studies on macrophages cultured on diamond demonstrated reduced levels of cytokine expression, indicating a downregulation of inflammatory response in the presence of diamond [133].

Direct comparison experiments between diamond and different substrates have yielded further promising results, when compared to TCP, neuronal stem cells pro-

liferated and adhered better on diamond substrates [192], [193], [194]. Furthermore, human epithelial cells demonstrated an affinity to diamond compared to glass substrates [195].

2.7.5.3 Diamond functionalization in biology

As mentioned previously, the surface functionalization ability of diamond is one of the most attractive characteristics of diamond in various applications. Two of the main types of termination that have been proved biologically relevant are hydrogen ($-$H) and oxygen ($-$O) termination. Oxygen termination is observed when the surface is functionalized with a range of carbon-oxygen bonds, such as ether (C$-$O$-$C), carbonyl (C$=$O) or carboxyl (COOH) groups [190], [196].

One of the key features of –O terminated diamond is its improved hydrophilicity, which can considerably enhance biocompatibility [197]. A range of studies have demonstrated superior adherence and proliferation of osteoblasts and epithelial cells on O-terminated diamond surfaces [198], [199], [200]. Furthermore, O-terminated surfaces promote the deposition of bone extracellular matrix [201]. However, one contrary study using bone implant coated surfaces demonstrated adhesion and proliferation only on mesenchymal stem cells deposited on H-terminated diamond [202]. O-termination has also been shown to promote oligodendrocyte differentiation, without affecting neuronal differentiation. There is still plenty of room for studying the effects of diamond termination on cell differentiation [203].

2.7.5.4 Diamond topography

Links are being established between the surface topography of diamond and the ability of different cell types to adhere and proliferate on them [204]. Studies have mainly focused on the proliferation of neuronal cell types on diamond. All studies have indicated that low roughness substrates support enhanced adhesion of neuronal cell types. For example, a study by Tong et al., has shown that the optimal roughness for rat cortical cell adhesion is around 20 nm [205].

2.7.6 Diamond in tissue engineering

Thanks to its excellent mechanical and biocompatibility properties, diamond has become an attractive material in the field for tissue engineering. Diamond is particularly prevalent in tissues that require scaffolds with modular stiffness. Poly(l-lactic acid) (PLLA)-nanodiamond complexes have demonstrated increased biocompatibility and differentiation potential of osteoblasts [206].

2.7.6.1 Diamond based medical devices

As CVD has become an efficient way of diamond synthesis, thin film diamond has been gaining popularity for many applications. Commercially, the prices of CVD are considered affordable, with a 0.5 mm thick and 1 cm^2 area film cost $50 USD. Since this kind of substrate can be cleaned and reused, this is a very cost effective proposition. Biomedical research based on diamond thin films is further facilitated by the supply of MCD diamond films, grown on silicon wafers. These substrates are comparatively cheaper than reagents regularly used in cell tissue culture, therefore making it a very attractive research proposition [207] [208] [6].

As a result, scientists are able to study, among other things, the ability of cells to adhere to the substrate. It has been shown that diamond films display the excellent properties of being both bioinert, and therefore not causing any inflammatory or coagulatory response, and also facilitating cell adhesion on their surface [209], [210]. This is a particularly interesting find, as most bioinert materials demonstrate poor cell adhesion properties [211], [212].

There has been a move for the coating of medical implants using nanocrystalline diamond (NCD). Recent advances include NCD and UNCD coatings for joint prosthesis microelectromechanical systems (MEMS) [213] and heart valves [214]. The non-coagulatory effects of diamond can be notable, as it has been observed that the new heart valves do not promote blood clotting and the healing times are quicker than regular valves [214].

Furthermore, their antimicrobial properties in conjuction with their increased

cell-adhesive abilities have made diamond coatings an appealing material in restorative implant surgery [215]. Apart from the bionert properties, the mechanical properties and resistance to tear of diamond are important. A temporomandibular joint (TMJ) implant coated with NCD was tested. This implant is in a part of the human body (in the jaw ligaments) that is subjected to frequent friction. Within two years of wear, results of Raman spectroscopy demonstrated minimal film damage and zero film loss [216].

Diamond is also used in disease modelling. The work of [217], on lab-on-chip devices has demonstrated that H-terminated NCD enabled high sensitivity and high throughput in the device. Further research from the same group showed that NCD spikes can facilitate more efficient cell lysis, therefore increasing the efficiency of lab-on-chip devices [218].

CVD diamond has been long established to be biocompatible and a desirable material for implant coating, thanks to being corrosion resistant and with excellent mechanical properties [178]. Further assays have shown the biocompatibility of BM--MSCs with nanocrystalline diamond (NCDs), which have indicated not only biocompatibility of the MSCs with the material, but also increased proliferation of the bone marrow cells on the FND surface [133].

Such results have prompted questions regarding the further use of nanodiamonds on stem cell research. Studies from institutes in Germany and Singapore have demonstrated that oxygen termination of NCDs has demonstrated greater adhesion of cells to their surfaces thanks to the carboxylic groups on their surfaces [219], [220]. Neurons were found to proliferate almost just as well on oxygen terminated diamonds as on biological substrates, with proliferation on hydrogen terminated NDs 70% of that on their oxygen terminated counterparts. Furthermore, the capability of boron doping the NCDs makes them an even better candidate for growth substrates, as boron makes the material electrically conductive, improving the conditions for neural cell proliferation [209].

Further experiments have shown the biocompatibility of the boron–doped

NCDs with hNSCs indicate that surface chemistry is not the only aspect affecting proliferation and cell adhesion of the cells on the substrate surface. Surface roughness and geometry appear to also play a role, with "rougher" surfaces where NDs have smaller radii and larger curvature, helping to promote further adhesion [210].

Diamond nanocrystallinity can also play a role in functions of mesenchymals cells such as osteoblasts in terms of key functions such as adhesion, proliferation and differentiation [221].

As mentioned previously, a few studies have been conducted in order to examine the interaction between ADSCs and nanodiamonds in a nanomaterial composite setting. Their exceptional mechanical properties and their large surface area, make NDs a promising candidate for its combination with a biodegradable polymer such as PLGA. This method brings better mechanical properties and longevity to the structure without obstructing its function [206]. Similar experiments, this time using PLLA result in scaffolds with similar mechanical properties to those of the bone, have also been carried out [222].

Furthermore, because of their large surface area, NDs are good candidates for drug delivery, which can also facilitate delivery of growth factors that can enhance osteogenic differentiation on MSCs [223]. The enhanced mechanical properties of these new scaffolds are very important in terms of mechanical properties, as they ensure that the potential scaffold for bone regeneration matches the mechanical properties of the bone it is grafted on, avoiding collapse due to inability to carry the body's load or in the opposite case, stress shielding and bone degeneration [224].

Chapter 3

Experimental methods

3.1 Introduction

In this chapter, the methods and materials used throughout this thesis are described. Background material is presented on the techniques utilised, which in turn gives a better insight to the results presented in later chapters.

3.2 Substrate degreasing

All borosilicate glass substrates were subjected to degreasing in order to remove impurities and residue dirt. This process results in clean, yet not sterile, substrates. Clean substrates ensure that the process of diamond and cell seeding would be carried out without the interference of other residues on the substrate. During the process, an ultrasonic bath was used. Upon completion, the samples were dried under N_2, supplied through a blow gun. The chemicals used and times of each process are described in table 3.1.

Table 3.1: Stages of substrate degreasing process in sequential order

Degreasing process		
Solvent	**Process duration**	**Target impurity**
Acetone	5 mins	Residue dirt
Isopropanol Alcohol (IPA)	5 mins	Residue acetone
dH_2O	10 mins	Residue IPA

3.3 Solution sonication

Neighbouring substances that measure in the micron scale and below are subject to large Van der Waals attractive forces. For the purposes of this thesis, all nanoscale substrates needed to be in as monodispersed state as possible. In order to achieve this, particles in aqueous solutions were subjected to ultrasonication, using a Sonics VibraCell sonicator. This apparatus uses sound energy at high frequency in order to break apart aggregates via the expansion and explosion of bubbles (cavitation). All substrates containing NDs used for experiments in this thesis were ultrasonicated for a minimum of 5 hours. Figure 3.1 demonstrates the ultrasonication set up used for the purposes of this thesis.

Figure 3.1: VibraCell ultra-power sonicator system with cup horn attachment used for the ultrasonication and monodispersion of nanodiamond solutions.

3.4 Nanodiamond coatings

Borosilicate glass coverlips (Cover glass, VWR, UK) were coated with NDs using a 0.05 g/l solution of monodispersed H-NDs in DI water (New Metals & Chemicals Corporation, Tokyo, Japan)) with diameter range 5-10 nm. These DNDs

were functionalised with hydrogen using a hydrogen anneal process, in a custom–made chamber where samples were heated 600 ^{o}C in 25 Torr of hydrogen for 5 hours. Prior to functionalisation, DNDs were dried by evaporating excess water. This is an established technique utilised in the Jackman group [143]. The solution was ultrasonicated again for a further 5 hours, in order to break up aggregates using cavitation, as described in the section above. The final result was the 0.05g/l H-ND solution. In chapter 5 of this thesis, the preferred method of ND seeding on degreased borosilicate glass substrates (Cover glass, VWR, UK) was ultrasonication. A lower-energy ultrasonicator bath was used for this purpose. The degreased substrates were immersed in the diluted ND solution and were treated in the ultrasonicator bath (Guyson Kerry KC 75W) for 10 minutes (excess time) [225]. Upon completion, the samples were dried under N_2 using a nitrogen flow gun in order to remove excess moisture and other debris. The resulting samples were uniformally coated with deagglomerated H-NDs [225].

3.5 Ozone treatment

An interesting feature of nanodiamonds compared to other graphitic nanoparticles is their ability to be functionalised with various groups on their surface [166]. This is due to the presence of an sp^3 dangling bond on the ND surface. In nanoscience this is particularly attractive property, the large surface area to volume ratio. These functional groups can enhance the properties of the diamond. Oxygen termination in diamond gives the material hydrophillic properties, as well as positive electron affinity. A range of techniques are used for oxygen termination, including silanisation, anodic oxidation, oxygen reactive ion etching (RIE) and ozone treatment [226]. The preferred method for oxygen termination of NDs throughout this thesis was ozone treatment. Ozone is preferred over oxygen as an oxidisation agent, due to its superior oxidisation properties. This is due to the presence of a weak O-O bond in ozone, which enables the easy formation of a free radicals ($O_3 \rightarrow O_2 + O\cdot$). Because of this, oxidation can occur at lower temperatures (200^{o}C vs 450^{o}C in air). The process followed for oxygen termination is described below:

1. Samples were placed on a heating stage inside a sealed chamber (UV ozone cleaner NL-UV253)
2. Pumping down to evacuate chamber (10^{-6} mbar)
3. Stage was heated for 30 minutes, until temperature of 200°C was achieved
4. Chamber was filled with O_2 until it reached 50 mbar pressure
5. O radicals were generated by using an ozone generator (10 g/h) for 1 hour

   This method of oxygen termination of samples has been used widely by the group. Oxygen termination has been confirmed using X-ray photoelectron spectroscopy (XPS) and has been published [225], [143].

3.6 Atomic Force Microscopy (AFM)

Atomic Force Microscopy (AFM) is a form of scanning probe microscopy (SPM). It is a micro-cantilever system, where a fine probe scans over a sample, resulting in a 3D topological map. From AFM data, other interesting information for the samples, such as height and frictional properties can be determined. The scanning component of the AFM consists of a cantilever which is made either out of Si or Si_3N_4. At the free end of the cantilever there is a sharp probe made out of the same material, whose radius is in the 10s of nanometres range. Imaging in AFM relies on the forces between the probe and the sample. Such force is not measured directly, rather with the use of Hooke's law, which states that

$$F = -kz$$

where k denotes the spring constant, which in this case is the stiffness of the cantilever, z denotes the vertical deflection and F denotes the forced measured. Therefore, cantilevers of different stiffness are utilized when scanning different materials.

The cantilever deflection is measured by means of laser beam. The laser beam

is projected onto the free end of the cantilever (on the opposite side of the scanning probe) and is then reflected from the cantilever. The reflected optical signal is then detected by a position- sensitive photo-detector. The detector then converts the signal into an electrical one.

When generating an image using an AFM a feedback loop is used in order to achieve high accuracy in the generation of a topographical map of the sample. This accuracy is achieved by keeping the force between the probe and the sample constant. In order to generate this feedback loop the deflected laser beam in the photo-detector is used as an input. The resulting output is the control of the distance along the z-axis between the probe support (which is usually a piezoelectric element) and the stage on which the sample being scanned is mounted. AFM can also be used in order to measure the interaction forces between tip and sample. This application is called force spectroscopy and can provide significant information regarding a range of properties of the samples measured, including mechanical properties. The resulting measurement is called the 'force – distance' curve. The tip of the cantilever is extended and retracted from the surface of the material and this deflection is measured as a function of piezoelectric displacement.

Force spectroscopy is especially useful in biological applications of AFM, as it can give a lot of insight in the the mechanical properties of fragile biological samples. In such applications another material can be added to the tip of the cantilever, such as a glass bead. In this case, the force measured is between the material and the surface of the sample of interest. The area scanned by the probe is larger and a mean force value can be derived from the force- distance curve.

For the purposes of this thesis, the surface roughness of the ND samples was measured using a Bruker Dimension Icon Atomic Force Microscope, in ScanAssyst PeakForce Tapping mode. Scans were performed on a 1x1 μm^2 area, on at least 3 different parts of the sample. Samples examined using this technique were Tissue Culture Polystyrene (TCPS), borosilicate glass slides and H-ND coated borosilicate glass slides. The roughness of the samples was determined using the Bruker

Nanoscope Analysis software in *roughness* mode.

3.7 Scanning Electron Microscopy (SEM)

A Scanning Electron Microscope (SEM) uses a focused beam of high-energy electrons in order to produce the image of a sample. Electrons are used in lieu of light in order to increase the resolution of imaging. SEM is used in order to produce images with resolution as low as 20 nm.

The images that result from SEM are due to the interaction between the electrons and a sample. The electrons generated in the SEM have large kinetic energies and their contact with the sample results in deceleration. These electron- sample interactions result in a range of signals. In the case of the SEM, it is the resulting secondary electrons that produce the image, by showing the morphology and the topology of the samples. Despite the collisions between high energy electrons and samples, SEM is considered a 'non-destructive' imaging method, which means that the sample can be imaged and analysed repeatedly.

For the purpose of this thesis, a Carl Zeiss Orion NanoFab SEM was utilised. The sample stage is contained in a high vacuum chamber. Therefore, the scanned samples are required to be dry. Consequently, biological samples imaged using this technique should be chemically fixed with agents such as gluteraldehyde and parafolmadehyde (PFA) in order to undergo structure stabilization. In this thesis, biological samples were fixed in 4% PFA and were dried in series of EtOH solutions of different concentrations.

3.7.1 SEM setup

The basic components of an SEM are: An electron source ('gun') an electron lenses, a sample stage, detectors for all signals of interest, a display/ data output devices (e.g. a computer). Additional infrastructure requirements include: A power supply, a vacuum system, a cooling system, a vibration free floor.

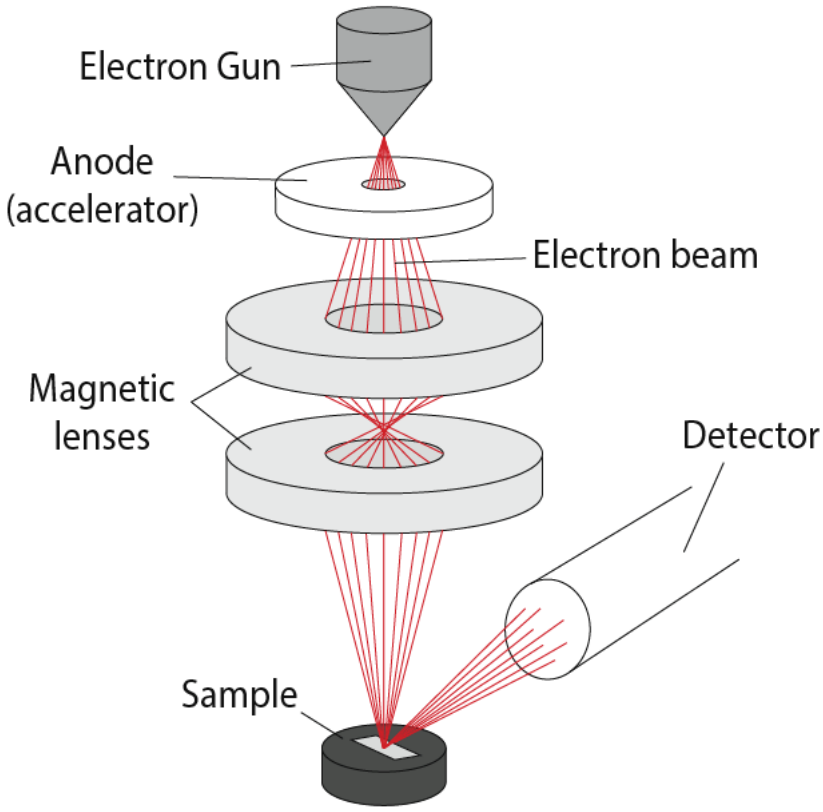

Figure 3.2: Schematic of typical SEM (adapted from https://www.eng-atoms.msm.cam.ac.uk/)

3.8 Nanoindentation

This is an indentation hardness technique which aims to test the mechanical properties of small volumes of material.

In traditional nanoindentation, a hard tip of known mechanical properties is utilised. That material can be a gem such as diamond or ruby. The probe is pressed into a material whose mechanical properties are unknown. The probe penetrates the object with an increasing load until it reaches a certain load pre-defined by the user. At that stage, load can be held constant in a time period determined by the user.

In order to best understand the mechanical properties of objects, different models are used for accurate calculation of a material's elastic and Young's modulus. In the case of biological tissue, the Hertz model is the model of choice in published literature [227]. According to this model, the examined material is an isotopic and

linear elastic solid occupying an infinitely extending half space. Another assumption made is that the probe does not deform and that there are no additional interactions between indenter and sample. Once these conditions are met, the Hertz model can be used in order to determine the Young's modulus of the material.

The Hertz model utilises different equations in order to determine Young's modulus. These equations are related to the shape of the probe. In the experiments demonstrated in this thesis, the indenter was of spherical shape, and the equation for the determination of the Young's modulus was

$$F = \frac{E}{1-\nu^2}\left[\frac{\alpha^2+R^2}{2} ln \frac{R+\alpha}{R-\alpha} - \alpha R\right]$$

with

$$\delta = \frac{\alpha}{2} ln \frac{R+\alpha}{R-\alpha}$$

where R is the radius of the spherical tip, E is the Young's modulus, ν is the Poisson's ratio, α is the radius of the indent and δ is the indentation of the substrate.

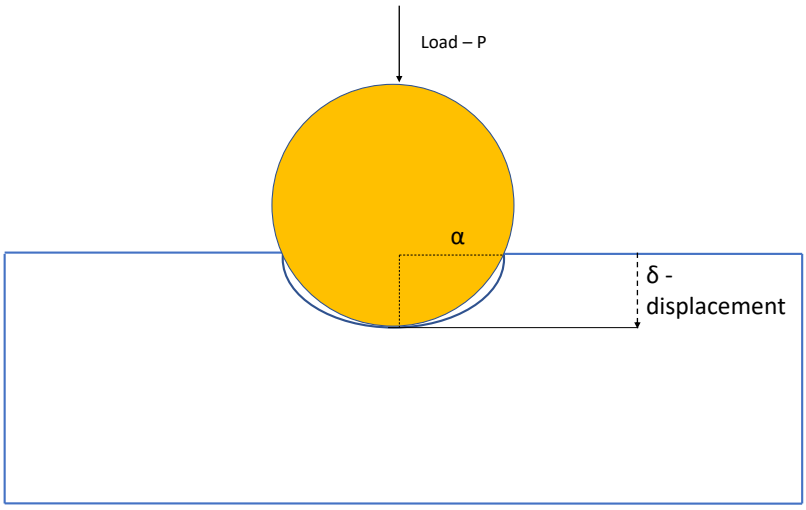

Figure 3.3: Spherical nanoindentation probe on a soft biological substrate. α indicates the radius of the indent, P indicates the load applied and δ indicates the displacement as a result of the probe.

3.8.0.1 Apparatus

Throughout this thesis work, an Anton-Paar Bioindenter (UHPT^3 Bio) Nanoindenter was utilised. This machine was especially designed for the examination of soft materials and biological tissues.

The apparatus as shown in figure 3.4 has the ability to apply loads up to 20 mN and is equipped with a 0.5 mm ruby spherical probe. The equipment applied the load on the z-axis and was able to probe multiple points on the substrate by means of a moving table, which could be controlled along the x-, y- and z-axes.

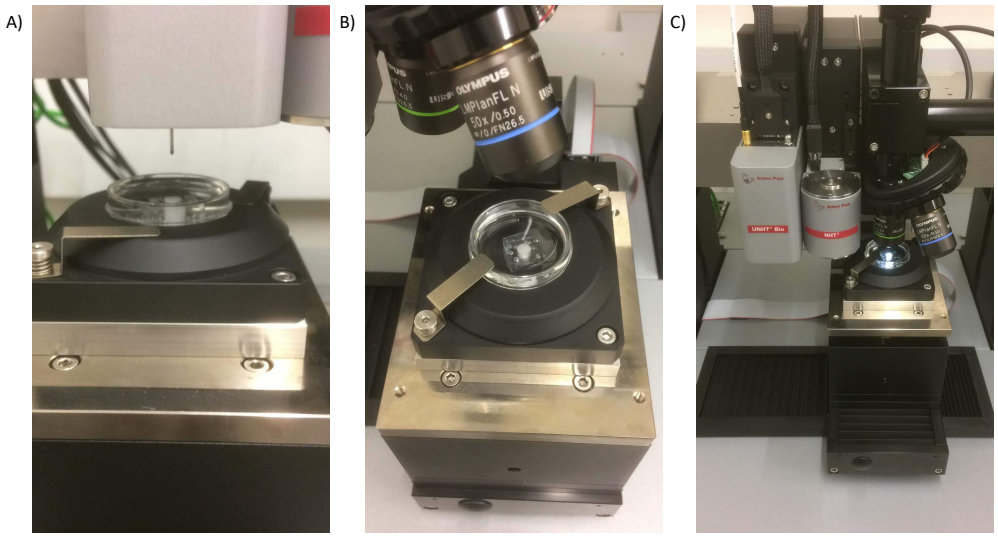

Figure 3.4: Experimental set up using the Anton Paar Bioindenter^{TM} UNHT^3. A) The ruby spherical probe before it engages with the H–ND–fibrin scaffold. B) The Petri dish containing the H–ND–fibrin scaffold below the microscope camera used in order to locate the optimal location on the surface of the sample for sample probing and C) Experimental set up including the UNHT^3 probe, the motorised precision table and the long working distance objectives.

3.9 Brightfield Microscopy

Bright field microscopy is one of the simplest modes of light microscopy. White light is transmitted from below the sample and the light observed by the eye pieces is the light that passes through the sample. The contrast in the observed image results from the different densities of the sample, which allow only specific

amounts of light to pass through. The resulting image is an image in greyscale [228].

3.10 Stereomicroscopy

A stereomicroscope is an optical microscope. It allows the observation of a specimen at low magnifications, therefore providing an holistic overview of small-sized specimens. [229].

3.11 Fluorescence Microscopy

Fluorescence microscopy relies on its specimen to exhibit autofluorescence. Fluorescence is stimulated by the absorption of a photon by a fluorophore. Once electrons relax from this excited state, energy is lost and as a result emission is shifted to longer wavelengths when compared to the excitation spectrum. This phenomenon is also known as Stoke Law.

In order to achieve maximum fluorescence intensity, the fluorophore is excited near the peak of its excitation curve, and therefore emits in a wide range of the visible spectrum. [230]

3.12 Polarised light microscopy

In its simplest form, a polarised light microscope (PLM) is brightfield microscope which contains two polarised filters: one at the top (*the analyser* and one below (*the polariser*) the specimen stage.

The polariser can be manually rotated and only allows light particles with vibration orientation along their polarising axis to pass. It is aligned in an east-west position (horizontal).

The analyser is aligned in a north-south position (vertical), bringing it to a 90^0 from the polariser, allowing light only moving in the north-south position to pass through.

This technique is most commonly applied to birefringent samples; there, the polarised light interacts strongly with the sample, therefore creating a strong contrast with the background [231].

3.13 Cell culture

hADSC and CSPC lines were expanded in two dimensions in tissue culture flasks with area of 175 cm^2 (T175 cell culture flask, Corning). Cells attached to the Tissue-Culture Grade Plastic of the flask with the aid of focal adhesions, multiprotein structures that contain integrin and facilitate the connection of the cellular cytoskeleton with the ECM [76], [77]. Cells were grown up to 80% confluency before passaging, in order to prevent loss of multipotency and spontaneous differentiation. Passaging included the following steps

1. Cell medium was removed from the flask.
2. Cells were washed $\times 3$ using PBS (without magnesium or calcium, as they inhibit trypsin activity).
3. Monolayer cell cultured was detached from flask wall by incubation with 0.05% v/v Trypsin / 1mM - EDTA for 5 minutes at 37^{o}C.
4. Trypsin action was deactivated by adding DMEM-Glutamax proliferation medium in the flask.
5. Detached cells in Trypsin-DMEM suspension were transferred in falcon tubes (Corning 430791 Conical-Bottom tubes). Trypsin is a pancreatic serine proteinase which aides in protein breakdown. In the case of tissue culture, it contributes to the breakdown of focal adhesions. EDTA is a metal chelator, which enhances the performance of trypsin. It ensures that trypsin will act quickly in the breakdown of the focal adhesions, as long incubation in trypsin can lead to cell damage.
6. Falcon tubes were placed in a centrifuge and cells were centrifuged at 1000g for 5 minutes until a pellet was formed.

7. Trypsin-DMEM medium was removed, and fresh DMEM-Glutamax medium was added.

8. Pellets were suspended in fresh medium.

9. Cell sample was taken and diluted in 1:10 Trypan Blue (Merck-Millipore) and counted using a haemocytometre under a light microscope. The dye can only enter compromised cells, hence aiding us to distinguished viable versus non viable cells under the microscope. In some cases, cells were also counted using a TC20 Automated Cell Counter (BioRad, Hercules, CA, USA). Trypan blue is a negatively-charged dye with 960 Daltons molecule diameter.

10. Between $2\times$ and 3×10^3 cells/ cm^2 were placed in new flasks [232].

3.14 Cell cryoconservation

In order to maintain cells at the desired passages when not needed, cells were kept in liquid nitrogen cryoconservation tanks. In those tanks temperatures down to -190^{o}C are present. There, cells are kept in a metabolic stasis state, while preventing contamination. In order to prepare cells for cryoconservation, cells underwent removal from tissue culture flasks as described above. In order to prevent cell damage at low temperatures and aide conservation, cells were kept in a special cryoconservation medium consisting of 90% v/v ES-FBS and 10% v/v dimethyl sulfoxide (DMSO) . DMSO acts as a cryoprotectant, as it prevents intracellular and extracellular crystals forming during freezing. These crystals can cause damage in the cell membrane and significantly decrease cell survival during the thawing process. ES–FBS also acts as a cryoconservation protector, being a macromolecule ([233]).

3.15 Cell differentiation

Complete protocols for cell differentiation can be found in results chapters 3 and 4. In this section the effect of the factors included in differentiation media is briefly discussed.

3.15.1 Chondrogenic differentiation media

The key components of this type of media were transforming-growth factor beta-1 (TGF - β-1), Dexamethasone (Dex) , Insulin-transferrin-selenium supplement (ITS) , and ascorbic acid. TGF β-1 is a 25 kDa cytokine that plays an important role in the signalling pathway of chondrogenic differentiation *in vivo*. Ascorbic acid can promote differentiation by promoting the formation of collagenous matrix and that matrix formation mediates activation of a signaling pathway, which promotes the differentiation programme ([234]). Dex is hypothesised to contribute to differentiation by promoting increased cell proliferation and the upregulation in expression in the master regulator gene *Runx2*, that is heavily involved in chondrogenic and osteogenic differentiation ([235]). Finally, ITS acts as a serum replacement in differentiaton cases where no ES-FBS or any other type of serum is supplied with the growth media.

3.15.2 Osteogenic differentiation media

In this type of media, the molecules Dex, ascorbic acid and β-glycerophosphate (β-Gly) are used. Dex and ascorbic acid have similar effects as in chondrogenic differentiation. In this case, the concentration of ascorbic acid is higher, as higher amounts of collagen matrix are needed. β-Gly promotes increased deposition of calcium, since it acts as the source of phosphate for the deposition of hydroxyapatite ([236]).

3.15.3 Adipogenic differentiation media

Here, the components are rosiglitazone, insulin. Dex and 3-isobutyl-1-methylxanthine (IBMX). IBMX in conjuction with Dex regulates PPAR γ, a transcription factor that promotes adipogenic differentiation. Rosiglitazone, speeds up and increases the rate of differentiation of precursor cells into adipocytes. Finally, insulin promotes mitotic activity and the activity of protein kinases in pre-adipocite cells ([237]).

3.16 Three dimensional cell culture

For the 3D culture of cartilage progenitor cells, fibrin was chosen as a suitable scaffold. Fibrin is a polymer resulting from the combination of fibrinogen monomers with thrombin polymerising factor. Fibrinogen and thrombin are the key components in blood clotting. For the purposes of this thesis, both fibrinogen (Merck-Millipore) and thrombin (Merch Millipore) were sourced from human plasma [125]. The fibrin scaffolds were reinforced with H–functionalised NDs, the same ones used in previous experiments in this thesis. The NDs were ultrasonicated in order to achieve monodispersion. NDs were suspended in PBS (Gibco), which is the dilution factor for both fibrinogen and thrombin. NDs were subsequently mixed with thrombin. Cells were first expanded in a monolayer culture, and upon reaching 100% confluency, they were trypsinised and mixed with the fibrinogen monomer at a concentration of 10,000 cells/ μl of fibrinogen. Thrombin diluted with the PBS- ND solution was added subsequently. Once thrombin was added, the material polymerised following the general gel condensing principle [238]. Figure 3.5 demonstrates how the 3D H–ND–fibrin cellularised constructs directly after assembly.

Fibrin gel was chosen for its superior properties compared to similar materials. It has a controlled degradation rate, excellent biocompatibility and its degradation products are biocompatible. Furthermore, it aids uniform cell distribution throughout the gel.

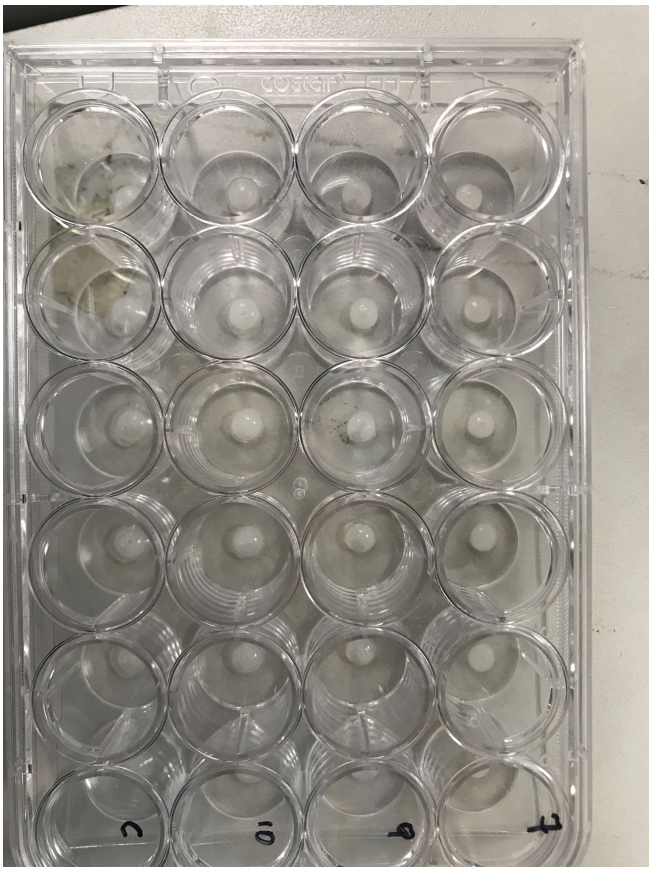

Figure 3.5: 24–well plate containing cellularised H–ND–fibrin scaffolds moments after its final polymerisation and prior to incubation in media. Concentrations of H–ND in scaffolds from right to left: 0.15g/l, 0.04g/l, 0.02g/l and no H–NDs.

3.17 Polymerase Chain Reaction (PCR)

PCR is a method widely used in molecular biology for the amplification of desired DNA sequences. The basic principle behind this technique is the complementarity of DNA bases and the principle of DNA elongation from 5' to 3' direction. There are various components required for a PCR reaction, such as Taq polymerase, which elongates the complementary DNA strand and is robust in high temperatures, deoxynucleotide triphosphates (dNTPs), which are pieces of DNA that are assembled together, and two primers, the 5' and 3' primer, each attaching at the 3' and 5' end of the template DNA strand, and acting as the starting point of elongation. PCR reactions occur in a thermal cycler, a piece of apparatus that controls the temperature of the reaction at any given moment.

3.17.1 Reverse Transcription PCR (rt-PCR)

This version of PCR used as a template single-stranded RNA. The single-stranded DNA is copied into a complementary single strand of DNA (called cDNA), which then adds as template for the amplification of the RNA signal, with a technique the same as the traditional PCR [239].

3.17.2 Quantitative- Real time PCR (qRT-PCR)

Quantitative polymerase chain reaction (Q-PCR) is a method by which the amount of the PCR product can be determined, in real-time, and is very useful for investigating gene expression [240].

Real-time PCR measures strength of light generated by a fluorescent dye. During DNA amplification, the fluorescent signal is created from a dye-labelled probe binding to DNA or from dye breakdown. During RT-PCR, DNA is amplified for a number of cycles. The cycle when the fluorescent signal surpasses background noise is called the C_T value.

Between two samples, one cycle difference in C_T value (δC_T) stands for a doubling of the amount of target. This relationship can be expressed as

$$The\ increase\ in\ the\ amount\ of\ amplified\ product = 2^{-\Delta C_T}$$

Standard deviation is calculated in order to determine the amount of variance from mean between C_T values of replicate real-time PCR reactions. It is given by the equation

$$\sqrt{\frac{\sum (x-\bar{x})^2}{n-1}}$$

DNA quantification with RT-PCR is performed by measuring a standard curve from a series of dilutions of independent replicate measurements of C_T values of positive control DNA. The control measurements are then compared against the log

of DNA concentration. This allows measurement of DNA concentration in the unknown sample with simple regression. [241]. Figure 3.6 demonstrates the concept.

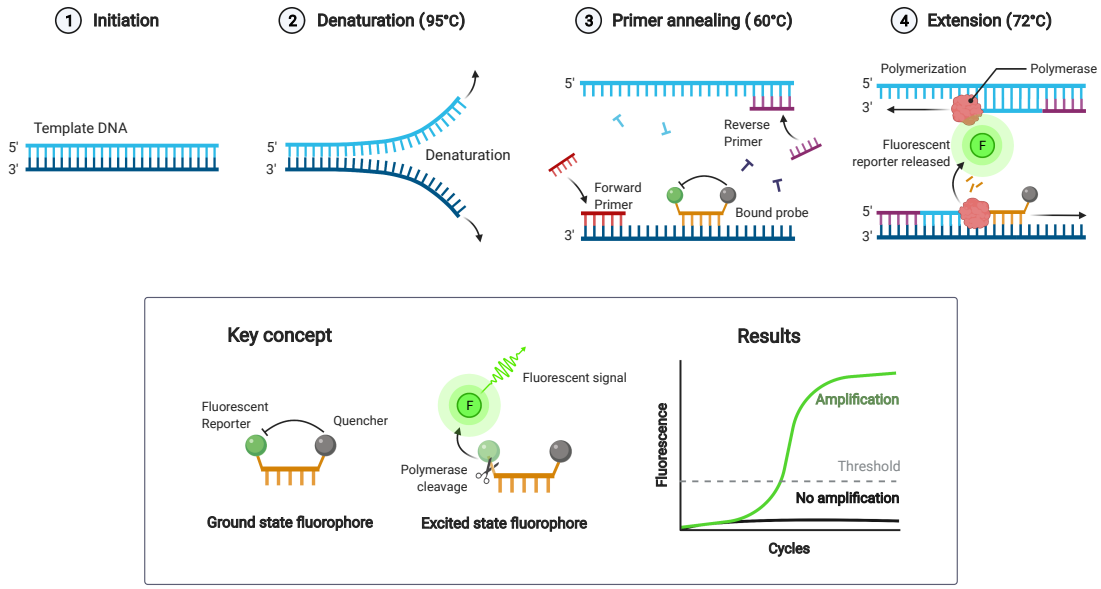

Figure 3.6: Schematic representing the process of a real time quantitative PCR (qrt-PCR).

3.18 Sectioning

Paraffin embedding is a widely used technique for the preparation of thin sections of biological materials for the purposes of histological analysis using light microscopy.

3D tissue samples were immersed in 10% neutral buffered formalin (NBF) in order to fix them. Formalin acts as a fixant by cross-linking of primary amino-groups. Post fixation, they are dried in order to be embedded in paraffin wax, a hydrophobic material.

Paraffin was the material of choice for embedding, as it has similar density to tissue and allows the tissue to be sectioned in sections between 3 and 10μm.

Sectioning was carried out using a microtome, a piece of equipment that allows for the cutting of sequential tissue samples of tunable thickness. The sections were

then immersed in a water bath in order to be smoothed out. The wax sections were then embedded on glass slides.

In order to remove the wax from the sections, the glass slides were left in a 65^oC oven overnight.

In order to completely remove wax, sections were then immersed in Histo-Clear, a solvent that removes wax completely. After Histo-Clear, the sections were immersed in increasing concentrations of ethyl alcohol, in order to achieve complete dehydration. The sections were then rehydrated by moving the sections down the ethyl alcohol concentration gradient and finally back into distilled H_2O. The rehydration steps are of essence, as tissue staining is only achieved in hydrated tissue [242].

3.19 Staining

3.19.1 Methylene blue stain

Methylene blue (or methylenium chloride) is an organic chloride salt. At 10% concentration it has the ability to penetrate every cell. Living cells are able to enzymatically reduce the dye and render it colourless, whereas dead cells cannot process the dye and therefore it remains blue [243]. The dye can be read by a photometer at an absorbance of about 650 nm.

3.19.2 Alcian blue stain

Alcian blue comes from a family of polyvalent basic dyes. It is able to stain acidic polyssaccharides such as glycosaminoglycans (GAGs), proteins expressed on the surface of cells differentiated towards chondrogenic fate.

The tissue parts the dye stains become a blue colour. The staining is pH-dependant. At pH 1, it stains only sulfated polysaccharides, whereas at pH 2.5 it also stains sugars that contain carboxyl groups. GAGs belong in the second group [244], [245], [246].

3.19.3 Alizarin red stain

Alizarin red, also known as 1,2-dihydroxyanthraquinone or Turkey red, is a naturally occuring dye, primarily used in the textile industry as a dye. It has the ability to stain the presence of calcified deposition of cells, an early indicator of osteogenic differentiation in tissue culture. As such, it acts as an indicator of matrix mineralisation, which is a crucial step in the formation of the extracellular matrix of bone [244], [247].

3.19.4 Picrosirius red stain

Also known as Sirius Red F 3B, this azo dye has the ability to stain collagen. The azo dye is able to bind covalently to collagen via a Michael reaction. While the red colour of the stain is non-specific to all types of collagen, when exposed to polarized light, Picrosirius red demonstrates a yellow colour when bound to collagen type I and a green colour when bound to collagen type III, which are specific to bone tissue [248].

3.19.5 Toluidine blue stain

This is a basic thiazine metachromatic dye, that shows great affinity for acidic tissue components. Because of this, toluidine blue is able to stain cartilage. The dye appears blue, but when bound to cartilage the colour tends more towards purple [249].

Chapter 4

Investigation of cell proliferation and morphology on oxygenated porous diamond coated structures

4.1 Introduction

Before understanding the effect of different nanodiamond coated surfaces on cartilage tissue engineering and cell differentiation, in this chapter the different nanodiamond substrates and morphologies were characterised. In addition, it was validated whether mesenchymal stem cells can proliferate and grow on a range of nanodiamond surfaces.

In vivo, the extracellular matrix (ECM) is the facilitator of cell adhesion and is partially responsible, through chemical and mechanical cues, for the direction of stem cell fate. Through *indirect* and *direct* mechanotransduction signalling, the ECM can cause the exoskeleton to move and change conformation, which in turn alters the shape of the nuclear envelope. This cascade of events eventually leads to the alteration of gene expression, through activation of different gene regions, as a direct result of the nuclear movement ([250], [251], [252], [253]).

Furthermore, the morphology of the substrate can have an effect on the adhe-

sion and organisation of cells ([254]). In the last decade, studies have moved from examining the effect of substrate organisation from the micrometre to the nanometre scale. Results point towards the direction of mammalian cells responding to nanoscale organisation ([255]).

The tissue-scaffold interface has been a well investigated topic in tissue engineering. One of the most important questions about the *in vivo* cell-interface is the interface between bone and prosthetic in hip and knee replacements. Amorphous carbon and diamond coatings have been used in order to establish better integration of implant and tissue, alongside modifications on the surface morphology of the implants ([256]).

In *in vitro* studies, patterned surfaces have been studied in order to establish links between improved differentiation and proliferation of stem cells ([257]).

A range of techniques have been utilised for the fabrication of such patterned surfaces. Some of the most popular ones include electrospinning ([258]), lithography methods ([259]), etching ([260]), and self assembly ([261]), ([262]). Each technique provides different patterns as well as different levels of control of spacing between each pattern structure.

Carbon and diamond patterned substrates are versatile platforms not only for biological, but for wider engineering purposes. Due to the biocompatbility and electrical conductivity of their base material, such structures point towards the dawn of a new era, when structures can provide the dual role of both electrical and mechanical stimulants of stem cell cultures.

In this chapter, a particular example of such a structure is examined. Scientists from the Diamond Sensors Laboratory in CEA, Paris Saclay, developed a structure of porous diamond with high electrochemical performance. These are polypyrole structures that have been coated with boron doped diamond (BDD).

The fabriaction process of this material utilises a conductive template material based on porous polypyrrole (PPy) . The rationale behind this was the combination

of the high surface area of the PPy with the excellent surface properties of diamond in order to create, amongst others, a material exhibiting high biocompatibility.

The basic principles behind its fabrication is the deposition of 20 μl of a $FeCl_3$, ethylene glycol and acetonitrile solution onto 1cm^2 polycrystalline boron doped diamond electrodes [263]. Those substrates were then exposed to saturated pyrrole vapour which enabled *in situ* polymerisation of pyrrole. The resulting PPy films featured a thickness of 10 μm. Subsequently, the material was coated with diamond nanoparticles with mean diameter of 25 nm, upon being exposed to an aqueous solution of poly-diallyldimethylammonium (PDDAC) , a technique developed by Girard et. al in 2009 [264]. Finally, a boron doped diamond layer of a few hundred nm was grown in a Microwave Plasma enhanced Chemical Vapour Deposition (MPCVD) reactor ([4]).

Furthermore, functionalised detonation nanodiamonds (DNDs) have been shown to support human neural stem cell (hNSC) adhesion and proliferation, in particular oxygen–functionalised DNDs (O–NDs) [143].

The initial aim for this chapter was to analyse the nanodiamond substrate morphologies. An additional aim was to validate if mesenchymal stem cells are able to proliferate and grow on the different nanodiamond based surfaces.

In experiments reported in this chapter, human adipose-derived stem cells (hADSCs) were cultured and imaged on different oxygen functionalised BDD and DND based structures in 2D, in order to examine their biocompatibility, as well as the effect of those structures on cell proliferation.

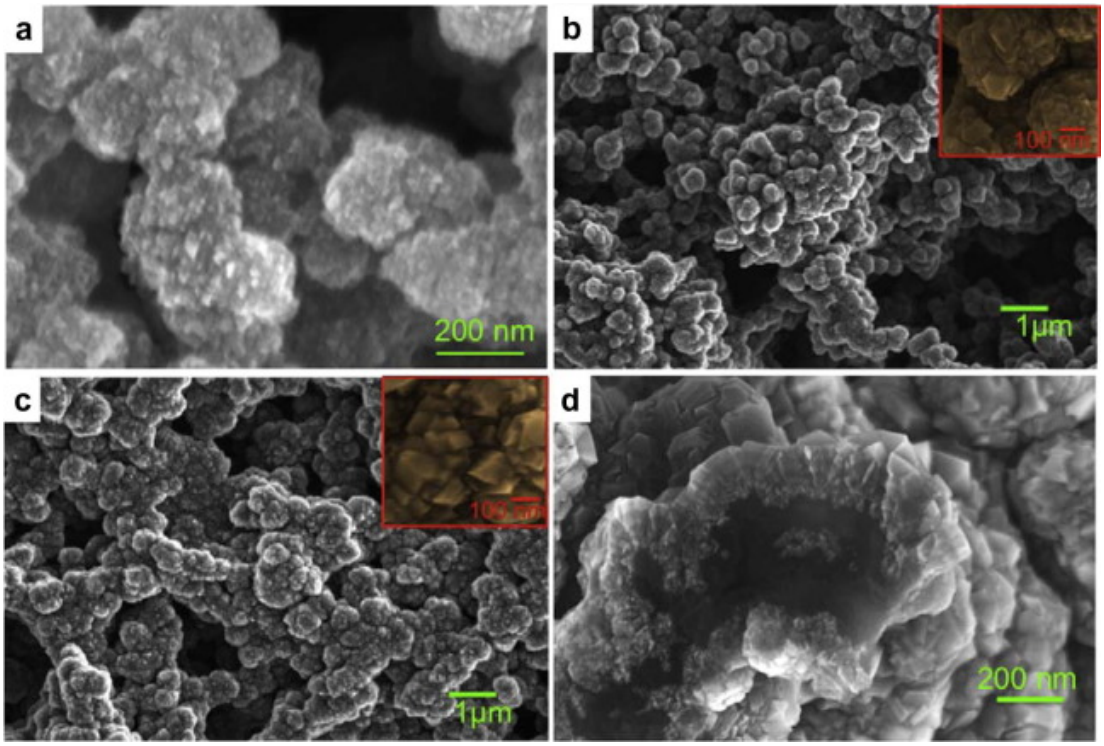

Figure 4.1: SEM images of boron-doped diamond (BDD) coated polypyrrole: (a) PPy film coated with high density of 25 nm diamond nanoparticles. (b) PPy film coated with a 90 nm thick BDD layer. The inset shows a higher magnification of the film. (c) PPy coated with a 170nm thick BDD layer. The inset shows a higher magnification of the film (d) cross section of the PPy film coated with a 170 nm BDD layer. Taken from [4].

In this chapter five different substrates were examined in order to establish the effect of substrate morphology on the organisation of 2D hADSC cultures. Through various imaging techniques (stereomicroscopy, Scanning Electron Microscopy (SEM), brightfield microscopy and fluorescence microscopy), the aim was to establish a link between the nature of this novel porous diamond substrate and culture morphology.

Three of the substrates match substrates further examined in chapter 5: TCPS (plastic), degreased borosilicate glass and oxygen-terminated NDs. Further tested substrates are the PPy diamond coated scaffolds, functionalised with oxygen under ozone, as well as degreased borosilicate glass coverslips, coated with PDDAC and seeded with NDs, which were then O-functionalised. The technique of ND seeding on those 2D samples matches the technique of diamond coating of the PPy samples.

4.2 Materials and Methods

All experiments were performed by the author. The 3D polypropylene scaffolds were kindly provided by Dr Emmanuel Scorsone from CEA Saclay, France.

4.2.1 Chemicals

Poly(diallyldimethylammonium chloride) (PDDAC) ($C_8H_{16}NCl$) (Sigma–Aldrich) was used as a coating polymer for borosilicate glass. Samples were fabricated according to the protocol presented in [264].

H-NDs as prepared by the protocol described in Chapter 3 were utilised for the samples seeded by ultrasonication. Samples seeded by the PDDAC method utilised DNDs.

4.2.2 Cell lines

The cell lines used for this experiment are shown in table 4.1.

Table 4.1: Cell lines and cell types used in experiments in this chapter.

Cell lines				
Cell line	Cell type	Passage	Patient condition	Experiment
hADSC	h20	P8	Parry Romber syndrome/ Facial atrophy	SEM imaging
hADSC	h37 GFP$^+$	P12	Hemifacial microsomia	Quantification assay

4.2.3 Cell culture

All samples were sterilised in 70% EtOH. Cells were plated on all substrates at a density of 3×10^4/cm^2 and were incubated at 37^{o}C under 5% CO_2 for 2 weeks. They were cultured using Dubecco's Modified Eagle Medium (DMEM), high glucose, Glutamax^{TM} (ThermoFisher Scientific). The medium was enriched with 10% embryonic stem cell-certified fetal bovine serum (ES-FBS) (Merck Millipore) and 1% penicillin-streptomycin antibiotic (Gibco™). The medium was changed every 3 days.

Fluorescent hADSCs were used in order to be able to image the opaque BDD-PPy substrates under the stereomicroscope. By using fluorescent cells, the cells cultured on the BDD-PPy opaque substrates could be imaged live, using a fluorescence stereomicroscope (Leica MZ26).

4.2.4 Fabrication of samples containing PDDAC coatings

Borosilicate coverslips degreased as per the process in chapter 2, were immersed momentarily in a 10% PDDAC solution for 10 minutes. They were then air dried under air flow in a fume hood for approximately 10 minutes.

Subsequently, the coverslips were vertically suspended in 0.05 g/l ND solution for 35 minutes and were then dried under N_2 flow.

4.2.5 Fabrication of borosilicate glass – ND samples

Borosilicate glass coverslips (Cover glass, VWR, UK) of 3mm diameter were cleaned and degreased as discussed in chapter 2. Subsequently, the degreased glass coverslips were ultrasonicated for 10 minutes (excess time) in H–ND solution suspended in DI water (0.05 g/l concentration). Afterwards, the substrates were dried under N_2 flow.

4.2.6 Oxygen termination

H–ND monolayers were treated with ozone in order to achieve oxygenation. The samples were treated in a custom made chamber combined with a commercially available ozone generator (Ozonia TOGC2-100201). Functionalisation was achieved by ozone flow for 1 hour under 50 mbar pressure and 200^{o}C. Upon completion of the process, samples were cooled down under ozone flow.

4.2.7 Samples utilised in this chapter

In summary, the samples used in experiments in this chapter are described in the table 4.2

Table 4.2: Description of samples utilised in Chapter 4

Samples		
Sample name	Type of material	Description
BBD–PPy	Boron doped diamond	Porous diamond fabricated as described in [4], functionalised with oxygen
O–PDDAC	DNDs	borosilicate glass substrate coated with PDDAC and subsequently submerged in DND solution, from a slightly modified protocol first described in [264]; sample was then functionalised with oxygen
O–ND	DNDs	borosilicate glass substrate coated with DNDs, and functionalised with oxygen
Plastic	Tissue Culture Polystyrene (TCPS)	Control tissue culture plastic sample, which is the substrate hADSCs are usually cultured on in 2D
Glass	Borosilicate glass	Control glass borosilicate sample

4.2.8 Sample fixation and drying

After 2 weeks in cell culture, cells were fixed using 4% PFA , in the technique described in chapter 2.

The BDD-PPy samples were subjected to further preparation for SEM imaging. They were post fixed with 1% osmium tetroxide for 1 hour and then washed $\times 3$ with DPBS. The cells were then subjected to a sequence of dehydration steps

- 50% EtOH (10 mins)
- 70% EtOH (10 mins)
- 80% EtOH (10 mins)
- 95% EtOH (two changes within 10 mins)
- 100% EtOH (three changes within 15 minutes)

Afterwards, the samples were subjected to chemical drying using HMDS .

4.2.9 Scanning Electron Microscopy

The BDD-PPy substrate with and without cells were characterized using a Carl Zeiss Orion NanoFab microscope. Images were used to calculate sample porosity, BDD grain size and to assess cell proliferation on the substrates.

The cells were fixed using 4% PFA and were subsequently dried as described in subsection 4.2.8 prior to SEM imaging.

4.2.10 Cell stereomicroscopy imaging

The eGFP$^+$ hADSCs were imaged live after two weeks of culture using a Leica MZ26 fluorescence stereomicroscope, using the GFP imaging filter fitted on the microscope.

4.2.11 Cell fluorescence imaging

The Olympus IX71 microscope (Carl Zeiss, Jena, Germany) equipped with a Hamamatsu ORCA-ER digital camera (Hamamatsu Corp., Bridgewater, NJ) was used in order to image the fluorescent cells grown on borosilicate glass, O-ND and O-PDDAC coated glass and on plastic. Fiji software was used for image processing.

4.2.12 Cell counting

Cells were counted using images taken with 5$\times$ objectives from both the IX71 Olympus and the Leica M205 Fa microscopes. Fiji was used to manually count the fluorescent cells. This technique was preferred over automatic counting using colour thresholding and a software like MATLAB, as GFP is present in the whole cell body, which is harder for software to distinguish compared to cell nuclei.

4.3 Results

4.3.1 Substrate characterisation

In figure 4.2 the surface morphology and roughness of the different 2D substrates are examined. The 2D substrates were characterised using AFM. The roughness of each substrate was assessed. From figure 4.2 and table 4.3, the roughness of the ND-seeded surfaces is comparable to the roughness of the TCPS (plastic). However, the glass roughness is lower.

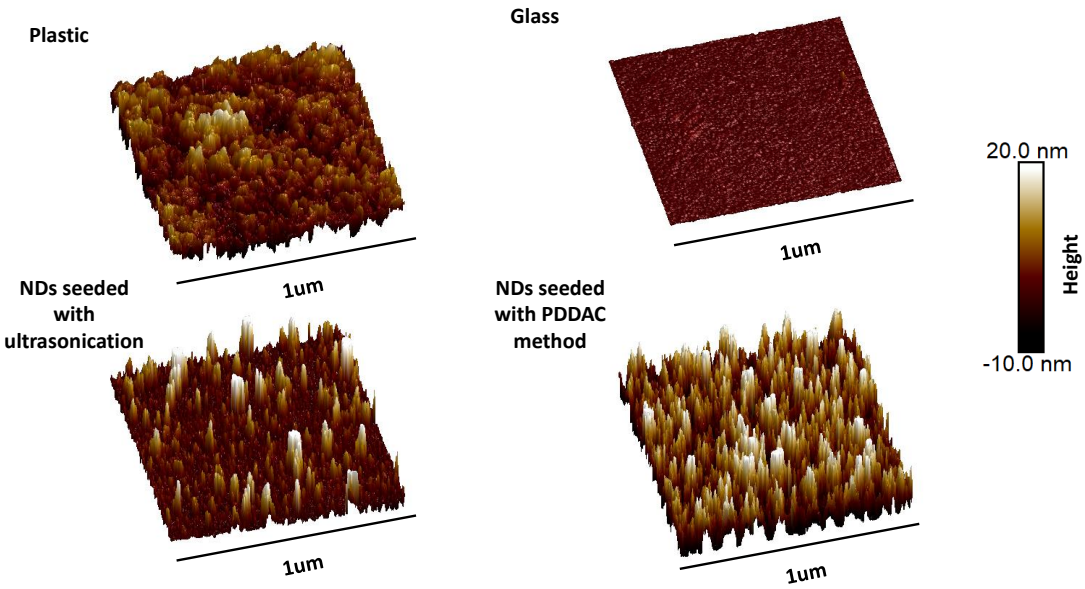

Figure 4.2: AFM topography of TCPS, Glass, O-ND and O-PDDAC substrates.

Table 4.3: Roughness of TCPS, glass, O–ND and O–PDDAC substrates

Root mean square roughness (Rq) (nm)	
Sample	Rq
TCPS	3.64 ± 0.84
Glass	0.28 ± 0.08
O–ND	3.28 ± 0.91
O–PDDAC	5.38 ± 0.93

When comparing the ND seeded substrates, it is evident that the substrates that were coated with PDDAC prior to ND seeding show a more homogeneous distribution of NDs compared to the counterpart that was directly seeded with NDs via ultrasonication. Furthermore, the samples coated with PDDAC display increased roughness compared to the ultrasonication seeded counterparts. This can be attributed to the longer exposure of the substrate to NDs (35 minutes vs 10 minutes for ultrasonication), as well as to electrostatic forces.

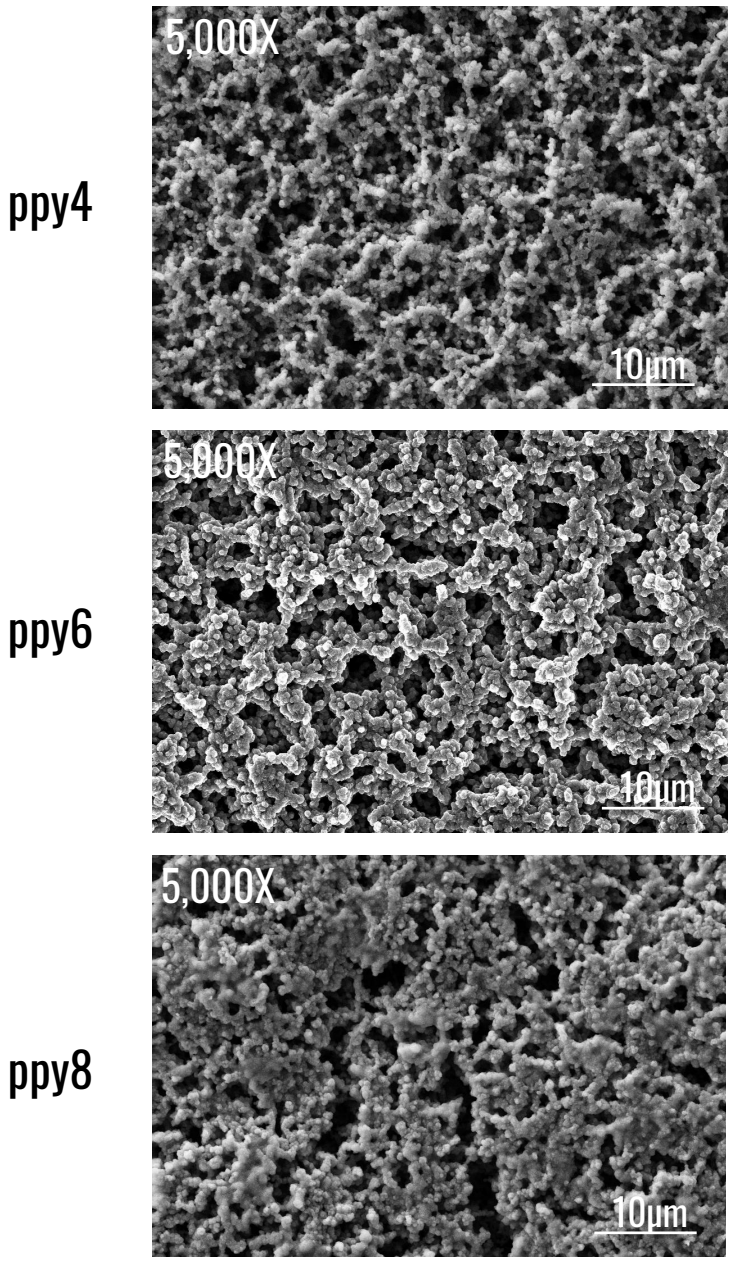

(a) SEM images depicting the porous structures of the BDD-PPy substrates.

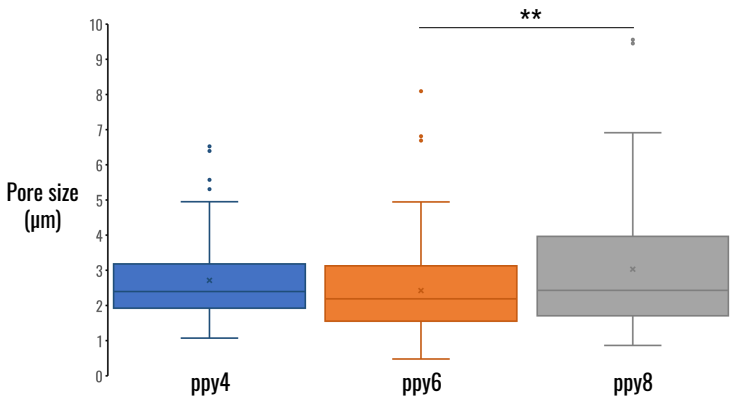

(b) Comparison of the average pore size in the three different BDD-PPy substrates.

Figure 4.3: Comparison of the morphology and average pore size between the three different BDD-PPy samples. Pore sizes were measured using ImageJ, with n=112 counts of pores per sample. Student's t-test was used for statistical difference, $^{**}p<0.01$.

In figure 4.3 the porosity of the different samples are examined. In order to examine the porosity, the diameter of pores on the surface of each sample was measured using Fiji. These three sample groups (PPy4, PPy6, PPy8) were manufactured under the same conditions. Grouping under each different name indicates similarities in structure and porosity. The average diameters are 2.71 μm, 2.42 μm and 3.03 μm for PPy4, PPy6 and PPy8 respectively, while their median diameters were 2.4 μm, 2.18 μm and 2.43 μm (n=112). Least variation is observe among the pores of PPy4, while the Student's t-test showed significant differences between the pore sizes of PPy6 and PPy8.

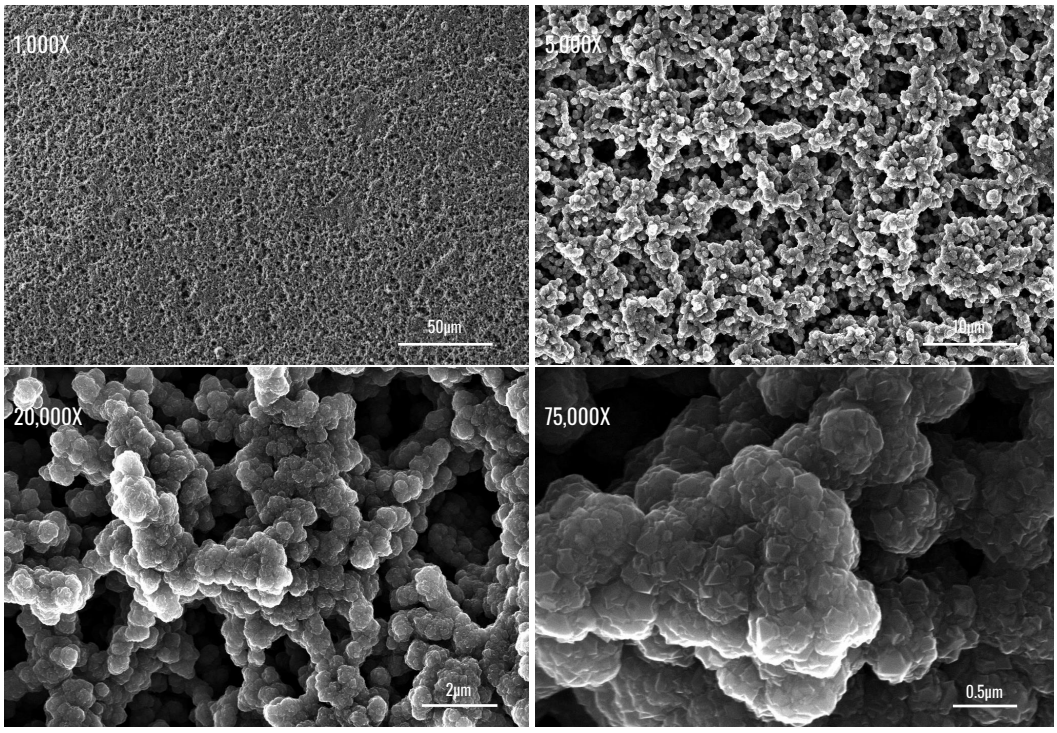

Figure 4.4: SEM imaging of the surface morphology of BDD-PPy6 under different magnifications.

In figure 4.4, the BDD-PPy6 scaffolds were examined under further magnification. The grain size of the boron-doped diamond coating these samples is 90 nm diameter.

4.3.2 hADSCs grown on porous BDD-PPy scaffolds

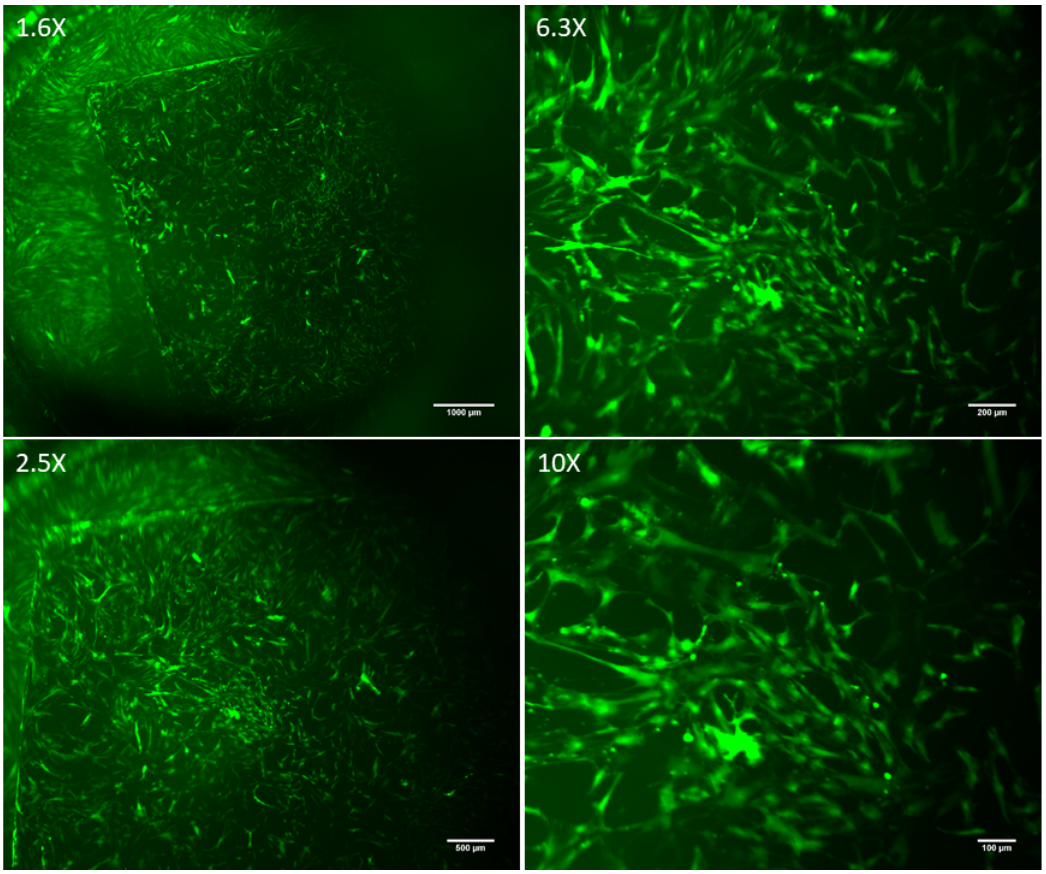

Figure 4.5: Stereoscopic image of eGFP^{+} fluorescent hADSCs growing on the BDD-PPy scaffolds.

Next the ability of mesenchymal stem cells, specifically hADSCs to grow and proliferate on different substrates was tested.

In figure 4.5, the eGFP^{+} hADSC cells were cultured for 2 weeks, until they achieved confluence. The cells ended up covering the scaffold fully, growing relatively uniformly throughout the structure. From these images, the cells appear elongated with long protrusions. However, the cells do not appear to have grown in any particular pattern nor do they demonstrate any type of organization.

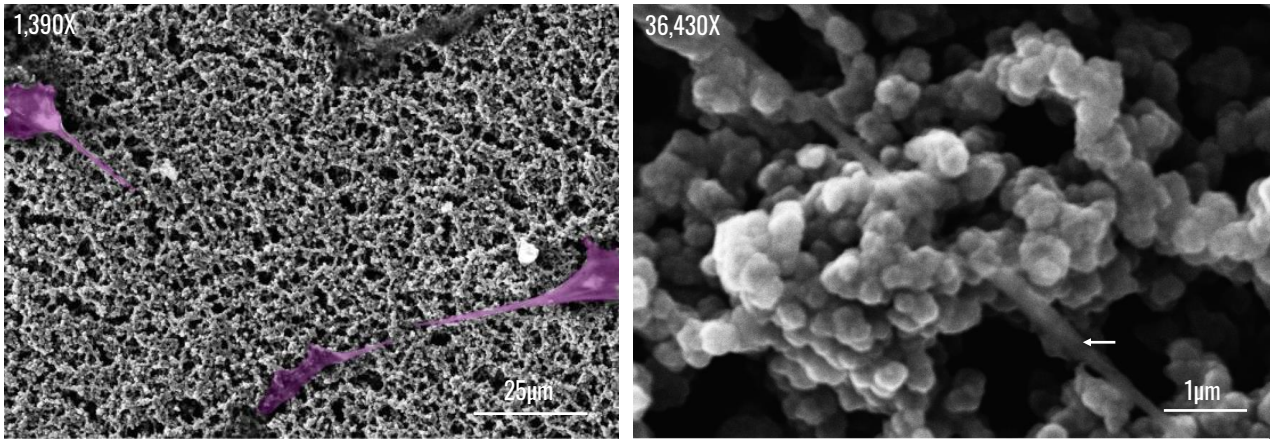

Figure 4.6: SEM imaging of hADSCs grown on the PPy6 substrate. For the left hand panel, cell bodies have been colorised using Inkscape.

In figure 4.6, the cells were imaged with higher magnification using SEM. From these images it is evident that the cells are utilising the porosity of the structures in order to adhere to the substrate.

4.3.3 hADSCs grown on 2-dimensional substrates

As a first experiment using hADSCs on 2D surfaces, proliferation of hADSCs on plastic, glass and O–ND coated substrates was observed.

In figures 4.7 and 4.8 $eGFP^+$ hADSCs were cultured for two weeks on four different substrates: TCPS (plastic) (n=5), degreased borosilicate glass (n=8), O-NDs (n=8) and O-NDs seeded on a surface treated with PDDAC (n=8). The cells cultured on the ND-seeded surfaces appear to grow in a more organised, striated manner compared to their counterparts grown on TCPS and glass. The difference between O–ND and glass surfaces is particularly pronounced.

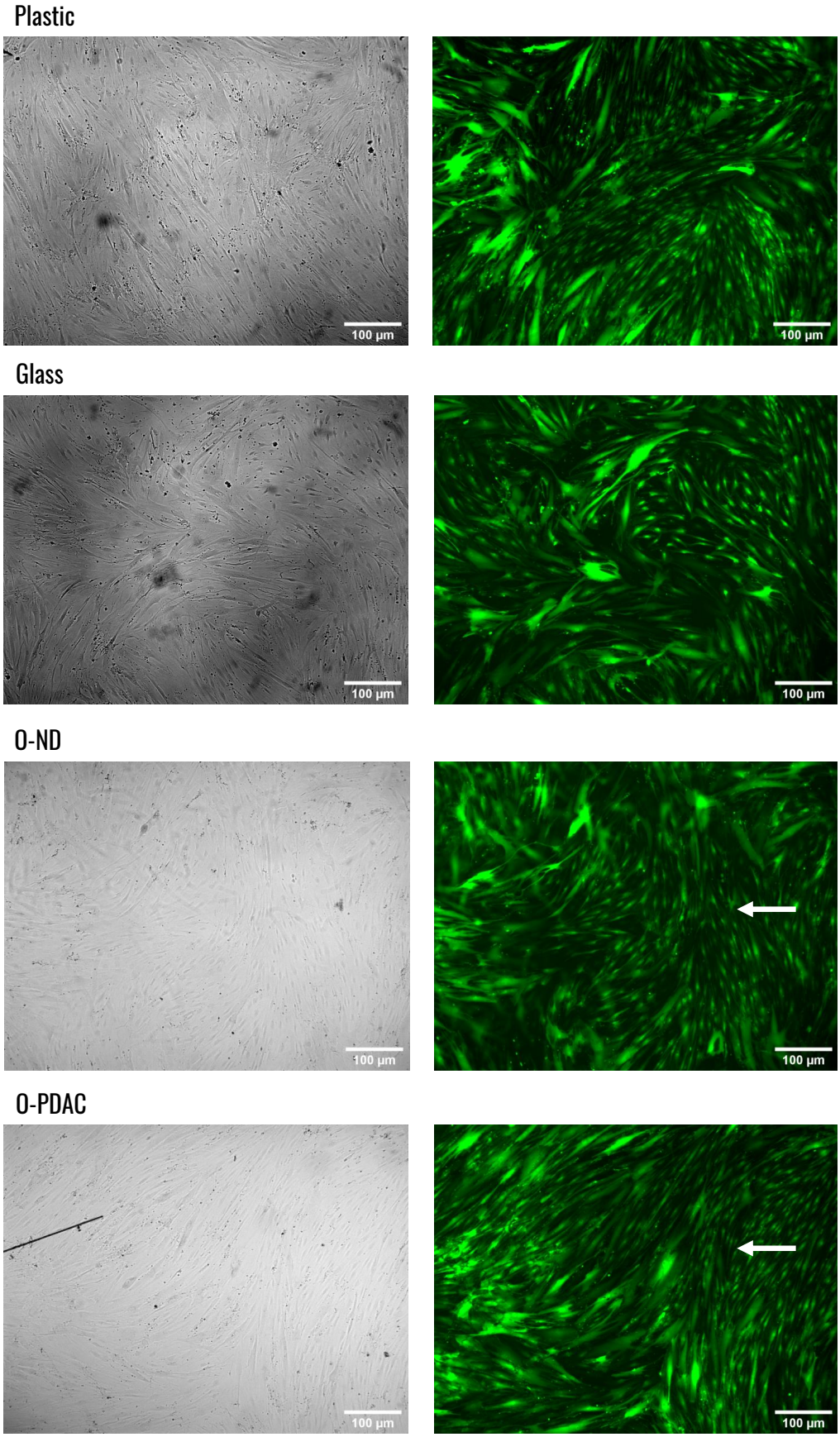

Figure 4.7: Brightfield (left) and fluorescence (right) microscopy of fluorescent hADSCs grown on different substrates, including two oxygen-terminated diamond substrates.

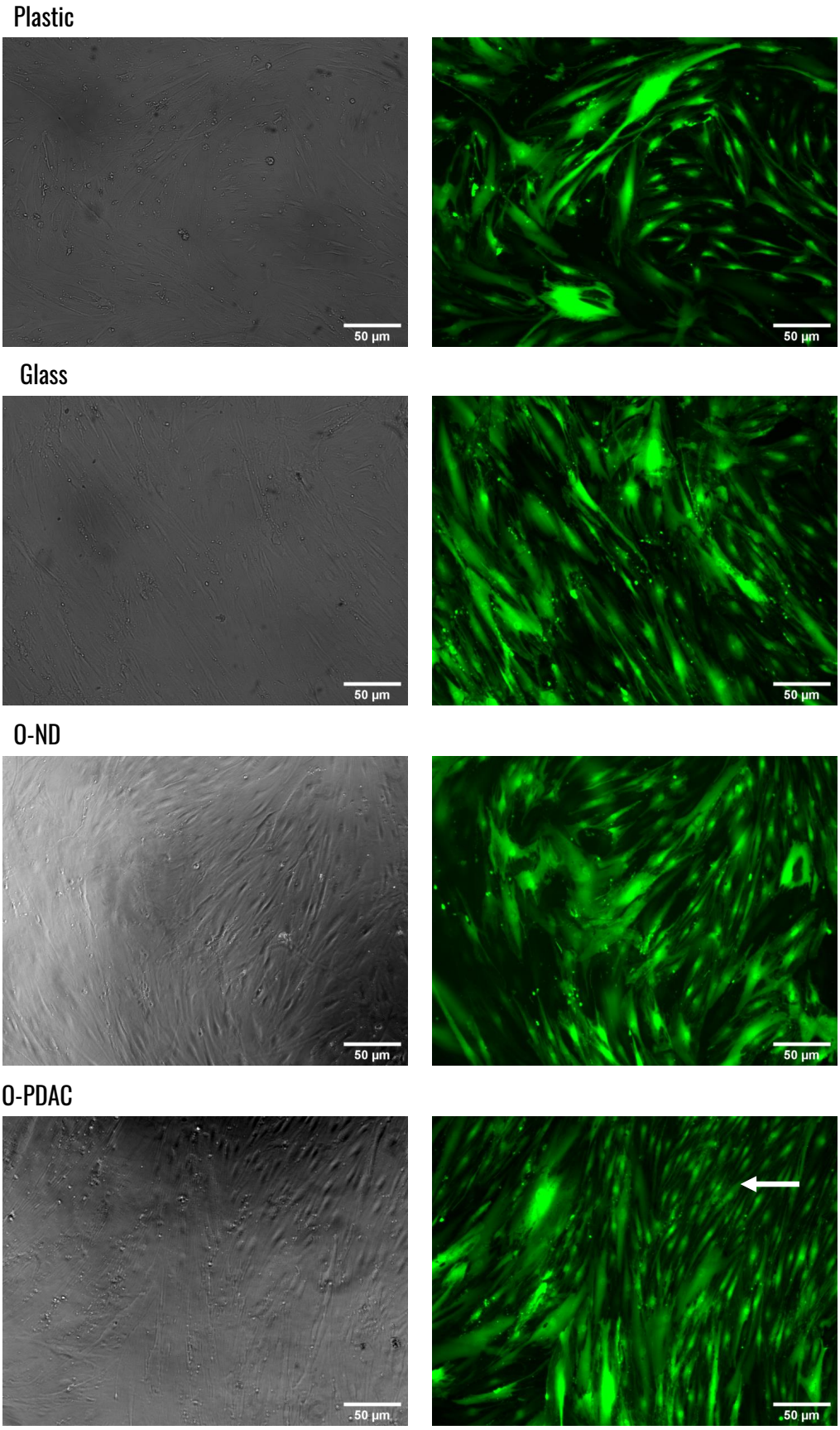

Figure 4.8: Brightlfield (left) and fluorescence (right) microscopy of eGFP^{+} fluorescent hADSCs grown on different substrates, including two Oxygenated diamond substrates.

4.3.4 Cell counting assay

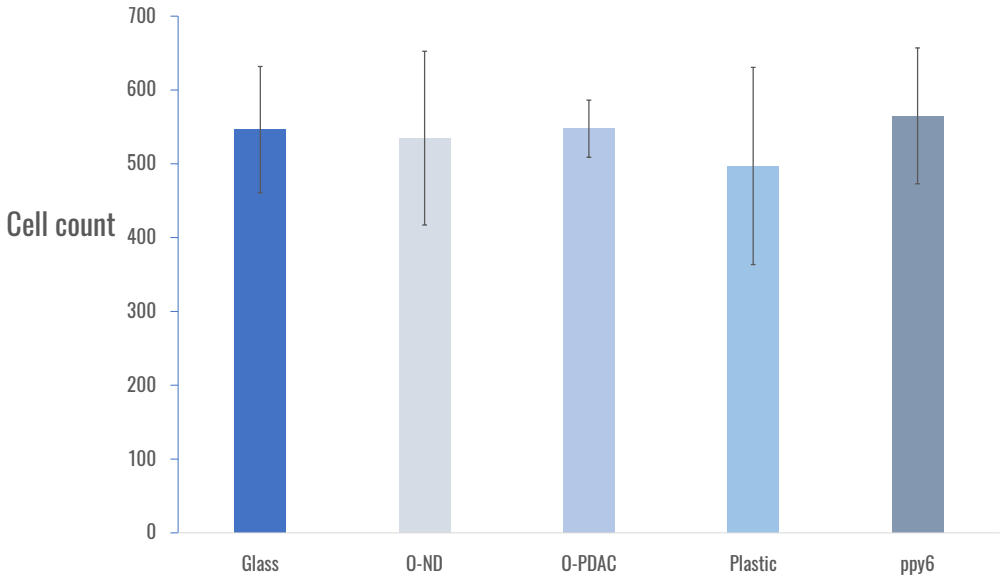

Figure 4.9: Cell count comparison among different substrates. Cells in 5 distinct fields were counted per sample. No statistical difference detected ($p<0.05$) with ANOVA test for variance and Posthoc Tukey HSD test.

Using the same magnification as the one in the figure 4.7 and the 10× magnification of the stereomicroscope, the eGFP$^+$ cells were manually counted within the area of the microscope captured. In figure 4.9, the cell count on all different substrates is compared. The cell count appears consistent between Plastic (n=5), glass (n=5), O–ND (n=5), O–PDDAC (n=5) and PPy6 (n=3). ANOVA and Posthoc Tukey HSD tests indicated no significant variance among samples.

4.4 Discussion

In this chapter, the effect of different diamond substrates on hADSC monolayer growth was observed. Mammalian cells have been shown to respond to nanopatterned surfaces. Figures (roughness and morphology) indicate increased patterning and roughness on the nanoscale. In figures 4.7 and 4.8 we can observe increased organisation of the fluorescent hADSCs on the substrates with increased roughness (O-ND, O-PDDAC and plastic) while they appear less organised on the glass substrate.

From the cell count data, it can be seen that the number of cells on each different substrate after two weeks is consistent. There are no large discrepancies between the number of cells on each different substrate. This is significant in two ways: one, cell proliferation and spreading is neither inhibited nor promoted by surfaces of different roughness and patterning; two, after two weeks of cell culture, there is no indication that cells on one type of substrate would have sustained higher cell death incidence compared to their counterparts.

Another interesting observation is the low standard deviation between the O-PDDAC samples. The number of cells on those substrates is more consistent compared to their counterparts. This could be an indication that the homogeneous distribution of NDs on the substrate could encourage homogeneous cell proliferation and sustained growth. This hypothesis could be tested with further experiments that examine the role of focal adhesions on the attachment of cells on these substrates, using an anti-FK or Vinculin antibody. Another assessment of the proliferation of cells over time can be a time series experiment where cells are imaged and counted at different times over a two week proliferation period.

An assessment of the effect of the O–ND, O–PDDAC and O-terminated BDD–PPy substrates on spontaneous differentiation of hADSC could be a further indicator on the effect of substrate morphology versus substrate functionalisation on cell differentiation. Since spontaneous differentiation levels on these substrates could potentially be low, an immunohistochemistry assay screening for Collagen-2, a protein expressed in the early stages of chondrogenic differentiation, could be utilised.

The significant difference in roughness between the O–ND and O–PDDAC substrate can be contributed by the formation of larger ND aggregates on the substrates coated with PDDAC prior to ND seeding. This higher aggregation can be attributed to the fact that the substrates were submerged on the solution for a significant amount of time (35 minutes versus 10 minutes for ultrasonication), as well as the different dynamics of deposition of the two techniques.

Despite the superior ND seeding observed on the borosilicate coverslips coated

with PDDAC, the process of creating the samples is time consuming and difficult to scale for biological experiments, which require significant amounts of replicates and potential repeats of experiments. Given that the ultrasonication ND method yielded satisfactory results in cellular experiments described on this chapter, for the rest of this thesis, the use of ND seeding using ultrasonication was utilised.

4.5 Conclusion

In this chapter, the morphology of 5 different substrates and the proliferation of hADSCs on each has been investigated. The cell count results have indicated that the different surface morphology does not affect significantly the number of cells on different substrates. Based on the results of this chapter, a further hypothesis can be formed that the morphology of the diamond substrate does not have an effect on cell behaviour on proliferation level. Rather, it is the chemical properties of nanodiamond that are enhancing the differentiation potential of these cells. Further investigation of this hypothesis is attempted in chapter 5 and 6.

Chapter 5

Investigation of functionalised nanodiamond as a platform for cartilage tissue differentiation in 2D

5.1 Introduction

Paediatric human adipose–derived stem cells (hADSCs) isolated from lipoaspirates and precursor cells derived from costal cartilage in the rib, have both shown good potential as precursor cells for cartilage tissue engineering ([265], [95], [94]).

hADSCs are an attractive cell type for autologous tissue engineering due to the minimally invasive character of tissue harvesting, as well as the tissue's relative abundance in the human body. hADSCs have also shown great aptitude for proliferatiation and differentiation on 2–dimensional cultures on tissue–culture plastic (TCPS).

However, there are still technical challenges when implementing differentiation of hADSCs. The main bottleneck is their lower affinity towards differentiation compared to other, more specialised skeletal stem cells. In this chapter, we aimed to examine whether novel nanodiamond coated substrates may sustain hADSC dif-

ferentiation on 2D surfaces. We have examined multiple novel nanodiamond coatings on 2D plastic or glass surfaces to establish whether these varied materials can sustain hADSC differentiation. The two novel nanodiamond coatings tested were oxygen and hydrogen terminated nanodiamonds, which were previously shown to sustain differentiation of human neural stem cells [143]. In addition to hADSCs we wanted to examine whether nanodiamond coated surfaces can act as a platform for differentiation of different stem cell types. For this purpose we have also used cartilage-derived stem-precursor cells (CSPCs) that were tested on 2–dimensional substrates and differentiated towards a 3–lineage fate (chondrogenic, osteogenic and adipogenic differentiation). This was done in order to test their differentiation ability, as well as to examine their behaviour on the different nanodiamond coated substrates. The results from this chapter allowed us to evaluate nanodiamond as a potential material for cartilage tissue differentiation in established 2D assays. This is a useful stepping stone before testing nanodiamond materials in more complex 3D structures.

5.2 Materials and Methods

.

5.2.1 Substrate degreasing

Borosilicate glass coverslips of 10 mm diameter were subjected to degreasing in order to remove residues of contamination. The coverslips were first placed in a glass beaker containing acetone and were incubated in an ultrasonicator bath for 5 minutes. The acetone was subsequently removed and the substrates were treated in isopropanol (IPA) for an additional 5 minutes in the ultrasonicating bath. Finally, IPA was removed and the substrates were treated for 10 minutes with de–ionised (DI) H_2O in the ultrasonic bath.

Afterwards, the coverslips were dried using N_2 flow from an nitrogen-gas gun.

5.2.2 Nanodiamond monolayer coatings

Borosilicate glass coverslips (Cover glass, VWR, UK) of 10 mm diameter were cleaned and degreased as discussed in chapter 4. Subsequently, the degreased glass coverslips were ultrasonicated for 10 minutes (excess time) in H–ND solution (5% w/v concentration). Afterwards, the substrates were dried under N_2 flow.

5.2.3 Oxygen termination

H–ND monolayers were treated with ozone in order to achieve oxygenation. The samples were treated in a custom made chamber in conjunction with a commercially available ozone generator (Ozonia TOGC2–100201). Functionalisation was achieved by ozone flow for 1 hour under 50 mbar pressure and a sample temperature of 200^{o}C. Upon completion of the process, samples were cooled down under ozone flow.

5.2.4 Primary cell lines

hADSC and cartilage derived progenitor lines were used in these two dimensional experiments. They are demonstrated in table 5.1.

Table 5.1: Cell lines and cell types used in experiments in this chapter.

Cell lines				
Cell line	Cell type	Passage	Patient condition	Experiment
hADSC	H20	P6	Parry-Romberg syndrome	Viability assay
hADSC	H20	P7	Parry–Romberg syndrome	2D chondrogenic differentiation study
CSPC	CH105	P6	'Bat'-ears (normal ear cartilage)	2D 3–lineage differentiation study

5.2.5 Cell expansion

The hADSCs were expanded in monolayers using the Gibco ^{TM} Dubecco's Modified Eagle Medium (DMEM), a proliferation medium supplied by LifeTechnologies^{TM}. The cells were expanded in monolayers on tissue culture polystyrene (TCPS), in T175 Corning cell culture flasks (Sigma–Aldrich). The cells were incubated at 37^{o}C at 5% CO_2 concentration in an incubator. The cells were passaged upon reaching no more than 80% confluence in order to avoid loss of pluripotency. Upon passaging, the old proliferation medium was discarded and the cells were washed three times using Phosphate– Buffered Saline (PBS) (LifeTechnologies). In order to detach the cells from the flasks, cells were treated with 0.05% Trypsin/ 1 mM EDTA and were subsequently incubated at 37^{o}C for 5 minutes. The cells were then gently shaken and detachment was examined under a light microscope. The action of trypsin was blocked by adding proliferation media back to the cell culture flask, as the proliferation medium contains serum, which acts as a blocker for trypsin. Moreover, the cell containing medium was then transferred in a falcon tube and were spun at 500g. The resulting cell pellet was suspended in 1 ml of fresh proliferation medium and was distributed in new T175 Corning cell culture flasks, which contained 25 ml of fresh medium, in equal volumes. The flasks were then gently shaken to ensure equal distribution of the cells on the TCPS surface and were then

placed in an incubator.

5.2.6 Cell cryoconservation

In order to be preserved for longer periods of time, cells that had reached around 80% confluency were expanded with the method described in the section above, and were removed from the cell culture flask. After trypsin deactivation, 20 μl of the cells were loaded on a Cell Counting Slide for TC10™/TC20™ Cell Counter, Dual–Chamber (BioRad) and were optically counted using a TC20™ Automated Cell Counter (BioRad). Once the count was established, the remaining cells were spun at 500g. They were then suspended in 1 ml of dimethyl sulfoxide (DMSO) and Fetal Bovine Serum, Embryonic Stem Cell quality (ES–FBS, Gibco^{TM}, LifeTechnologies) at a concentration of 10% v/v and 90% v/v respectively and were transferred in a Mr Frosty^{TM} Cryoconservation container (ThermoFisher), in order to ensure 1^{o}C/ minute drop in temperature, and were placed in a –80^{o}C freezer for 2 days. The vials were later transferred in liquid nitrogen storage at –150^{o}C.

5.2.7 Cell differentiation

The 2D diamond substrates were placed in 48–well tissue culture plates with flat bottoms (Corning), with diameter of 11 mm and volume of 1.6 ml.

Cells were plated on all substrates at a density of 5×10^4/cm^2 and were incubated at 37^{o}C under 5% CO_2 until they reached 100% confluence on the samples. They were cultured using Dubecco's Modified Eagle Medium (DMEM–GlutaMAX), high glucose, Glutamax (ThermoFisher Scientific). The medium was enriched with 10% embryonic stem cell–certified fetal bovine serum (ES–FBS) (Merck Millipore) and 1% penicillin–streptomycin antibiotic (Gibco Life Technologies). Medium was changed every 3 days.

Upon reaching confuence, the DMEM–GlutaMAX medium was replaced with the differentiation media described in tables 5.2, 5.3 and 5.4. Each well received

400 μl of differentiated media. The media was replaced every 2 days. The cells were incubated in differentiation media for 21 days.

5.2.8 Cell differentiation media

For both the hADCS and CSPC differentiation assays, the following differentiation media recipes were followed. The recipes are demonstrated in tables 5.2, 5.3 and 5.4

Table 5.2: Factors and concentrations of components of chondrogenic differentiation media

Factor	**Concentration**
DMEM–GlutaMAX	87.5%
Dexamethasone	0.1 μm
Transforming growth factor (TGF β–1)	10 ng/ ml
Insulin–transferin selenium (ITS)	100×
Ascorbate–2–phosphate	50 μm
ES–FBS	10%
Pen–Strep	1%

Table 5.3: Factors and concentrations of components of osteogenic differentiation media

Factor	**Concentration**
DMEM–GlutaMAX	87.5%
Dexamethasone	0.1 μm
β – glycerolphosphate	10 mM
Ascorbate–2–phosphate	100 μm
ES–FBS	10%
Pen–Strep	1%

Table 5.4: Factors and concentrations of components of osteogenic differentiation media

Factor	**Concentration**
DMEM–GlutaMAX	87.5%
Dexamethasone	1 μ m
IBMX	500 μM
Rosiglitazone	1 μM
Insulin	10nm/ml
ES–FBS	10%
Pen–Strep	1%

5.2.9 Cell fixation post differentiation

After 21 days of incubation in differentiation media, the differentiation medium was removed from all wells. Cells were then incubated in 4% paraformaldehyde (PFA) at room temperature for 15 minutes. After this time period, PFA was removed and the cells were washed 3× using DPBS (Thermo Scientific). During each wash, the cells stayed in DPBS for 10 minutes.

Upon removal of the last round of DPBS, cells were subjected to colourometric assays.

5.2.10 Methylene blue assay

For this colorometric assay, the methylene blue solution was prepared by mixing 1% methylene blue powder with 0.01M borate buffer (pH 8.5). Cells were incubated with For this colorometric assay, upon washing with PBS, the cells were incubated with 400 μm/well of methylene blue solution at room temperature for 30 minutes. After incubation, the dye was removed and residual methylene blue solution was removed using 0.01M borate buffer. After the washing step, samples were transferred into a new well plate. A mixture of 1:1 (v/v) ethanol and 0.1 M HCl was used in order to extract the methylene blue dye. Upon gentle shaking in order to mix the dye with the solution, 100 μl of solution from each well were transferred to a new well in a 96 well plate. The subsequent extracted dye was measured for its absorbance at 650 nm by a spectrophotometer (Revelation v4.21 Dynex Technologies, inc). The absorbance measurements were then normalized to the surface area of the samples.

5.2.11 Alcian blue assay

The Alcian blue solution was prepared by mixing 1% Alcian Blue 8GX powder (BDH, Crawley, UK) in 0.1 HCl. Cells were incubated with 400 μl/well of Alcian blue stain for 24 hours. The Alcian blue dye was then extracted using Guanidine–HCl 6M. The plates was placed on a shaking platform and were incubated overnight

at room temperature. Before use, aliquots of Alcian Blue 1% solution were filtered using Whatman filtering paper (Thermos Scientific) in order to exclude powder residue. The subsequent extracted dye was measured for its absorbance using a plate reader at OD 595 nm.

5.2.12 Alizarin red assay

The Alizarin red solution was prepared by mixing 1% of Alizarin Red powder (Sigma–Aldrich) in dH_2O. The pH was adjusted to 4.1–4.3 using 0.5 % ammonium hydroxide. The final solution was stored at room temperature away from sunlight. Before use, aliquots of Alizarin red 1% solution were filtered using Whatman filtering paper (Thermos Scientific) in order to exclude powder residue.

5.2.13 Cell brightfield imaging

The Olympus IX71 microscope (Carl Zeiss, Jena, Germany) equipped with a Hamamatsu ORCA–ER digital camera (Hamamatsu Corp., Bridgewater, NJ) was used in order to image the cells grown on borosilicate glass, O–ND, glass and on plastic. The CSPCs were stained with Alcian Blue, Alizarin red. CSPCs differentiated into adipogenic fate were also imaged after fixation. The hADSCs were imaged prior to staining with Alcian Blue, but post–fixation. Fiji software was used for image processing.

5.2.14 Cell stereomicroscopy imaging

The Alcian blue and Alizarin red–stained CSPCs were imaged before dye extraction using a Leica M205 FA fluorescence stereomicroscope.

5.2.15 Pixel intensity measurement

The whole images were considered as regions of interest (RoI) measured in ImageJ. Arbitrary units were used on a scale of 0 to 4096 for intensity. The image values were inverted to account for lower pixel intensity correlating with higher degree of staining. Measurement values were combined into distributions based on

each substrate treatment.

5.2.16 Statistical analysis

Each distribution was tested by ANOVA variance for statistical difference between other tested distributions with different conditions. Post–Hoc Tukey's HSD test was used to determine significant difference between individual distributions.

5.3 Results

5.3.1 Viability assay of hADSC of 2D functionalised ND substrates

In order to understand better the viability of hADSCs on the substrate, we performed a staining assay using methylene blue dye. The amount of dye absorbance determines the viability of the cell population on the 2D substrate with higher absorbance indicating lower viability. We cultured hADSCs for a week, and used the assay in order to determine the cell count under each condition. Cell count is related to absorbance, with higher absorbance linked to higher cell count. The results are demonstrated in the figure below.

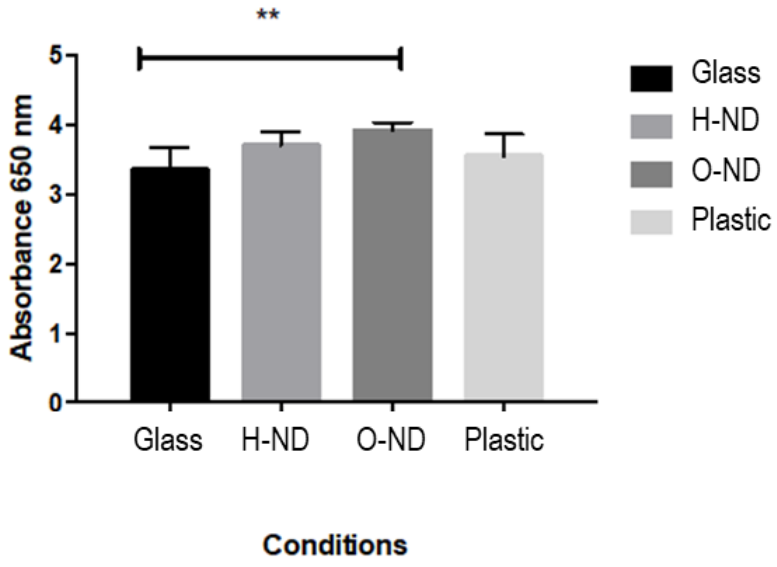

Figure 5.1: Absorbance of methylene blue at 650 nm extracted from cells stained after a week of incubation on four different substrates. Statistical difference tested with Anova variance and Post–Hoc Tukey HSD test ($p<0.01$)

hADSCs were incubated on 4 different substrates for one week. The results in the figure 5.1 demonstrated small, but statistically significant increase ($p<0.01$) in methylene blue absorbance for the cells cultured on the O–ND surface when com-

pared with the cells grown on glass. This result indicates that the a greater number of hADSCs adhered strongly to the O-ND substrate compared to the glass substrate. hADSCs viability was not statistically different when O–ND surface coated material was compared with tissue culture plastic (TCPS), which is the standard surface in 2D hADSC culture.

Overall, the results suggest that not only both H–ND and O–ND coated surfaces can support viable tissue hADSC culture, but also that there is potentially increased cell proliferation on O-NDs compared to the other substrates, including TCPS which is the most commonly used material in 2D tissue culture. This result could be further explored and potentially quantified using high throughput screening assays. For example, a label free assay utilising xCELLigence real-time cell analysis could quantify cell adhesion [266], [267].

5.3.2 Differentiation of hADSCs on 2D functionalised ND substrates

Once the hADSC cell viability was tested we observed cell differentiation on different 2D surfaces and substrates. hADSCs were previously shown to provide a cell source for differentiation into cartilage tissue, however they do not tend to show as high expression of GAGs as CSPCs in Alcian Blue assays..

The hADSCs were exposed to 4 different 2D surface test conditions, TCPS (plastic), borosilicate glass or O–ND and H–ND coated borosilicate glass. In addition differentiation medium was used, creating two different tested populations, one with and one without an established differentiation trigger.

After 21 days, qualititative and quantitative markers of hADSC differentiation on the 2D surface were observed.

In figure 5.2 qualitative observation of hADSC after 21 days on different 2D surfaces can be seen. From the images it is clear that cell differentiation is taking place on the surfaces that were submerged in differentiation medium. From the images it is not clear whether O–ND or H–ND coating increase cell differentiation and further quantitative measurements of differentiation markers were used.

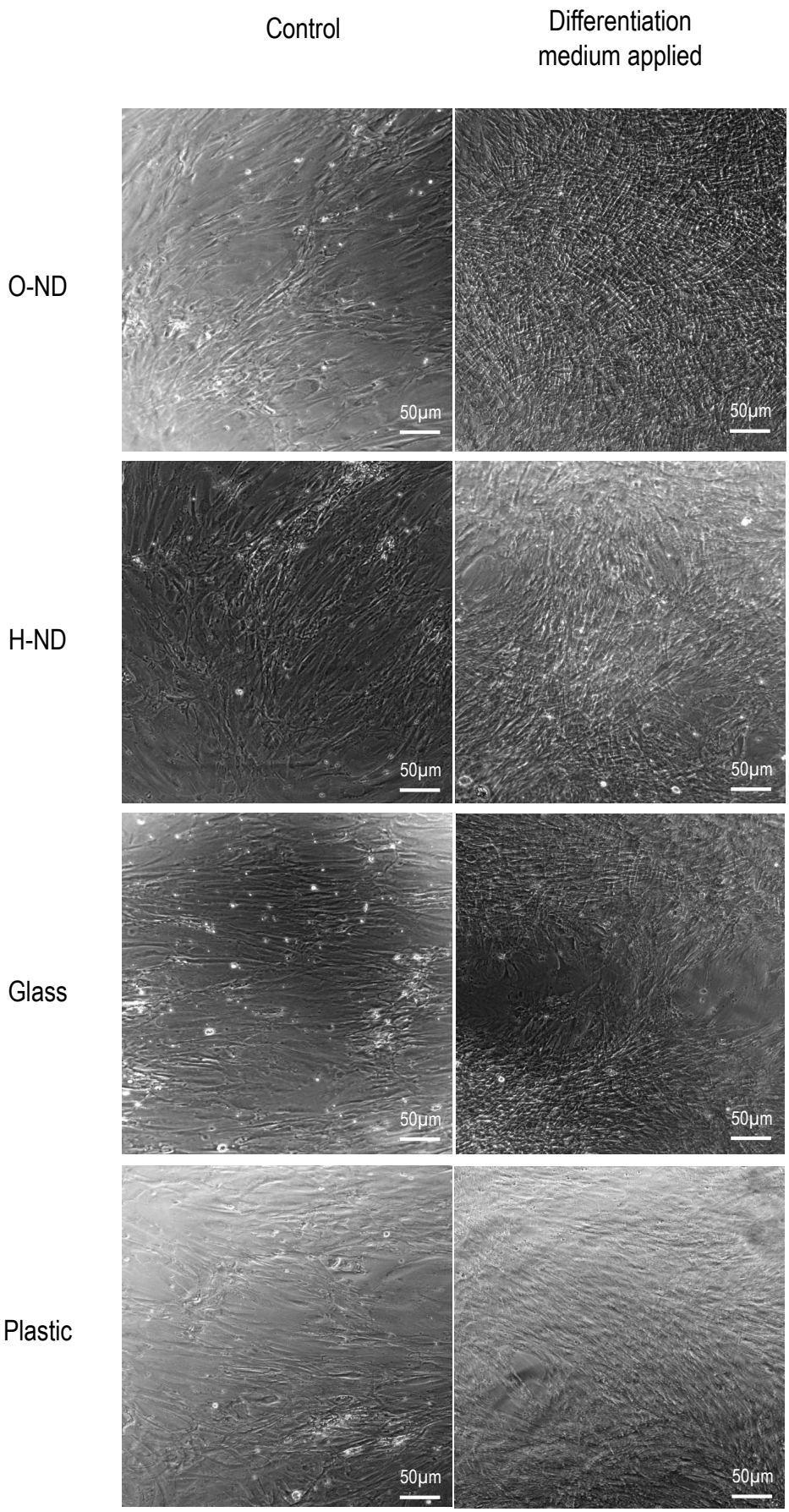

Figure 5.2: hADSC cell differentiation on 4 different surfaces with or without differentiation medium added. Increased cell density is observed in all samples treated with differentiation media, indicating hADSC hypertrophy. Scale bar = 50 μm.

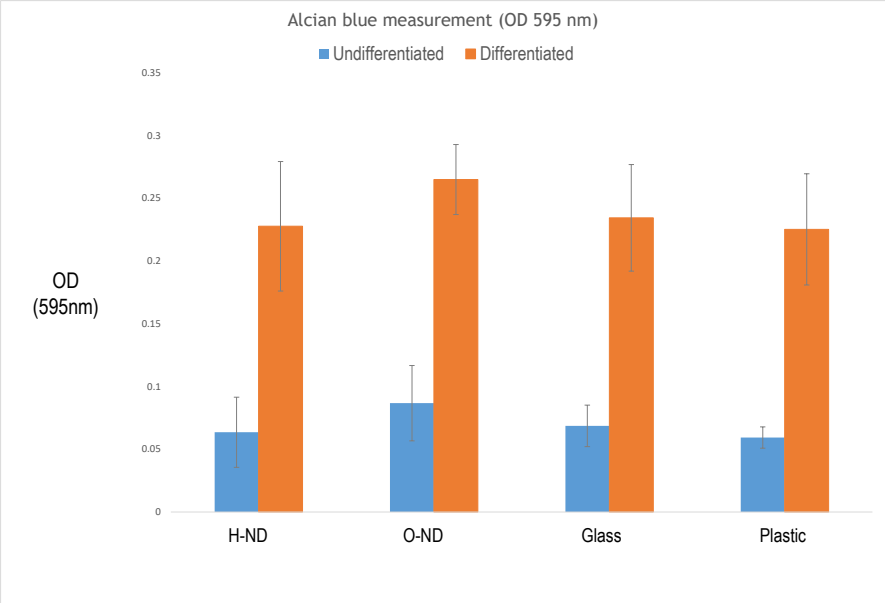

Figure 5.3: Absorbance of Alcian blue extracted from chondrogenically differentiated hADSCs after 21 days of differentiation in identical media, on four different substrates (TCPS, borosilicate glass H–NDs and O–NDs - both seeded in borosilicate glass. Statistical difference tested with Anova variance and Post–Hoc Tukey HSD test ($p<0.05$)

In the figure 5.3 we can observe results of Alcian blue stain absorbance. Increased levels of Alcian blue absorbance indicate increased levels of dye binding to the proteoglycan GAG, that points towards increased levels of chondrogenic differentiation. Alcian blue staining was used to compare the levels of glycosaminoglycan (GAG) expression for hADSCs grown across 4 different substrates both with and without differentiation media. GAGs are components of cartilage extracellular matrix (ECM) and as such can indicate the chondrogenic hADSC differentiation. The cells were grown on 4 different types of substrates (from left to right): On borosilicate glass coverslips covered with hydrogen–functionalised NDs, on borosilicate glass coverslips covered with oxygen–functionalised NDs, on plain, degreased borosilicate glass and directly on the plastic of the wells in a 48–well plate. Within the figure 5.3 the orange columns indicate GAG levels in hADSCs exposed to differentiation medium and the blue columns indicate GAG levels in hADSCs not exposed to differentiation medium. The data were compared separately for the differentiation and non-differentiation group.

Differentiated cells: None of the surfaces and surface treatments have shown to induce statistically significant difference of the GAG levels in hADSCs. However hADSCs differentiated on O–ND–seeded coverslips contained incrementally highest levels of GAG expression. Furthermore, the variability of the GAG expression in the hADSCs on the O–ND–seeded coverslips is the smallest in comparison to cells differentiated under different conditions as indicated by the smallest error bars. This points towards a more uniform cell fate and higher levels of chondrogenic differentiation.

Undifferentiated cells: Alcian blue binding on undifferentiated hADSCs on different surfaces was also observed, albeit in much lower levels compared to the differentiated hADSCs. No statistically significant difference in Alcian blue staining was observed among the cells on four tested substrates and surfaces. However as with the cells exposed to differentiation medium, the highest GAG expression was found in cells on O–ND–seeded coverslips. It is possible that the slight increase in GAG expression can be due to the spontaneous differentiation of hADSCs into chondrocytes.

5.3.3 Differentiation of cartilage stem-progenitor cells on 2D functionalised ND substrates

5.3.3.1 Chondrogenic differentiation

While hADSCs are easier to source in the clinical setting, CSPCs demonstrate greater chondrogenic potency, while still maintaining the ability of tri-lineage differentiation. Because of this, for the purposes of evaluating cell differentiation with different functionalised nanodiamond and other surfaces, CSPCs can provide a stronger differentiation outcome and may be preferable to hADSCs for this proof of concept.

Therefore cartilage stem-precursor cells were also incubated in 2D on borosilicate glass coverslips seeded with O–NDs, H–NDs, as well as plain borosilicate glass coverslips and TCPS (plastic) for 21 days. Similarly to hADSC, two different population groups were tested, one with and one without being submerged in the chondrogenic differentiation media. As with hADSCs, both qualitative and quantitative differentiation observations were taken.

In figure 5.4, bright field images of the fixed and stained differentiated CSPCs are shown. It is clear that the differentiation medium has induced CSPC differentiation and the cells are exhibiting the chondrocyte phenotype. On the undifferentiated panel, the cells have mostly retained their precursor cell morphology. From this qualitative observation it is not possible to conclude whether any of the 4 different surfaces tested had any effect on cell differentiation and quantitative markers of cell differentiation were used.

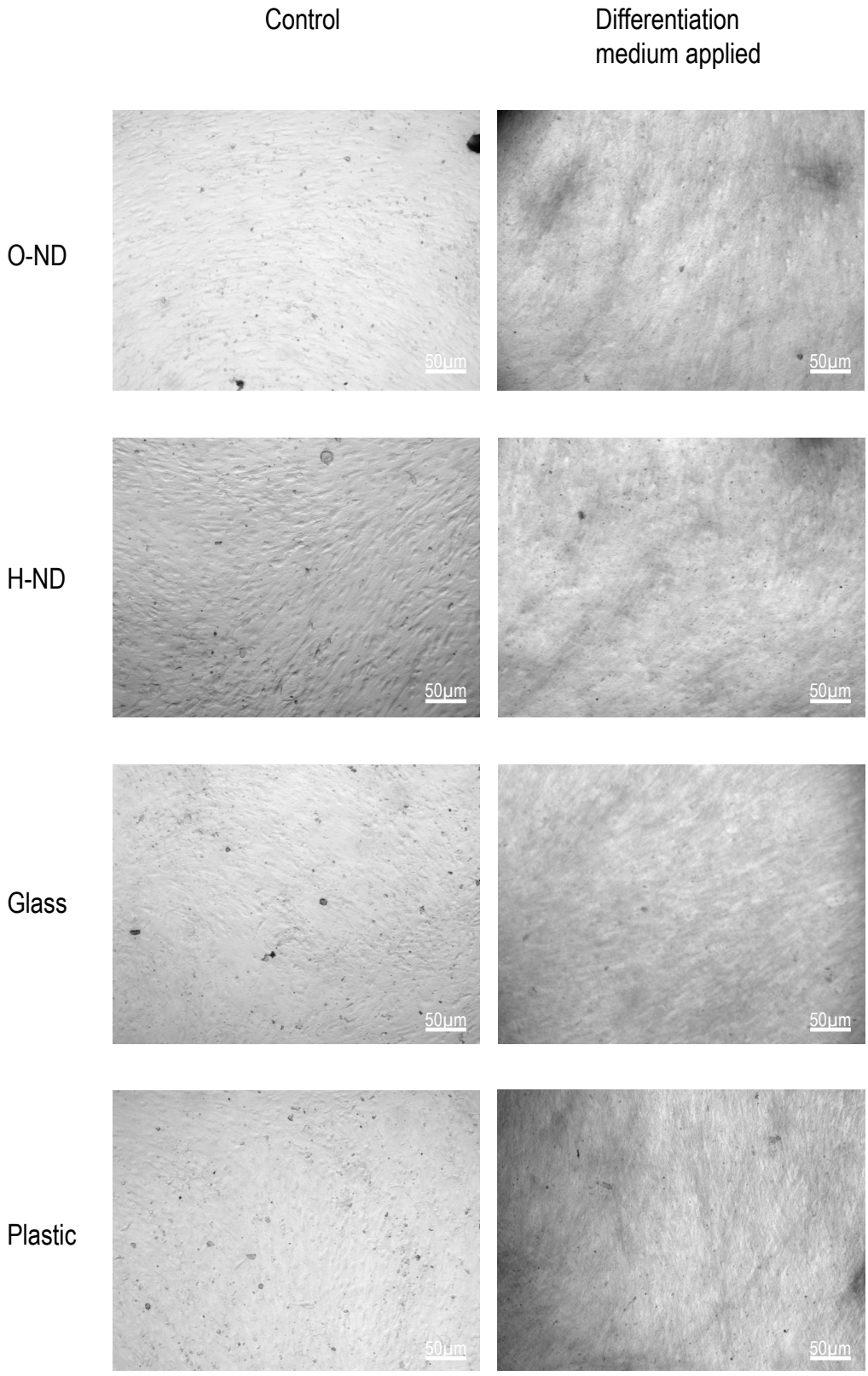

Figure 5.4: Brightfield images of CSPCs. CSPC differentiation on 4 different surfaces with or without differentiation medium added. Increased cell density is observed in all samples treated with differentiation media, indicating cell hypertrophy. Scale bar = 50 μm.

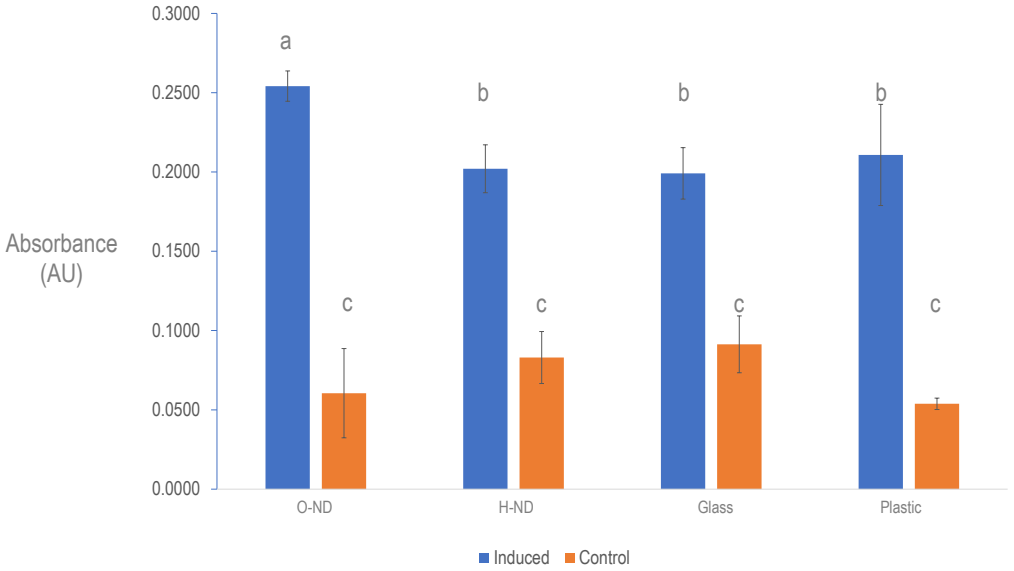

Figure 5.5: Absorbance of Alcian blue extracted from chondrogenically differentiated cartilage stem-precursor cells after 21 days of differentiation in identical media, on four different substrates. Number of replicates n=6. Statistical difference tested with Anova variance and Post–Hoc Tukey HSD test (p<0.05). *a* denotes statistical difference among induced samples. *b* denotes induced samples and *c* denotes control samples with no significant statistical difference among them.

To observe differentiation markers quantitatively, GAG expression was measured with the absorbance of Alcian blue stain, in the same manner as with hADSCs. Since GAG expression is a well known marker of differentiation, differences in Alcian blue absorbance can provide clues on the differentiation potency of the CSPCs grown on the nanodiamond coated and plain surfaces.

In figure 5.5 it can be observed that CSPCs submerged in the differentiation media, grown on O–ND coated borosilicate glass demonstrate a significant increase in chondrogenic differentiation rate in comparison to those grown on glass alone or all the other tested surfaces.

CSPCs that were not submerged in the differentiation medium had significantly decreased Alcian blue absorbance in comparison to CSPCs that did have the differentiation medium treatment. This result indicates lower binding of the Alcian blue stain on the cells, correlating to lower expression of GAGs and therefore decreased differentiation activity. This is expected, as differentiation medium, drastically increases the GAG expression and the same result has been observed in hADSCs as

well.

Lastly, differences in Alcian blue absorbance between CSPCs grown on the four different surfaces, but untreated with differentiation medium are not statistically significant.

The results indicate that while O–ND and H–ND coating alone is not sufficient to trigger GAG expression and CSPC differentiation, in combination with differentiation medium, O–ND coating increases CSPC differentiation.

5.3.3.2 Osteogenic differentiation

To further explore the differentiation potential of CSPCs on 2D functionalised surfaces, validation of tri-lineage differentiation was performed for the CSPCs. In particular, the aim was to characterise any positive or negative effects H–NDs and O–NDs may have on CSPCs tri-lineage differentiation.

For this purpose, on top of the chondrogenic differentiation, in this experiment osteogenic differentiation was tested.

In this experiment, cells grown on 2D surfaces consisting of borosilicate glass, TCPS (plastic), or H–ND or O–ND coated glass were attempted to be differentiated into osteogenic lineage. The cells were incubated in osteogenic media for 21 days to induce differentiation.

In figure 5.6 a qualitative observation of the CSPC osteogenic differentiation after 3 weeks can be seen. The osteogenically differentiated cells started demonstrating condensation. For the cells exposed to H–NDs and O–NDs, the cell monolayer started becoming topically denser, peeling off and concentrating at the edges of the well, visibly different to the TCPS and glass surface monoloyer. Cells cultured on glass and TCPS formed differentiating cell monolayers on the surface.

This initial qualitative data indicates that both H–ND and O–ND coated surfaces are visibly influencing CSPCs osteogenic differentiation, not observed in the case of glass and plastic surfaces alone.

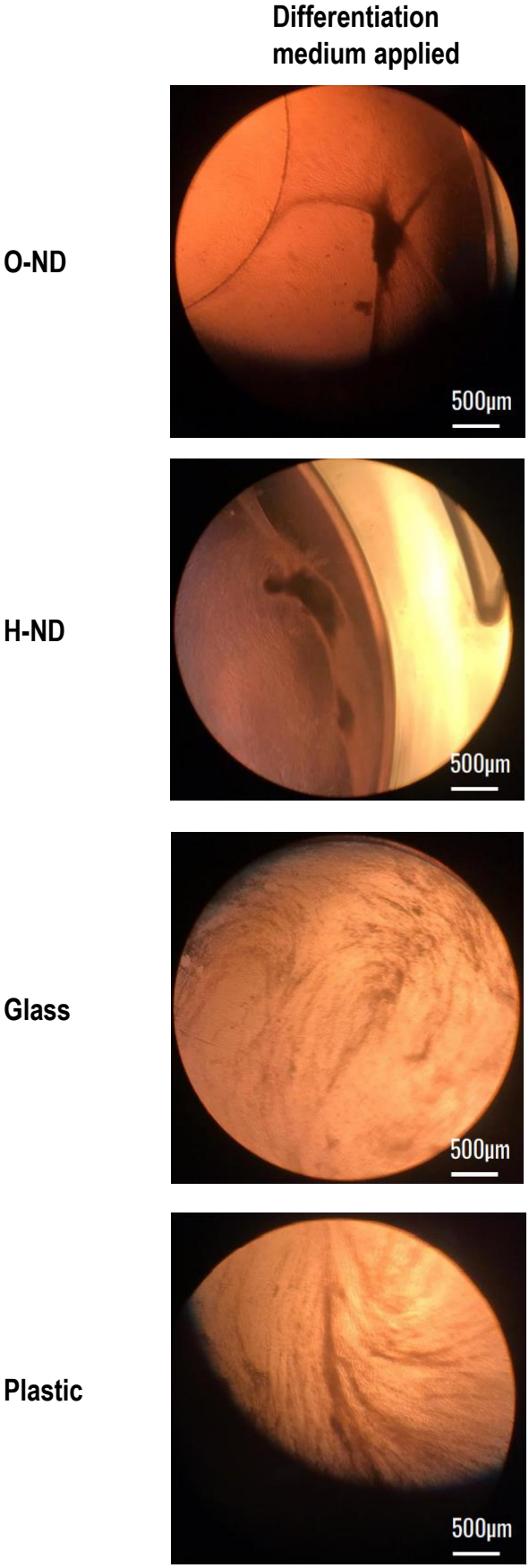

Figure 5.6: Macroscopic images of tissue formations of cells undergoing osteogenic differentiation on day 21. Cells were live and in their differentiation media when these images were taken. Scale bar = 50 μm

CSPC cells undergoing osteogenic differentiation create calcium deposits, which are a clear marker for cell differentiation. For observation of calcium deposits in the cell monolayers, the samples were stained with 1% v/v Alizarin red dye.

In order to investigate the effect of direct contact of cells with the substrate, the stain strength of Alizarin red from the cells that were directly in contact with the coverslips was measured. These results can be seen in figures 5.7 and 5.8. In figure 5.7 the accumulation of calcium deposits can be qualitatively assessed. The increased accumulation of calcium could be observed with darker colouring of the mass on the substrate. However, qualitatively it is difficult to draw conclusions from the cells differentiated on the four substrates. Quantitative measurement was needed.

In figure 5.8 the results of quantitative measurement of Alizarin red stain reporting calcium deposit level can be seen. Cells in osteogenic differentiation medium on all surfaces have shown a statistically significant increase in calcium deposits in comparison to cells not exposed to differentiation medium.

More importantly, out of the cells in the differentiation medium, CSPCs grown on H–ND coated surface demonstrated a statistically significant 34% increase in calcium deposits. Interestingly CSPCs grown on O–ND coated surface did not display higher levels of calcium, even though phenotypically in figure 5.6 they both show similar differentiation pattern.

Overall these results show that the H–ND coated surface stimulated calcium deposits in CSPCs during osteogenic differentiation. In addition both the H–ND and O–ND coated surfaces resulted in visibly more differentiated cell mass.

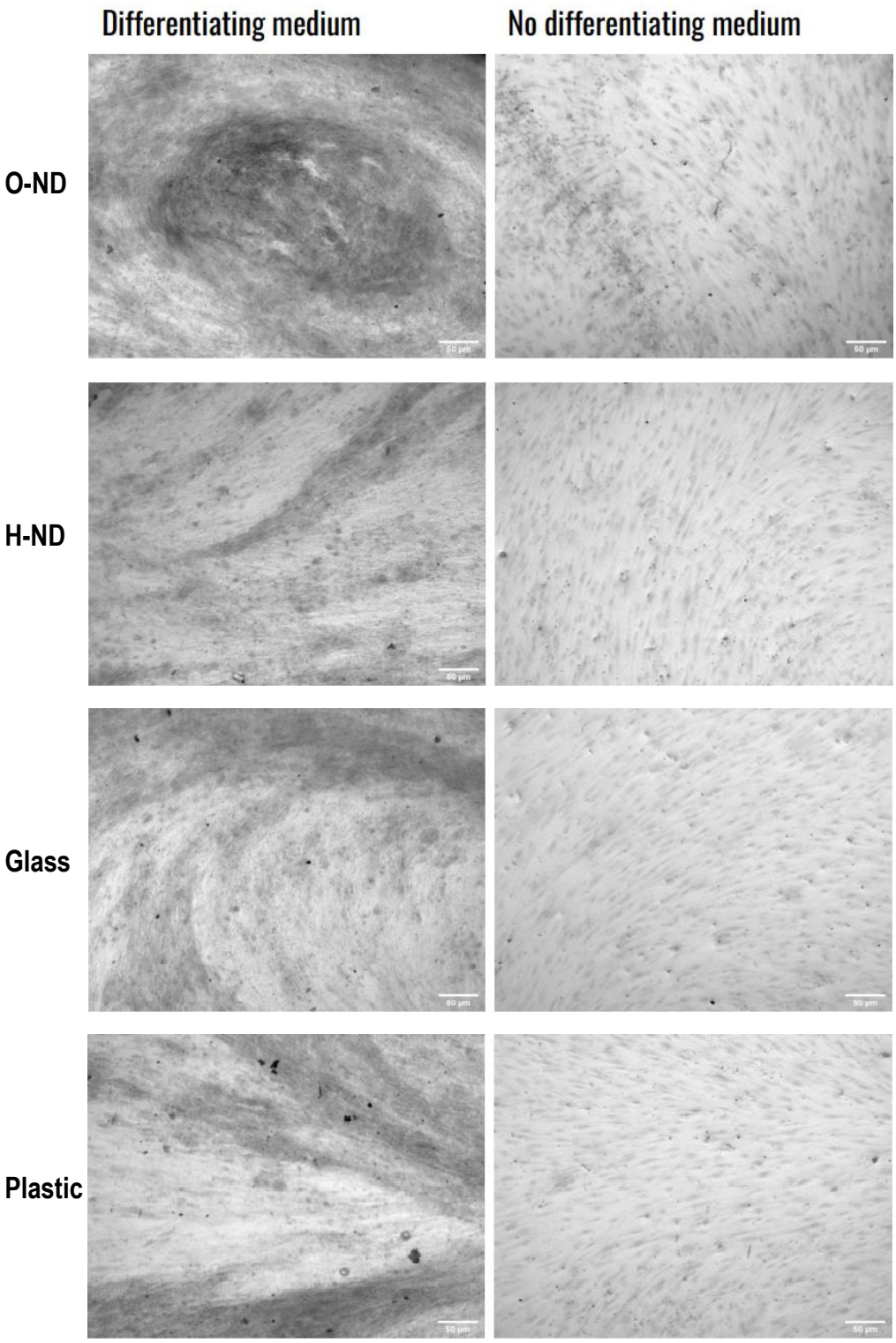

Figure 5.7: Brightfield microscopy images of CSPCs that have undergone osteogenic differentiation. On the left panel there are cells that have been treated with osteogenic differentiation medium for 21 days. The darker regions indicate calcium deposits stained with Alizarin red. On the right panel are cells that have been treated with regular DMEM–GlutaMAX medium. Scale bar $= 50\ \mu$m

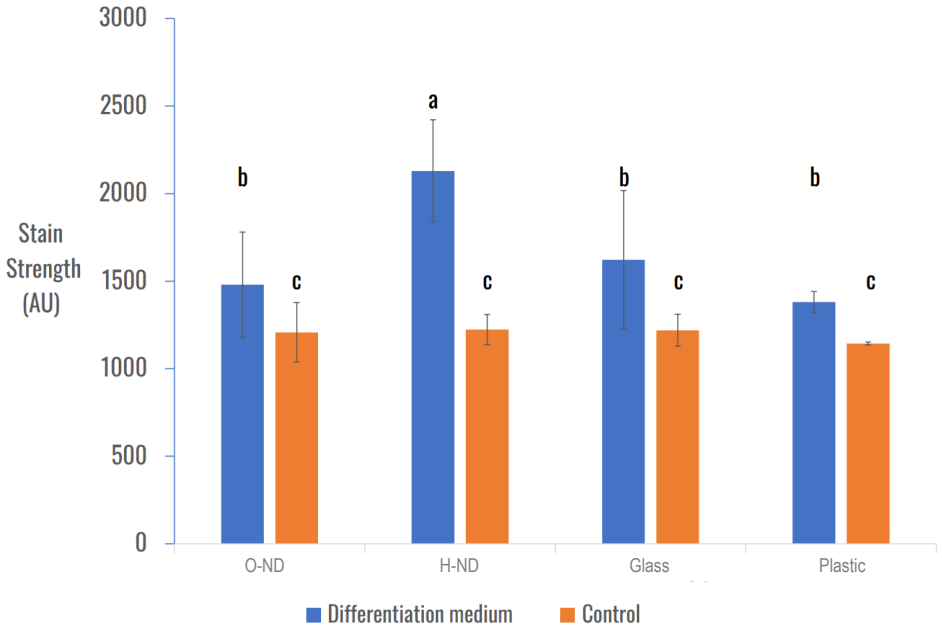

Figure 5.8: Figure shows osteocyte differentiation on different substrates as a function of calcium deposits as indicated by 1% v/v Alizarin stain strength as a measure of pixel intensity. Measured in Fiji ([5]) (n=4). Statistical difference tested with Anova variance and Post–Hoc Tukey HSD test (n<0.05). *a* denotes statistical difference among induced samples. *b* denotes induced samples and *c* denotes control samples with no significant statistical difference among them.

Additionally it was observed that cell growth and differentiation were not limited directly to the surface that was being tested, but CSPCs also started to grow on the adjacent plastic wall surrounding the tested surface. Since these cells weren't in direct contact with the surface, we wanted to observe whether the H–ND coated surface contact is necessary for the higher levels of calcium deposits or whether this phenomenon translates across the whole cell mass, even to cells growing on adjacent plastic.

Similarly to the previous observation, Alizarin red dye was used to report the level of calcium in differentiating CSPCs. In figure 5.9 the amount of calcium levels can be qualitatively assessed. Since the differences in calcium accumulation in cells across the four surfaces could not be resolved visually, quantitative measurement was used.

In figure 5.10, a very similar pattern to figure 5.8 can be observed. Cells grown

in differentiation medium have statistically significant increase in calcium deposits compared to cells without differentiation medium. Interestingly CSPCs grown in differentiation medium adjacent to H–ND coated surface shown statistically significant 30% increase in calcium deposits in comparison to all other tested surfaces.

This data provide evidence that the differentiating CSPCs do not have to be in direct contact with nanodiamond surface to show higher calcium deposits. Being part of the same growing cell mass suffices to increase a hallmark signal of osteogenic differentiation.

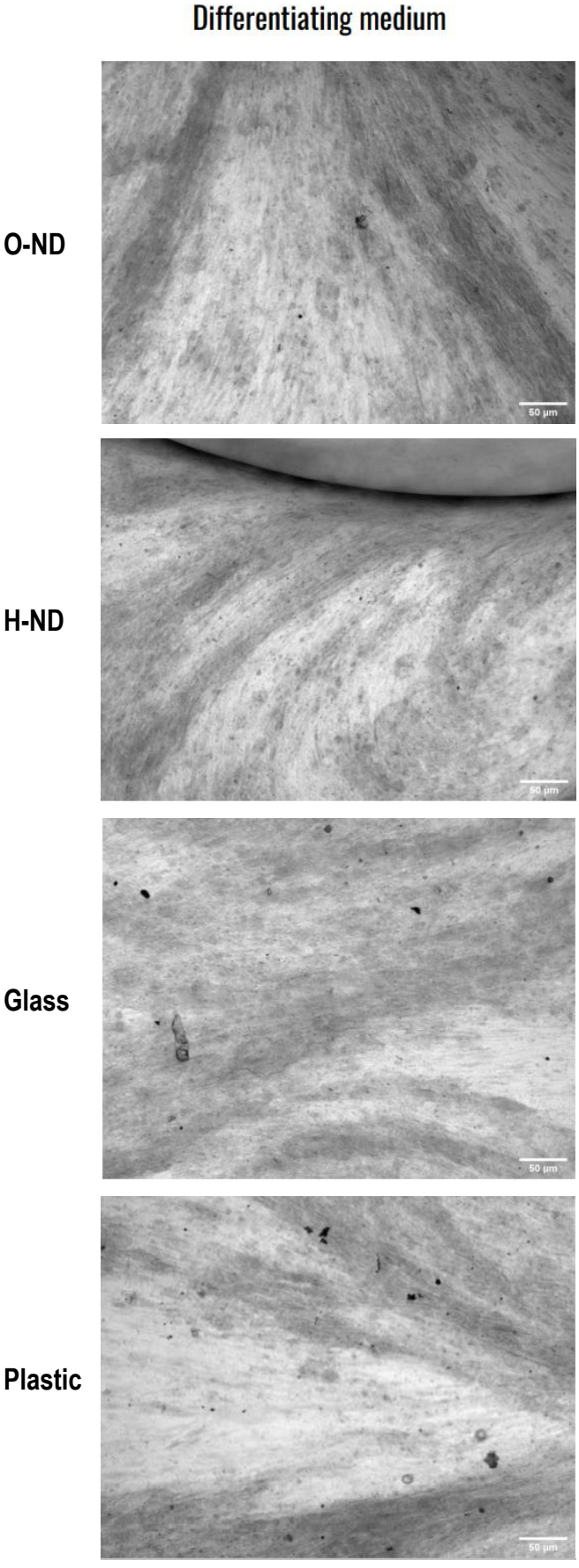

Figure 5.9: Brightfield microscopy images of CH105 cartilage progenitor cells that have undergone osteogenic differentiation. Cells have been treated with osteogenic differentiation medium for 21 days, were fixed with 4% and were subsequently stained with 1% Alizarin Red solution. The darker regions indicate calcium deposits. These are cells grown on plastic that was part of the wells with coverslips in them. Scale bar = 50 μm

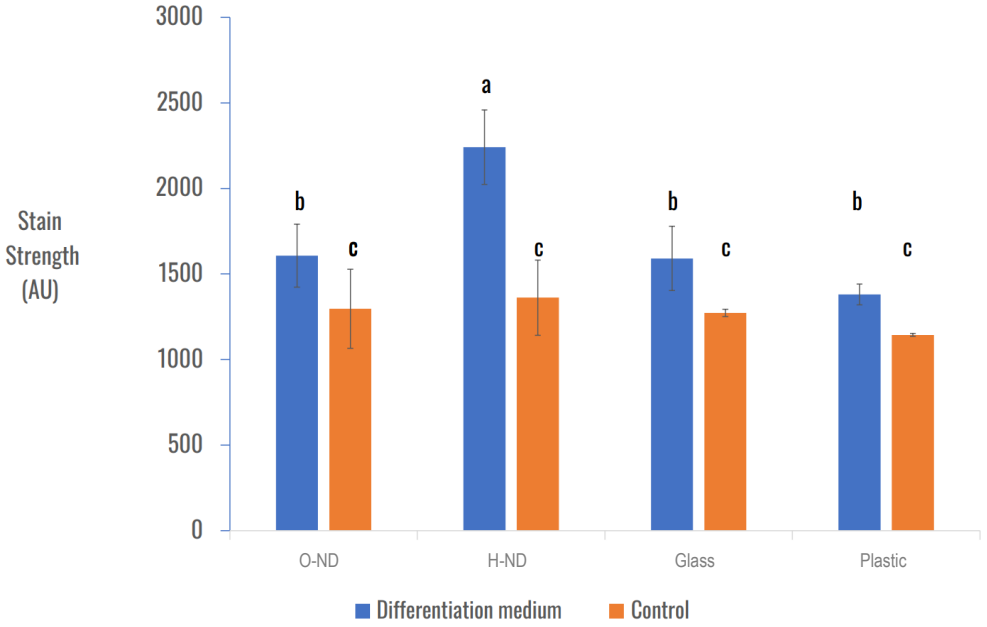

Figure 5.10: Osteocyte differentiation on plastic which was in contact with different diamond and non–diamond substrates, as a function of calcium deposits as indicated by 1% v/v Alizarin stain strength as a measure of pixel intensity. Measured in Fiji ([5]) (n=4). Statistical difference tested with Anova variance and Post–Hoc Tukey HSD test (p<0.05). *a* denotes statistical difference among induced samples. *b* denotes induced samples and *c* denotes control samples with no significant statistical difference among them.

5.3.4 Adipogenic differentiation

To complete the testing of CSPC differentiation on different 2D surfaces and fully explore the tri-lineage differentiation, CSPCs were also tested for adipogenic differentiation.

As previously, four surfaces were tested for 2D monolayer cell growth, borosilicate glass, TCPS (plastic) and O–ND and H–ND coated glass. CSPCs were subjected to adipogenic differentiation medium for a period of 21 days after which the level of cell differentiation was observed.

In figure 5.11 the effect of different surfaces on CSPC adipogenic differentiation can be seen. The tell-tale qualitative sign of adipogenic differentiation is formation of dark coloured fat droplets. It can be seen that cells on plastic and glass accumulate a certain baseline level of fat droplets. CSPCs differentiating on H–ND and O–ND coated surfaces also displayed fat droplets indicating adipogenic differentiation, clearly visible under microscope. This level of differentiation was strong enough to deem quantitative measurement redundant.

Overall it can be observed that both O–ND and H–ND nanodiamonds do not inhibit CSPC adipogenic differentiation.

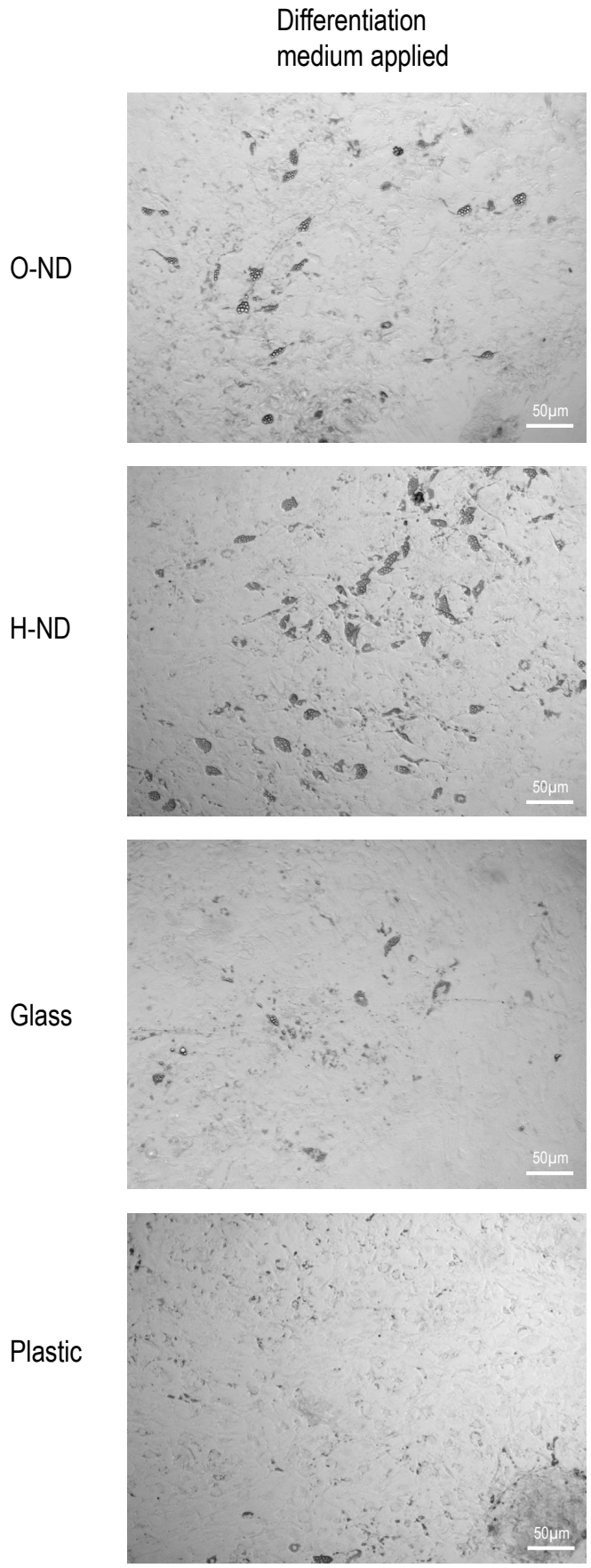

Figure 5.11: Brightfield microscopy images of cartilage precursor cells differentiated into adipocytes, while incubated on four different substrates. Fat droplets are evident in all 4 different conditions indicate successful differentiation.

5.4 Discussion

As an overall conclusion of this chapter, cells grown on oxygen–terminated NDs have shown an aptitude towards chondrogenic differentiation. Even though statistically significant increase was observed only for the cartilage stem precursor cells on the O–ND surface undergoing chondrogenic differentiation, modest increase in chondrogenic differentiation was also seen for hADSCs on oxygen–terminated NDs. Overall it was shown that both hADSCs and CSPCs prefer the O–ND substrate compared to other substrates, including macroscopic diamond surfaces terminated with oxygen.

This can be attributed to a number of reasons. O–NDs have been shown to make for surfaces of higher hydrophilicity, compared to H–ND substrates ([143], [268]).

The effect of O–NDs has been mainly studied on cells that are directed towards neuronal fate and less so on skeletal tissue stem cells [143], [269], [270], despite the fact that biocompatibility has been with cells of osteocyte origin ([222]).

The differences observed among O-–ND and H–ND coated surfaces and the other substrates, indicates that there are differences in the interaction between cellular proteins and the functional groups of the NDs. H– and O-NDs have positive and negative surface charges, respectively ([271]). It has been shown that chondrogenesis is upregulated in 2D hydrophilic environments, which is in line with results presented in this chapter [272].

Cell adhesion is one of the most important aspects of the differentiation initiation and has been shown to play a crucial part in embryogenesis ([273]). Cell adhesion is important in clinical procedures such as bone transplants in order to promote cell integration and cell progenitor differentiation ([274]). It can be speculated that cell adhesion is being facilitated by O–NDs and that can help chondrogenic differentiation. It is interesting to note that O–NDs had a similar effect on both hADSC and cartilage-progenitor cells, indicating that O–NDs are not only positive towards the progenitor-type cells, but also have an active effect towards this chondrogenic

differentiation.

A fact that should seriously be considered is the effect of hydrogen–terminated NDs on osteogenic differentiation. As seen in figure 5.6, H–NDs promote osteogenic differentiation. However, it has been shown that osteocyte cell lines prefer O–NDs over H–NDs for their proliferation [202] when grown on H– and O– functionalised NCDs. Experiments on osteogenic differentiation of Sarcoma-osteogenic (Saos-2) cells on H– and O–terminated NCD have indicated that osteogenic differentiation of these cells on O–terminated NCD surfaces were significantly higher compared to their H–ND counterparts [199]. However, both of these experiments were conducted on NCD with different cell types. This result prompts further investigation in the differentiation of hADSCs and CSPCs on H– and O–NDs and direct comparison between cells grown on functionalised NCD versus NDs is required.

5.5 Conclusions

In this chapter it has been demonstrated that different types of nanodiamond functionalisation can have different positive effects on the same cell line that has been guided to different differentiation paths.

Multiple factors such as adhesion and hydophilicity may play a part. O–NDs are shown to be favoured by cells guided towards chondrogenic fate, whereas osteogenic differentiation has been promoted by H–NDs. Adhesion of different cell types on O- and H-terminated ND substrates can be further characterised by means of AFM, as demonstrated by Rezek et. al [202], [275]. AFM can be utilised in order to quantify the elastic modulus of cells adhering to the substrates, as well as adhesion between AFM tip and sample.

Future work needs to validate the effects of NDs on the gene expression during the early stages of differentiation. This can be achieved by mRNA extraction and qRT–PCR examination of key gene markers for all types of tri–lineage differentiation.

Chapter 6

3-dimensional diamond–fibrin scaffolds for skeletal tissue engineering

6.1 Introduction

The ultimate goal of tissue engineering is to create 3–dimensional scaffolds, that can sustain cell differentiation and proliferation and produce a functional tissue. Such scaffolds should be able to not only sustain the cells mechanically and chemically, but to also be compatible with the patient and be able to degrade at a rate similar to that of the tissue generation.

Carbon-based materials have long been preferred in skeletal tissue regeneration. For example, diamond-like carbon (DLC) coatings have been a standard in bone replacement surgeries and carbon nanotubes are heavily examined as potential candidates for bone tissue engineering, due to both their biocompatibility and excellent mechanical properties [276].

However, nanomaterials have also been confronted with certain scepticism. Due to their small size, when incorporated in degradable scaffolds, nanomaterials such as NDs can escape and translocate to different parts of the body, with un-

predictable results. Studies have been conducted using fluorescent NDs (FNDs) in simple organisms such as *C. elegans* [277] to more complex human tissues such as blood [183] and organisms such as mice [278] and swine [279]. Such studies suggest that NDs can be a safe material for biomedical applications.

It has been argued that while stem cell differentiation is possible both in 2D and 3D, 2D culture will have no tissue–like cytoarchitecture. Therefore, in order to better assess the potential of NDs to promote skeletal cell differentiation, a 3D culture environment is needed [280].

Nanodiamonds have been investigated as potential candidates for 3D culture mainly in relation to bone tissue engineering. In the past decade Zhang et. al have demonstrated in two studies the potential of NDs in bone differentiation by enhancing the Young's modulus of PLLA and PLGA scaffolds [222], [224]. Recent studies have also demonstrated the potential of ND-polycaprolactone (PCL) scaffolds for bone tissue engineering [281]. However, 3D studies of the effect of NDs in cartilage tissue engineering have been limited to studying the antibacterial properties of Ag–functionalised NDs [282].

For the purposes of this chapter, cartilage precursor cells were selected due to their ability to differentiate into both chondrogenic and osteogenic lineage [283], and because they are able to differentiate in hydrogel environments [284].

When assessing the most suitable materials for the creation of 3D scaffolds, H–NDs were chosen due to their demonstrated sustaining of chondrogenic and osteogenic differentiation of cartilage progenitor cells in chapter 5.

The aim for this chapter is to show that chondrogenic differentiation of CSPCs can be enhanced in fibrin scaffolds containing H–NDs.

6.2 Materials and methods

6.2.1 Cell lines

The cell lines used for this experiment are shown in table 4.1.

Table 6.1: Cell lines and cell types used in experiments in this chapter.

Cell line			
Cell line	Cell type	Passage	Patient condition
CSPC	CH105	P8	'Bat'-ears (Normal ear cartilage)

6.2.2 Diamond

H–NDs from Carbodeon were used in the substrate (Carbodeon uDiamond ®Hydrogen D, 2.5 wt%). The H–ND undiluted solution was ultrasonicated for 5 hours using a VCX500 Vibra-cell sonicator with the cup horn accessory.

Subsequently, 5 ml of H–ND solution was diluted with equal amounts of DPBS (Sigma Aldrich) and were subsequently serially diluted in order to achieve a range of concentrations from 25g/L to 0.04 g/L.

The diluted solutions were then ultrasonicated using a Guyson Kerry KC 75W ultrasonic bath for 5 hours.

6.2.3 Fibrinogen, thrombin and fibrin

Lyophilised human plasma fibrinogen 341576-1GM and lyophilised high activity human plasma thrombin 605195-100U (Merck Millipore) were used for the assembly of scaffolds in this experiment.

Fibirnogen was reconstituted in 23.370 ml of DPBS and was diluted to a final concentration of 33 mg/ml.

In order for the thrombin solution to reach its final concentration of 1 international unit/ ml, thrombin was reconstituted in 200 μl of DPBS, the DBPS-H–ND solution was used as the final dilutant, in order to achieve final concentration of 1 unit/ ml.

6.2.4 Preparation of acellular scaffold moulds

A mould milled from a nylon block with dimensions of 200 mm $\times$ 50 mm with 3 cylindrical protrusions of 1 ml in volume was used as a cast for the 3D moulds. The moulds were made out of silicon, using the SYLGARD 182 elastomer kit (Dow). SYLGARD elastomer and the hardening agent were mixed at a 10:1 ratio and the mixture was immediately poured into the nylon master mould. The mixture was left to set for 48 hours at room temperature.

Upon setting, the moulds were removed from the 3D printed nylon cast. The side of the mould that was previously in touch with the 24-well plate cover was adhered to a microscopy glass slide (Thermo Scientific) in order to create a seal, which would prevent the fibrin from leaking prior to setting.

6.2.5 Assembly of acellular scaffolds

A H–ND/DBPS solution of 0.2 g/l concentration was ultrasonicated for 5 hours using a VCX500 Vibra-cell sonicator with the cup horn accessory. Upon ultrasonication, the solution was serially diluted using DPBS in order to achieve concentrations of 0.05 g/l and 0.02 g/l.

The solutions were then used in order to dilute reconstituted thrombin described above to a final concentration of 1 unit/ ml.

Equal volumes of thrombin–H–ND mixture and fibrinogen were mixed in a 0.5 ml Eppendorf tube. 1 ml of the mixture was then pipetted in the silicone moulds. The complex was then introduced to a 37^{o}C oven for 30 minutes until set.

Upon setting, the moulds were cut in thirds using a single edge razor blade. Each mould with a set scaffold was then transferred into a 60 mm tissue culture plate (Corning).

6.2.6 Mechanical testing of scaffolds

An Anton Paar UNHT^{3} Bio indenter was used, with the following settings.

Parameter	Value
Acquisition rate	20 Hz
Linear loading maximum depth	10000 nm
Loading rate	0.03 mN/ min
Unloading rate	0.03 mN/ min
Indenter	Spherical
Material	Ruby
Poisson ratio	0.25

Table 6.2: Parameters used to measure the Young's modulus of the H–ND–fibrin scaffolds.

Three scaffolds per condition were selected, with four unique points identified on the surface of each scaffold. Three repeat measurements were then made per point.

6.2.7 Assembly of cellularised scaffolds

In order to sterilise the selected nanodiamond dilutions, they were placed in 0.5 ml Eppendorf tubes (Sigma Aldrich) and were heated with steam to 121^{o}C at pressure of 15 p.s.i for 30 minutes. In order to avoid evaporation, the Eppendorf tubes were sealed with Parafilm (Pechiney Plastic Packaging Inc) tape and were wrapped in aluminium foil to prevent steam from escaping.

Upon sterilisation, the selected dilutions were sonicated in a Guyson Kerry KC 75 W ultrasonic bath for 3 hours.

Ch105 cells expanded as described in Chapter 3. Upon reaching confluency, the cells were removed from flasks and subsequently all growth media was removed from the cells, upon centrifugation at 1000 rpm for 60 seconds. Cells were then resuspended in fibrinogen, at a concentration of 20000 cells/ μl of fibrinogen.

Equal volumes of thrombin and fibrinogen were used for the final assembly, namely, 12.5 μl of the thrombin–H–ND solution and 12.5 μl of the fibrinogen–Ch105 solution.

The resulting scaffolds had a total volume of 25 μl and contained approximately 250000 cells per scaffold, as estimated by the content of cells in 1 μl of

fibrinogen.

6.2.8 Differentiation process

Overall, 72 cellularised fibrin–H–ND scaffolds were prepared. The table below indicates the experimental set up.

ID	H–ND conc. (g/L)	Type of differentiation		
		Chondrogenic	Osteogenic	No differentiation
No H–NDs	0.00	6	6	6
7	0.2	6	6	6
9	0.05	6	6	6
10	0.02	6	6	6

Table 6.3: Collection of cellularised fibrin–H–ND platforms prepared by H–ND concentration and differentiation conditions. The numbers in 'Type of differentiation' column show the amount of biological samples used.

The scaffolds were treated with media as described in Chapter 3 for 3 weeks before harvesting.

6.2.9 RNA extraction

Scaffolds were frozen in TRIzol at -80^{o}C before RNA extraction.

To maximise the surface area of the scaffolds and therefore optimise the area from where RNA is extracted, scaffolds were homogenised using either an RNAse-treated mortar and pestle, or, in case of tougher scaffolds, using a Tissuelyser (Qiagen) and 5 mm Stainless Steel beads (Qiagen).

RNA extraction was then performed using TRIzol Reagent (Ambion, Life Technologies) allowing sequential precipitation of RNA. Samples were homogenised in 0.4 ml TRIzol per 10^6 cells and were subsequently treated with 180 μm of chloroform per 1 ml of TRIzol and were incubated at room temperature for 15 minutes. Samples were then spun in a centrifuge at 12000g for 15 minutes at 4^{o}C. The aqueous phase (top layer) resulting from centrifuging was then transferred into clean Eppendorf tubes. 0.5 ml of of isopropanol was added to

the aqueous phase per 1 ml of TRIzol used in the homogenisation step. Upon 10 minutes of incubation at room temperature, the mixture was centrifuged at 12000g for 10 minutes at 4^{o}C. The resulting supernatant was removed and the resultant pellet was resuspended in 1 ml of 75% ethanol per 1 ml of TRIzol used for lysis. Samples were then vortexed briefly in order to ensure that the pellet was suspended in ethanol, and were then spun in a centrifuge at 7500g for 5 minutes at 4^{o}C, The supernatant was discarded and pellets were respun for an additional 30 seconds to ensure that all ethanol was removed. Pellets were then air dried for 15 minutes. They were then resuspended in 80 μl of RNAse–free diethylpyrocarbonate (DPEC) water (Qiagen) and were incubated in heat block at 55^{o}C for 15 minutes. The RNA concentration was examined using the Nanodrop One Microvolume UV-Vis spectrophotometer (Thermo Fisher Scientific).

The extracted RNA quality was assessed by monitoring both the nucleic acid 260/280 absorbance ratio in order to examine for protein contamination, as well as the 260/230 ratio in order to assess for phenol contamination resulting from TRIzol treatment. Nucleic acid has absorbance maxima of 260 nm, protein has absorbance maxima of 280 nm, and phenol and other contaminants have absorbance maxima of 230 nm. Extracted RNA with values greater than 1.8 was selected for further examination.

6.2.10 Histology

6.2.10.1 Paraffin embedding

Scaffolds were fixed in formalin solution, 10% overnight at 4C. They were then washed 3$\times$ 30 minutes in DPBS in order to remove residual fixative.

Embedding was performed by the Histopathology department at UCL Great Ormond Street Hospital Institute of Child Health (UCL GOS-ICH), London.

6.2.10.2 Sectioning

Samples were cut on a HM340E manual rotary microtome (ThermoFisher Scientific) using Feather S35 microtome blades. The resulting sections were floated in a water bath in order to eliminate distortions and when then mounted on SuperFrost Plus Adhesion slides (Thermo Fisher Scientific). They were then air dried for 60 minutes and heated for 60 minutes at 70^{o}C in order to remove residual wax.

6.2.10.3 Staining

All histological sections were cleared in Histo-Clear for 5 minutes and Cell rehydration Sections were rehydrated by descending ethanol solutions as follows: 2 $\times$ 5 minutes in 100% ethanol, 3 minutes each in 95% and 70% ethanol and finally 2 $\times$ 5 minutes in distilled water (dH_2O) .

Picrosirius red stain: 0.5 g Sirius red F3B - Direct red 80 (Sigma–Aldrich), 500 ml of saturated aqueous solution of picric acid (Sigma–Aldrich). For the process, acidified water was prepared by adding 5 ml of acetic acid (glacial) to 1 litre of distilled water.

The sections were then stained in Picrisirius red stain for 2 hours. Slides were then washed in two changes of acidified water. Water was removed from the slides with vigorous shaking.

Toluduine blue working solution was prepared by mixing toluidine blue O (Sigma Aldrich) in 70% solution and was then mixed with 1% sodium chloride (pH 2.3) in order to make up a working solution with pH between 2.3 and 2.5.

Sections were stained with Toluiduine blue working solution for 2 minutes at room temperature and were then rinsed in dH_2O until waste water ran clear.

1% Alizarin Red powder (Sigma Aldrich) was dissolved in dH_2O in order to make the staining solution. pH was adjusted to 4.1-4.3 using 0.5% ammonium hydroxide.

Sections were stained in 1% Alizarin Red solution for 2 minutes at room tem-

perature and rinsed in dH_2O until refuse water ran clear.

Alizarin red and Picrosirius red stained slides were dehydrated by immersion in 70%, 95% and 100% ethanol, for 3 minutes each. Sections were mounted using Permount (Sigma–Aldrich), and left to dry in a fume hood for 36 hours. Mounted sections were stored at room temperature. Toluidine blue stained sections were air dried for a minimum of 24 hours.

6.2.10.4 Imaging

Stained sections were examined using an Axioplan 2 Upright Epifluorescent microscope (Zeiss), using the following modes:

Brightfield for sections stained with Toluidine blue, Alizarin red and Picrosirius red.

Phase contrast for imaging sections stained with Procisirious red in order to examine for the presence of collagen fibres.

6.2.11 Gene expression analysis

6.2.11.1 cDNA composition

SuperScript IV reverse transcriptase (RT) enzyme (Thermo Fisher Scientific) was used for retrotranscription. Two negative controls were produced during the process:

- One consisting of a duplicate of one sample (selected at random) but without the RT enzyme added.
- One consisting of the RT enzyme and synthesis mix but with no RNA and just nuclease free water.

Samples were maintained at -20^{o}C.

6.2.11.2 q-RT PCR

The following primers were used in this chapter. Primers were ordered from Sigma-Alrich and were resuspended in DPEC (Sigma-Aldrich) in order to make up a final concentration of 100 μm, per instructions of the manufacturer. cDNA was amplified using SYBR Green Mix (Sigma-Aldrich) in an Applied Biosystems 7500 Fast real time PCR system (Thermo Fisher Scientific). Housekeeping gene 60s ribosomal protein L19 (RPL19) was used in order to normalise gene expression.

Gene		Primer sequence	Length (bp)
Sox9	Forward Primer	GCTCTGGAGACTTCTGAACGA	132
	Reverse primer	CCGTTCTTCACCGACTTCCT	
Runx2	Forward Primer	ACGAAGGTTCAACGATCTGAGAT	81
	Reverse primer	TTTGTGAAGACGGTTATGGTCAA	
Agg	Forward Primer	AGTCCTCAAGCCTCCTGTACTCA	185
	Reverse primer	CGGGAAGTGGCGGTAACA	
ColX	Forward Primer	ACGCTGAACGATACCAAA	101
	Reverse primer	TGCTATACCTTTACTCTTTATGGTGTA	
Collagen 2	Forward Primer	GGCAATAGCAGGTTCACGTACA	78
	Reverse primer	GATAACAGTCTTGCCCCACTTACC	
Osteocalcin	Forward Primer	ACACTCCTCGCCCTATTG	249
	Reverse primer	GATGTGGTCAGCCAACTC	
GAPDH	Forward Primer	TGATGACATCAAGAAGGTGGTGAAG	240
	Reverse primer	TCCTTGGAGGCCATGTGGGCCAT	
L19	Forward Primer	GCGGAAGGGTACAGCCAAT	130
	Reverse primer	CAGGCTGTGATACATGTGGCG	
Osx	Forward Primer	CGGGACTCAACAACTCT	308
	Reverse primer	CCATAGGGGTGTGTCAT	

Table 6.4: Primers utilised for the qRT PCR anaylsis in this chapter. Primers were designed in order to withstand temperatures between 50-55^{o}C and were diluted in DPEC according to instructions from the manufacturer (Sigma-Alrich).

6.2.11.3 Analysis

For the purposes of the q-RT PCR analysis, the fibrin scaffolds containing no H–NDs and treated with no differentiation media were used as controls. Gene expression was normalised against L19 gene expression. Final analysis performed on the qRT–PCR data was delta–delta C_T analysis.

6.2.11.4 Statistical analysis

Sample distributions for each group with a different differentiation path (none, chondrogenic, osteogenic) were tested separately by ANOVA variance for statistical difference. Post–Hoc Tukey's HSD test was used to determine significant difference between individual ND treatments.

6.3 Results

6.3.1 Initial screening of fibrin-based scaffolds

Before selecting the fibrin based scaffold for 3D cell differentiation, three different fibrin-based materials were tested to examine their ability for 3D scaffold use. The results can be seen in table A.1.

Table 6.5: Outcomes for initial screening of different Fibrin-based materials for their use as 3D cellular scaffold.

Fibrin-based scaffold	**Outcome**
Fibrin collagen composite	Did not work - Did not allow for high enough ND concentration
Low concentration fibrin (12 mg/ml) with fluorescent NDs	Did not work - Low polymerisation and Unsuitable for observation (See Appendix A)
Fibrin (33 mg/ml) with H–NDs	Worked - Polymerisation and suitable for observation

Out of the materials tested only 33 mg/ml fibrin with H–NDs satisfied the working requirements for a 3D cellular scaffold. The scaffold polymerised and was shown previously to sustain chondrogenic differentiation as a stand alone material. In addition the H–NDs were chosen because of the results in chapter 5.

6.3.2 Limit of H–ND fibrin scaffold polymerisation

In order to select suitable H–ND–fibrin scaffolds to be cellularised and treated with differentiation media, scaffolds that maintained their structural integrity needed to be selected, see table 6.6.

There was a clear pattern in the polymerisation of the H-ND-fibrin scaffolds. Above a ND concentration of 0.6 g/L, the scaffolds did not maintain structural integrity upon incubation in a 37^{o}C oven for 30 minutes.

Scaffolds 1-5 were further incubated for up to 4 hours at 37^{o}C, however they did not polymerise further.

Scaffold 6 was recreated on 3 separate occasions and failed to fully polymerise each time, despite being incubated uninterrupted for up to 4 hours.

As a result of this experiment, scaffolds **7**, **9** and **10** were selected for further experiments.

Table 6.6: Different concentrations of H-NDs in fibrin scaffolds and the result of polymerisation. Samples 7-10 maintained structural integrity after 30 minutes of treatment in a 37^{o}C oven for 30 minutes and remained intact upon remaining in room temperature conditions for 48 hours in PBS. Sample 6 was only partially integral after 30 minutes. Highlighted samples were selected in order to carry out the subsequent experiments in this results chapter.

Sample ID	H–ND concentration (g/L)	Polymerisation outcome
1	12.5	No polymerisation
2	6.25	No polymerisation
3	3.13	No polymerisation
4	1.6	No polymerisation
5	0.8	No polymerisation
6	0.4	Partial polymerisation
7	**0.2**	**Polymerisation**
8	0.08	Polymerisation
9	**0.05**	**Polymerisation**
10	**0.02**	**Polymerisation**

6.3.3 Mechanical testing of fibrin - ND scaffolds

6.3.3.1 Elasticity of fibrin - H-ND scaffolds

Upon establishing the limit of H-ND concentration that allowed for the polymerisation of the fibrin scaffolds, their Young's modulus was tested.

Bioindentation was chosen to measure the Young's Modulus of the 3D scaffolds using the Anton-Parr Bioindenter UNHT^3. Before the Young's modulus of the H–ND fibrin scaffold with three H–ND concentrations could be measured, different methods of scaffold fabrication were tested. The outcomes can be seen in table 6.7. The working technique involved a disposable silicone mould for scaffold fabrication. However to enable bioindentation measurement, the scaffold was never removed from the silicone mould; instead the mould was cut open to reveal the flat scaffold surface for measurement.

Table 6.7: Outcomes for H–ND fibrin 3D scaffold fabrication with different approaches.

Fabrication method	**Outcome**
96 well plate and syringe extraction	Unsuccessful - Structure compromised
PDMS mold	Flat surface collapsed
Disposable silicone mould	Worked - mold and scaffold cut open allowing bioindenter measurement

In figure 6.1 the Young's modulus of all samples are in the range between 1-5MPa. The highest Young's Modulus measurements were observed for the control sample, not including outliers. The greatest distribution variance was observed in the sample containing 0.05 mg/ml.

Despite no significant difference observed among all four conditions, there is some indication showing that the fibrin scaffold which contained no H–NDs demonstrated a higher Young's Modulus compared to the samples containing H–NDs at various concentrations.

When comparing median values among the samples containing H–NDs it appears that there is no clear trend towards the samples containing higher concentrations of H–NDs.

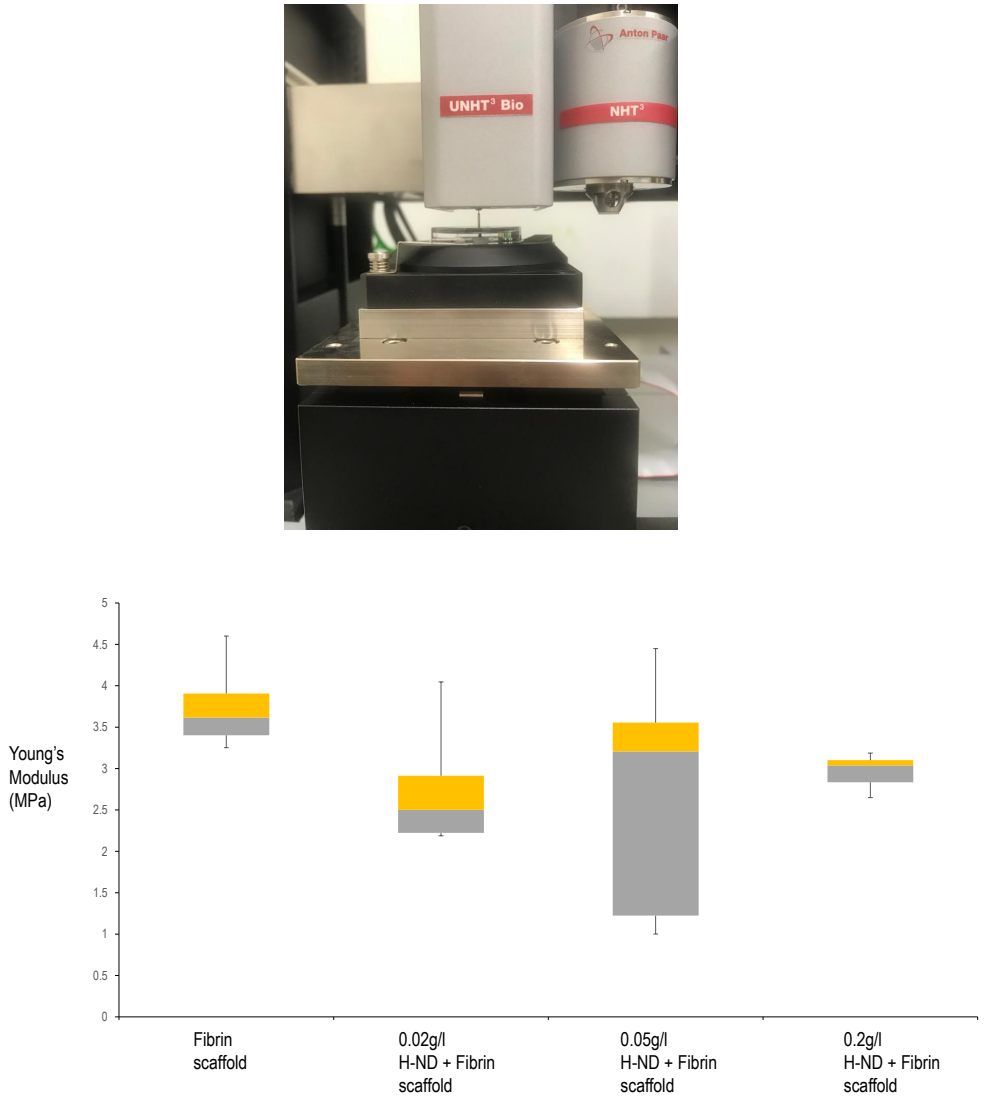

Figure 6.1: Top: Experimental set-up of nanoindentation probe approaching H-ND-fibrin scaffolds for the examination of the scaffold's Young's Modulus. **Bottom:** Quantitative description of elasticity for fibrin based 3-dimensional scaffolds with different concentrations of H–NDs incorporated. Young's modulus examination of fibrin - H-ND scaffolds using the Hertz indentation method. The box plot shows distribution of elasticities in n=3 samples per condition, with 4 technical replicates per sample at different positions on the scaffold. The box plot shows distribution median with a line within the box. The box itself stands for 50% of the data closest to the median. The lines below and above the box stands for 2 quadrants containing data distributed 25% and more away from the median. No significant difference was observed among all four. Statistical test performed was 2-way analysis of variance (ANOVA) found no significant difference in the group ($p<0.01$).

While fibrin Young's modulus at concentration of 33 mg/ml has been observed previously, similar measurements of fibrin scaffolds containing H–NDs are novel and these observations confirm that H–NDs potentially interfere with the ability of fibrin to crosslink. However, further observations are required in order to statistically prove this hypothesis.

6.3.4 Histological examination of differentiated 3-dimensional tissues

6.3.4.1 Detection of Glycosaminoglycans with toluidine blue stain

Glycosaminoglycans (GAGs) are key cellular markers of chondrogenic differentiation. GAG presence was used to observe the level of chondrogenic differentiation of CSPCs in 3D H–ND fibrin scaffolds. Toluidine blue stain was used to stain sections of all samples for presence of GAGs. Samples treated with no differentiated media had low structural integrity, and therefore only small amount of sections were acquired. Samples treated with differentiation media retained better structural integrity, and therefore larger sections were stained. In figure 6.2, Toluidine blue dye stained cells that expressed glucosaminoglycans (GAGs) show a purple colour. Other parts of the structure, containing cells, diamond and fibrin were stained blue. In figure 6.2 middle section, it is evident that GAGs are present throughout the structures, due to the even dispersion of purple colouring throughout. Sections from the structures containing 0.05 g/L and 0.2 g/L of H–NDs indicate denser cell population.

The structural integrity of the scaffolds containing cartilage precursor cells undergoing osteogenic differentiation is lower and the samples are stained primarily blue. The toluidine blue is not turning purple in these samples, because GAGs are specific to chondrogenic differentiation.

The Toludine blue staining of these samples indicated overall successful chondrogenic differentiation of the samples treated with chondrogenic differentiation media, as well as signs of cell hypertrophy in these sections.

These results are in line with attempts to induce chondrogenic differentiation in fibrin scaffolds in literature [285], [286], [287] and will be examined further in the discussion section of this chapter.

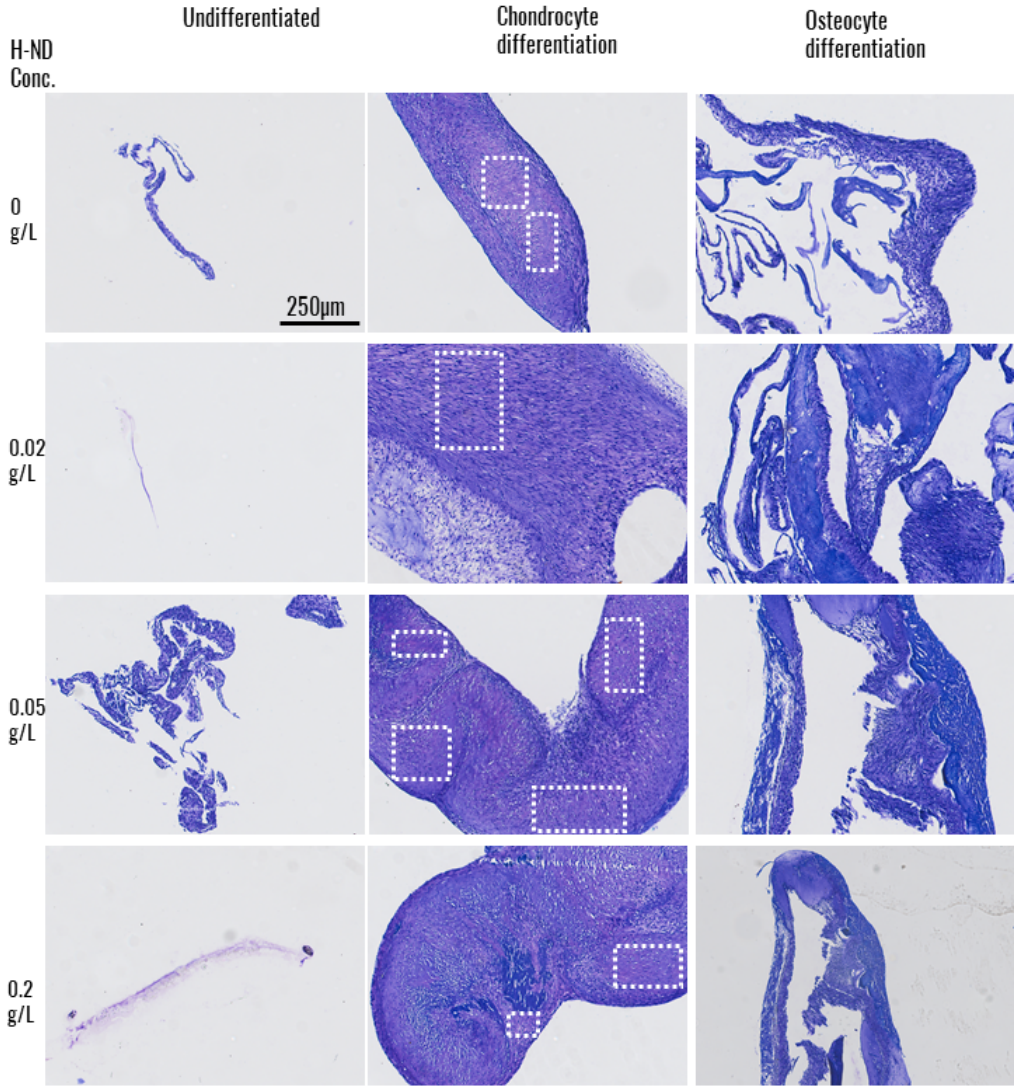

Figure 6.2: Histology sections of the 3-dimensional fibrin-ND-cell scaffolds stained with toluidine blue stain. The scaffolds treated with no media have low structural integrity, with the blue stain indicating the presence of cell nuclei. Purple stain indicates presence of glucosaminoglycans (GAGs) in the chondrogenically differentiated group. Squares highlight areas of GAG staining. Pictures represent 3 biological replicates, in which at least 4 independent fields were examined. All scalebars are 250 μm; Magnification 10$\times$

6.3.4.2 Detection of collagen with Picrosirius red staining

Collagen accumulation is an indicator of cells undergoing chondrogenic differentiation. Picrosirius red dye was used to indicate the presence of collagen in the 3D H–ND fibrin scaffolds containing differentiated cells. When examining stained samples sections, those that are seen with bright red colouring indicate the presence of collagen. That is further confirmed once sections are exposed to polarised light, as the stained collagen fibres are the only structure visible when imaged in polarised light mode.

In the figure 6.3 it can be seen that due to low structural integrity, the H–ND–fibrin scaffolds which were not treated with differentiated media produced very small sections with no presence of collagen, as is further confirmed by the lack of fibres indicated in the polarised light section images in figure 6.4. The brighter areas in the undifferentiated samples containing H–NDs are possible artefacts and do not indicate the presence of collagen.

Scaffolds treated with chondrogenic differentiation media were well stained with picrosirius red and showed the presence of collagen. This can be seen in figure 6.3. That is further confirmed in figure 6.4, where the corresponding polarised light images show collagen fibres, with brighter areas of higher density of collagen fibres.

The staining of the scaffolds undergoing osteogenic differentiation does not indicate presence of collagen. Despite the fact that marginally brighter red areas are indicated in the samples containing 0.05 g/L and 0.2 g/L H–NDs, the polarised light images of 6.4 do not indicate presence of collagen fibres, rather small light artefacts.

The presence of collagen in the chondrogenically differentiated sections indicates successful chondrogenic differentiation, as the cells have began depositing extracellular matrix [288] and since picrosirius red does not stain fibrin, it can be assumed with confidence that the matrix deposition is in fact related to successful differentiation. In the discussion section, the significance of this result will be expanded upon.

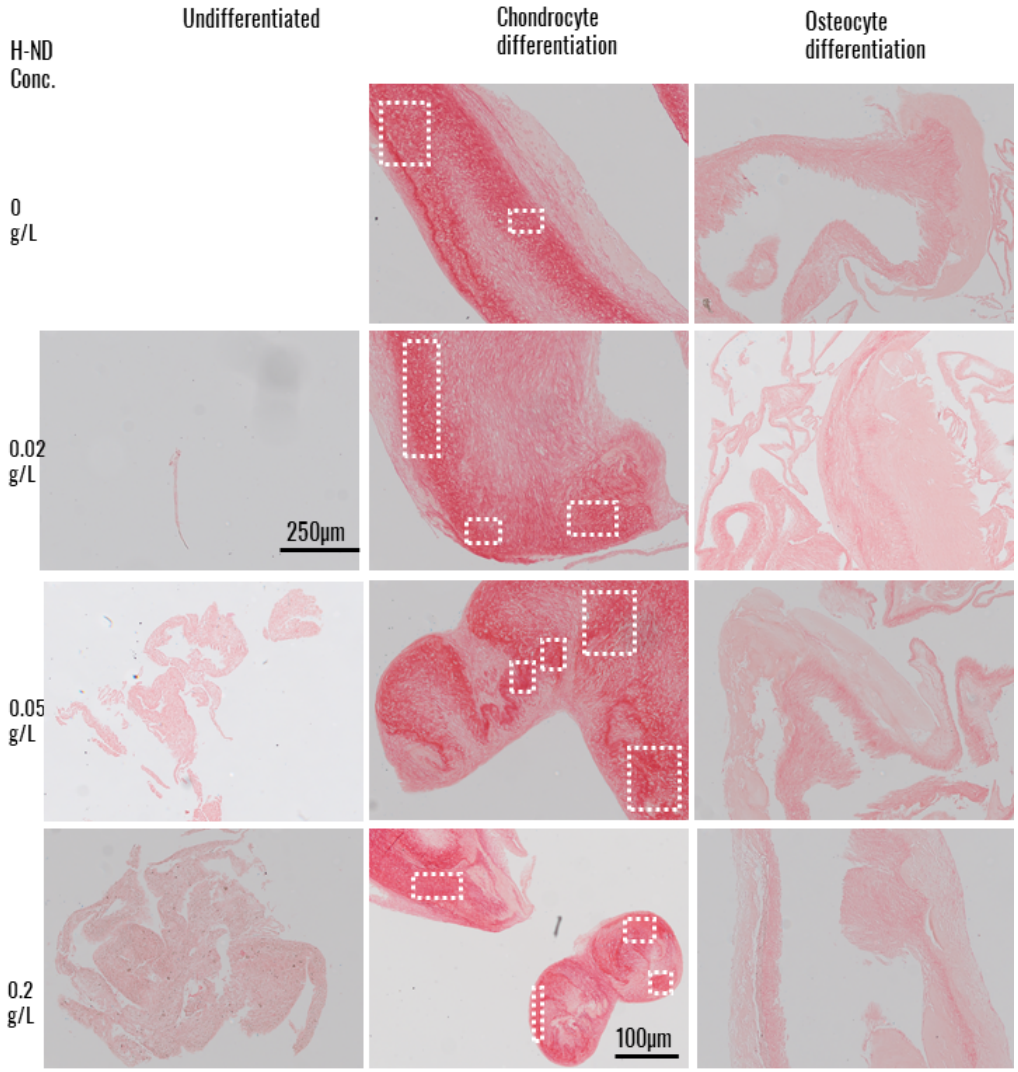

Figure 6.3: Histology sections of the 3-dimensional fibrin-ND-cell scaffolds stained with picrosirius red stain. The scaffolds treated with no media have low structural integrity, with the pale pink indicating the presence of fibrin. Bright red staining indicates presence of collagen in the chondrogenically differentiated group. Some areas with collagen staining are indicated in squares. Pictures represent 3 biological replicates, in which at least 4 independent fields were examined.

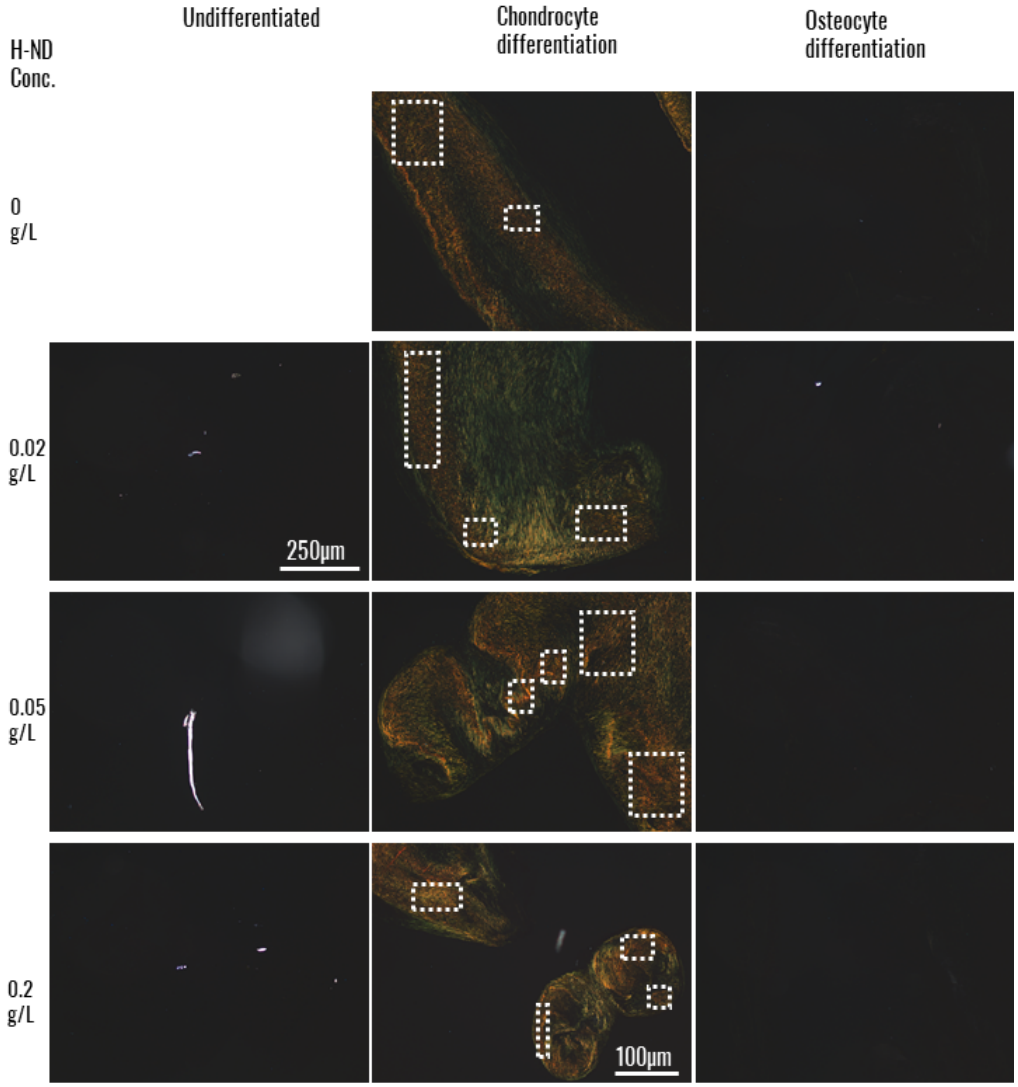

Figure 6.4: Histology sections of the 3-dimensional fibrin-ND-cell stained with picrosirius red. The polarised light images indicate the presence of collagen fibres. Some areas with collagen staining are indicated in squares.. Pictures represent 3 biological replicates, in which at least 4 independent fields were examined.

6.3.4.3 Detection of calcium deposits with Alizarin red staining

Alizarin red is a stain that binds to calcium deposits, which are linked to osteocyte differentiation. In figure 6.5 it can be seen that samples with no differentiation media demonstrated low structural integrity and do not appear to contain calcium deposits, which would be demonstrated with bright red colours. In addition it can be seen that sections of samples that have undergone chondrocyte differentiation do not demonstrate calcium deposites, as a uniform pink stain around the fibrin scaffold is observed. In addition in figure 6.5 it can be seen that sections of 3D scaffolds with cells having undergone osteocyte differentiation appear to have lower structural integrity in comparison to their chondrocyte differentiated counterparts.

Calcium deposits would have been observed as bright red patches within the scaffold. In figure 6.5 it can be seen that samples containing no H–NDs and 0.02g/L H–NDs in the fibrin scaffolds do not appear to contain any calcium deposits, as there are no bright red staining spots. However, samples containing 0.05 g/L and 0.2g/L of H–NDs in the H–ND–fibrin scaffold appear to have certain areas stained bright red, however it cannot be determined that these are calcium deposits - indicators of osteogenic differentiation or just dye trapped between cell aggregates without osteogenic differentiation.

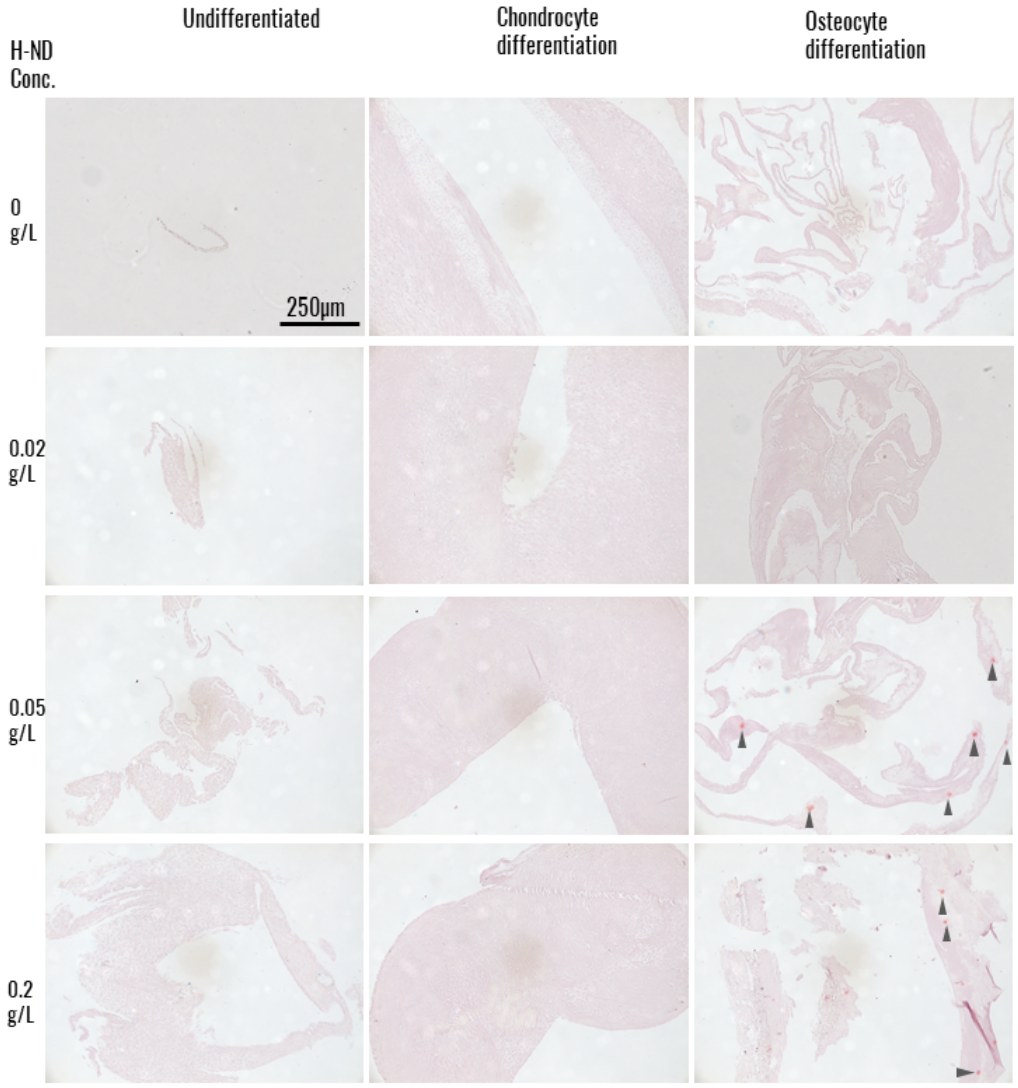

Figure 6.5: Histology sections of the 3-dimensional fibrin-ND-cell scaffolds stained with Alizarin red stain. The scaffolds treated with no media have low structural integrity, with the pale pink indicating the presence of fibrin. Bright red spots of accumulated Alizarin red are indicated with arrows. Pictures represent 3 biological replicates, in which at least 4 independent fields were examined.

6.3.5 qRT-PCR examination of differentiation on 3-dimensional tissues

6.3.5.1 Examination for cartilage markers with gene expression

To further examine the level and the impact of H–NDs on CSPC differentiation, gene expression analysis of well known gene markers of chondrogenic and osteogenic cell fate was used.

Initially Sox9 gene expression levels were measured. Sox9 is a gene expressed in the early stages of chondrogenic differentiation.

Statistical analysis of samples was performed only within each group (undifferentiated, osteogenic, chondrogenic) to compare for the effect of different H–ND concentrations on samples treated with the same differentiation media. Overall there is no statistical difference among samples when compared within the same sample type (undifferentiated, osteogenic, chondrogenic) as indicated in figure, due to low sample number (n=3). See figure 6.6.

The highest levels of Sox9 expression are observed in the samples that were not treated with differentiation media. There is high variance among the replicates of the samples containing 0.2 g/L of H–NDs in the fibrin scaffolds.

The samples treated with osteogenic differentiation media demonstrated the second highest levels of expression of Sox9. Lower variance is observed in the samples containing the highest concentrations of H–NDs.

Samples that have undergone chondrogenic differentiation show the lowest levels of expression of Sox9, as well as the lowest variance among samples.

Overall, the low expression of Sox9 in the samples undergoing chondrogenic differentiation is not surprising, as Sox9 is a marker expressed in the early stages of chondrogenic differentiation [289]. The cells were grown on H–ND fibrin scaffolds for 21 days, which is likely too long to maintain the Sox9 signal. However, the expression of Sox9 is an early indicator of osteogenic differentiation through its

interaction with Runx2, a marker examined further in this chapter [290],[291].

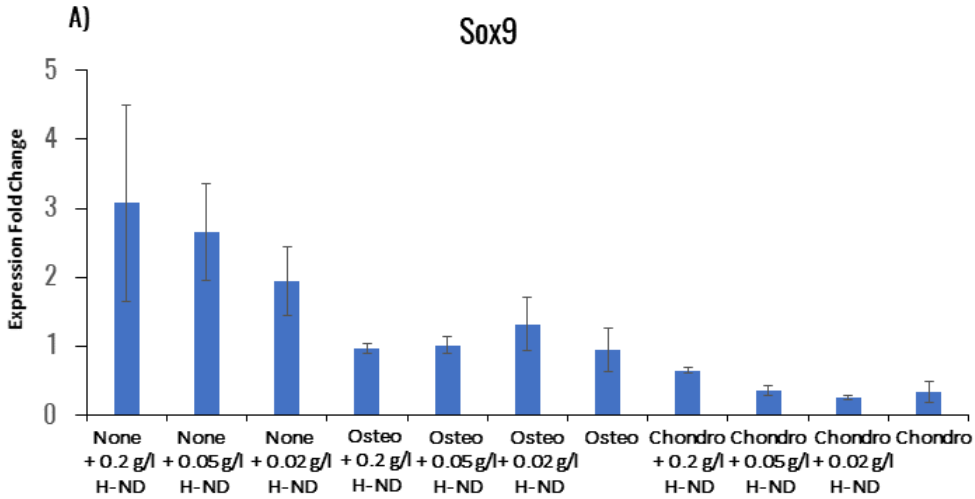

Figure 6.6: Examination of expression of Sox9 in samples treated with no differentiation media, osteogenic and chondrogenic differentiation media. Samples represent 3 biological replicates. Expression measurements were normalised against L19 expression and a control sample of cells cultured in a fibrin scaffold containing no H–NDs with no differentiation media for 21 days. ANOVA statistical test of variance was used to observe statistical difference in each group, $p<0.05$.

6.3.5.2 Gene expression of markers of differentiated cartilage

To further obtain levels of differentiation of CSPCs in H–ND fibrin 3D scaffolds, more gene expression markers were measured. Aggrecan and ColX are gene expression markers associated with differentiated cartilage.

In figure 6.7 it can be seen that the expression of Aggrecan is statistically significantly upregulated in samples that have undergone chondrogenic differentiation with H–ND concentration of 0.2 g/l and 0.05 g/l in the 3D H–ND fibrin scaffolds. The samples with 0.02 g/l H–ND concentration in the scaffold have significantly less Aggrecan expressed. This result shows higher H–ND concentrations within the fibrin scaffold have a positive effect on Aggrecan expression during chondrogenic differentiation.

In figure 6.7 it can be seen as expected Aggrecan was not strongly expressed in CSPCs undergoing osteogenic differentiation, with only baseline expression found.

Col10 is present in all samples that have undergone chondrogenic differentiation (figure 6.7), with high variance being observed in the samples containing the higher concentrations of H–NDs (0.2 g/l and 0.05 g/l) in the H–NDs–fibrin scaffolds.

While some Aggrecan marker was expressed in the samples that have undergone osteogenic differentiation, almost no Col10 expression was observed in the same samples.

In figure 6.7 it can be seen that some Col10 expression was found in samples that did not undergo differentiation but which contained H–NDs of 0.2 g/l concentration in the H–ND–fibrin scaffolds. However the increase was not statistically significant.

Overall, the results indicate that the samples that have undergone chondrogenic differentiation have done so successfully, as Col10 indicates deposition of ECM and Aggrecan is a proteoglycan associated with appropriate function of cartilage [292], [293].

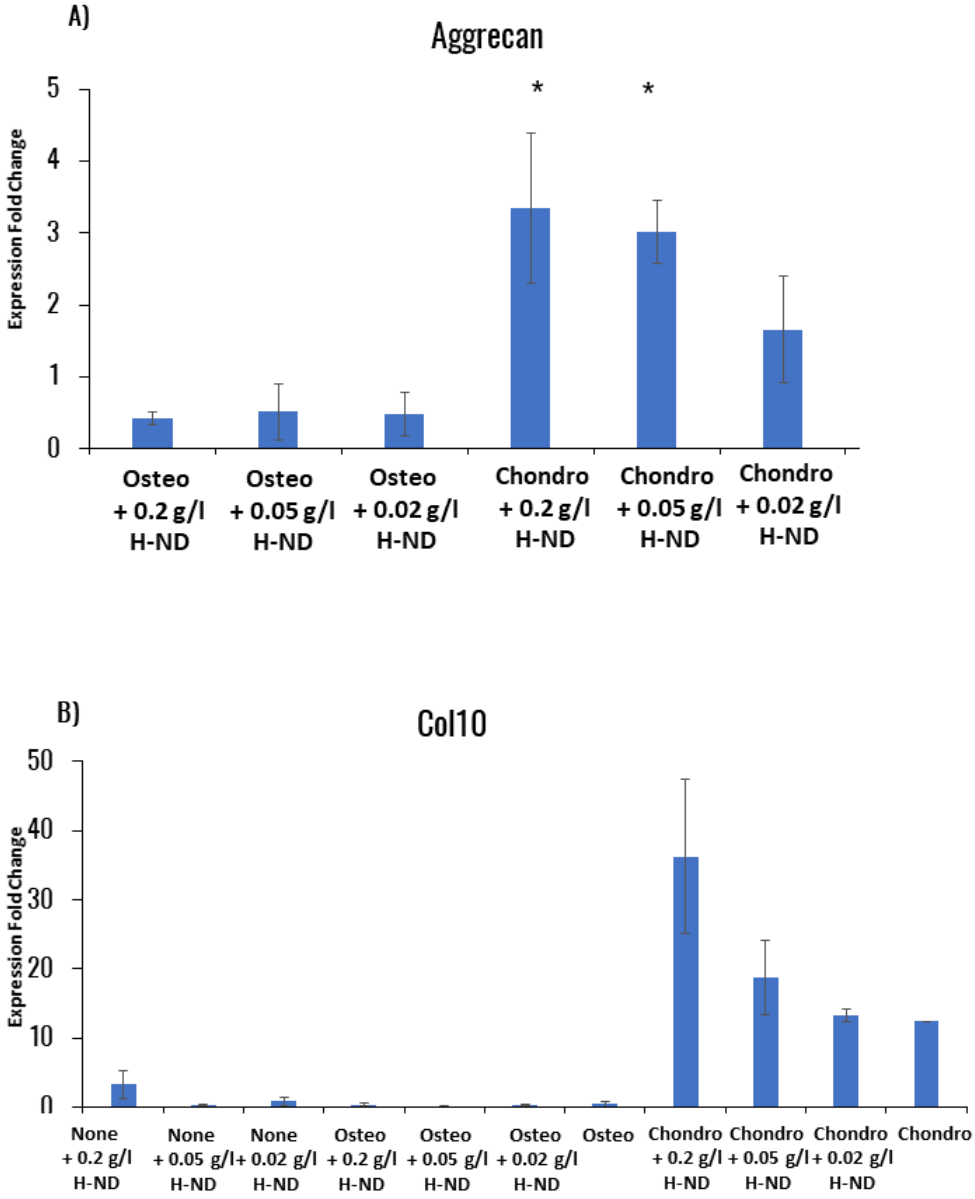

Figure 6.7: Examination of Aggrecan and Col10 expression. Samples represent 3 biological replicates using qRT-PCR. Expression measurements were normalised against L19 expression and a control sample of cells cultured in a fibrin scaffold containing no H–NDs with no differentiation media for 21 days. Samples treated with no differentiation media, as well as samples not containing H–NDs in the fibrin scaffolds, did not express significant amounts of Aggrecan to be included in this figure. Statistical difference was analysed with ANOVA test of variance, with post-hoc Tukey HSD test, $*p<0.05$.

6.3.5.3 Examination for osteogenic differentiation markers

Osterix and Runx2 are two gene markers involved in the early stages of osteogenic differentiation.

In figure 6.8 it is shown that both Osterix and Runx2 markers have statistically significant upregulation in cells that have undergone chondrogenic differentiation in the H–ND–fibrin scaffold containing 0.2g/L of H–NDs.

Following the observations in figure 6.8 there is a variance in the expression of Osterix in the samples that have undergone osteogenic differentiation, as well as cells that have undergone chondrogenic differentiation in the sample containing 0.02 g/L of H–NDs within the fibrin scaffold.

Runx2 expression baseline expression is observed in samples that have not been treated with differentiation media (figure 6.8). Runx2 expression in samples that have undergone osteogenic differentiation appears to be lower compared to their counterparts that have been treated with chondrogenic differentiation media. The variance in levels of expression of Runx2 among samples that have been treated with the same differentiation media is relatively low, as is the variance of Osterix expression in the samples that have undergone osteogenic differentiation.

Upregulation of Runx2 and Osterix expression in mesenchymal stem cells undergoing chondrogenic differentiation has been previously observed in hADSCs and chondrogenic progenitor cells and can indicate hypertrophic chondrocyte and osteocyte presence, early indicators of endochondral ossification [294], [295], [296].

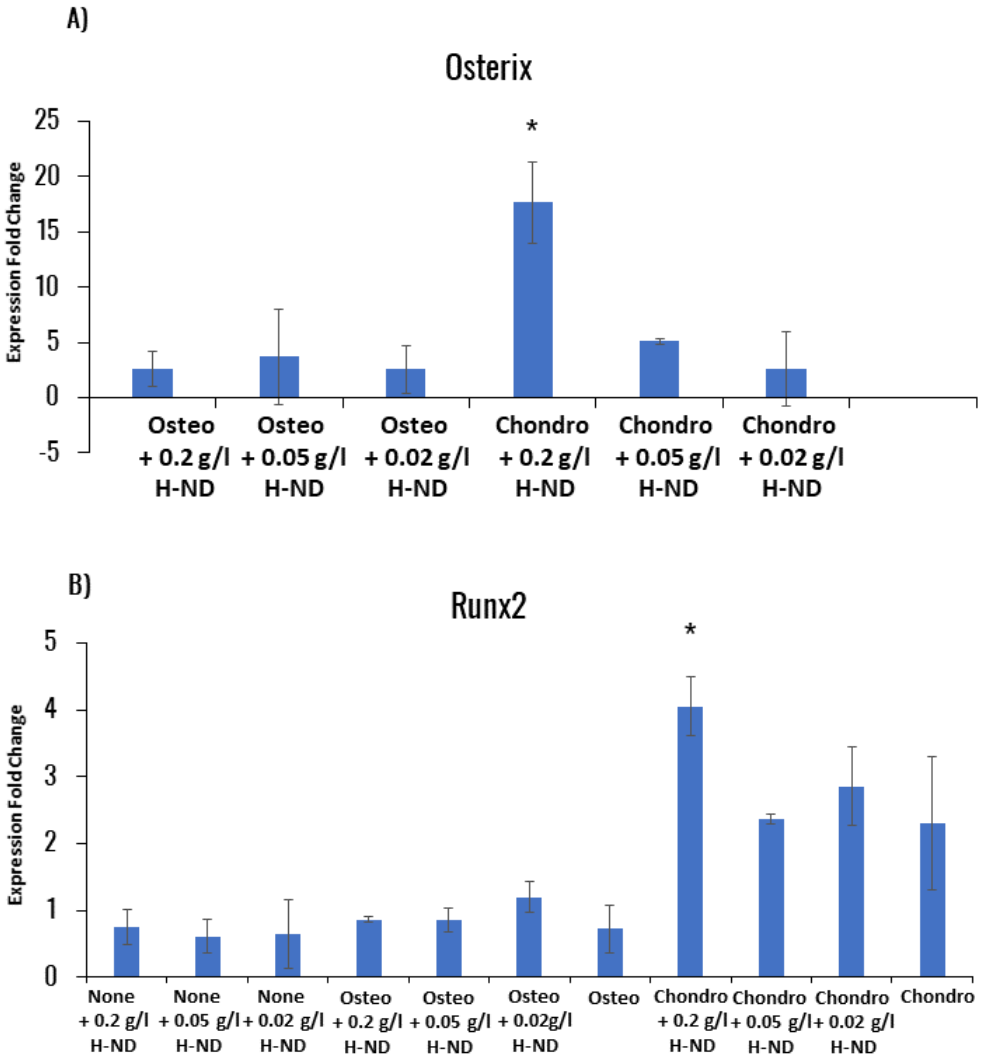

Figure 6.8: Examination of expression of Osterix and Runx2 in samples. Samples represent 3 biological replicates. Expression measurements were normalised against L19 expression and a control sample of cells cultured in a fibrin scaffold containing no H–NDs with no differentiation media for 21 days. Samples treated with no differentiation media, as well as samples not containing H–NDs in the fibrin scaffolds, did not express significant amounts of Osterix to be included in this figure. Statistical analysis was done with ANOVA test for variance with post-hoc Tukey HSD test. *$p<0.05$.

6.4 Discussion

6.4.1 Polymerisation and mechanical properties of scaffolds

Polymerisation of the H–ND–fibrin scaffolds was observed at lower concentrations of H–NDs, implying that H–NDs may affect the activity of thrombin and subsequently the cross linking of fibrinogen fibrils. Although such phenomenon has not been observed with larger particles (c. 150 μm) incorporated in fibrin scaffolds [297], fibrinogen fibrils and H–NDs are similar in diameter, which could interfere with cross linking. In order to further examine this theory, transmission electron microscopy (TEM) of the scaffolds can provide an insight into the position of H–NDs in the scaffolds. A technique used by Cheng *et al.* in 2007 utilised nanodiamonds' unique spectroscopic signal in order to track bioconjugated NDs in lung epithelial cells using Raman imaging [298]. This technique could be utilised in order to track the position of the NDs within the hydrogels.

Overall, when comparing acellular fibrin scaffold samples, the Young's modulus of scaffolds containing H–NDs is lower compared to that of acellular scaffolds containing no H–NDs. This result is in line with the assumption that H–NDs can interfere with fibrin polymerisation, as lower Young's modulus implies less crosslinking. In order to further examine this hypothesis, experiments with even lower concentrations of H–NDs compared to the ones utilised in this thesis could be used. Incorporation of larger NDs in diameter can potentially demonstrate the enhancement of the mechanical properties of these scaffolds. An experiment where H–NDs of larger diameters are incorporated in fibrin scaffolds while maintaining the same wt % concentration could indicate whether scaffold stiffness in conjunction with the chondroinductive properties demonstrated in this chapter can further enhance differentiation. Since studies on the enhancement of the mechanical properties of scaffolds for the purposes of osteogenic differentiation have demonstrated successful results [222], [224], [281], potential enhancement of the osteogenic properties of these scaffolds can be examined. On the other hand, studies incorporating NDs of similar diameter to the ones utilised in this chapter have also achieved increased

substrate stiffness when combined with polymers such as Gelatin methacrylamide (GelMA) [299].

6.4.2 Differentiation of chondrocyte progenitor cells in H–ND–fibrin scaffolds

Markers such as Agg and ColX are indicators of chondrocyte differentiation, especially in the later stages of differentiation (days 15-21) [186], [300]. Sox9 is a differentiation marker appearing at the earlier stages of chondrocyte differentiation [120].

High concentrations of H–NDs have significantly stimulated Agg gene expression. Together with presence of the ColX marker, this indicates terminal differentiation of chondrocytes, an interesting result in chondrogenesis, as it an indicator of endochondral calcification [301], [302].

Unfortunately, ColII detection was not possible during this thesis, due to issues with optimisation of ColII primers for the purposes of qRT-PCR. However, expression of GAGs, picrosirius red stain of collagen and detection of Sox9, ColX and Agg in the chondrogenically differentiated samples can be considered as sufficient indicators.

Detection of collagen 2 could have confirmed that the cartilage produced during these experiments is either hyaline or articular cartilage. This can be suggested as future work on further gene expression analysis.

The presence of Osterix, RunX2 and ColX gene expression markers in the cells treated with high concentration of H–NDs that have undergone chondrocyte differentiation further affirms the hypothesis that cells are undergoing endochondral ossification [303], [304], [305]. The levels of gene expression of Agg, Osterix and Runx2 for cells cultures in scaffolds with the highest concentrations of H-NDs indicates a potential link between concentration of H–NDs and acceleration of chondrocyte differentiation and/ or endochondral ossification in cells. However, lack of calcium deposits in the chondrogenically differentiated sections indicates that os-

sification did not advance to calcification levels within 21 days. This result can pave the way for further examination of these scaffolds, and their potential as tools for bone differentiation by means of endochondral ossification, potentially by increasing the time in culture of the H–ND–fibrin scaffolds undergoing chondrogenic differentiation.

As discussed in 6.4.2, no significance difference appears in the Young's modulus among the fibrin scaffolds utilised in the chapter of this thesis. Therefore, scaffold stiffness can be disregarded as a factor in the acceleration of chondrogenesis.

Detection of Sox9 gene markers in cells that were not incubated in differentiation media means that further experiments that can determine potential spontaneous differentiation of chondocyte progenitor cells in H–ND–fibrin scaffolds could be explored. Such experiments can involve for example: Incubation of chondrocyte progenitor cells in H–ND–fibrin scaffolds for longer periods of time and subsequent examination of chondrogenesis markers. Fabrication of fibrin scaffolds with lower concentration of H–NDs and subsequent repetition of experiments described above in order to further understand the effect of H–ND concentration in endochondral ossification and chondrocyte hypertrophy. Based on results of chapter 5, chondrocyte progenitor cells tend to proliferate faster than hADSCs in chondrogenic differentiation media. Therefore, the potential of hADSCs as precursor cells for cartilage that does not undergo endochondral ossification can be examined.

6.5 Conclusions

In this chapter, the potential of H–ND–fibrin 3–dimensional scaffolds as platforms for skeletal tissue engineering have been examined. Overall, there are indications that the concentration of H–NDs in the fibrin scaffolds can accelerate the process of chondrogenesis and endochondral ossification. The presence of H–NDs in fibrin scaffolds does not inhibit, neither promote osteocyte differentiation under osteogenic differentiation media treatment.

Further experiments should be carried out in order to better understand the potential of H–ND–fibrin scaffolds as a platform for spontaneous chondrocyte or osteocyte differentiation, the potential of hADSCs as cartilage precursor cells in H–ND–containing 3D cultures as well as the potential of the H–ND–fibrin scaffolds as a platform for osteogenesis through endochondral ossification.

Chapter 7

General Conclusions

This thesis has demonstrated functionalised detonation nanodiamond as a potential material for skeletal tissue engineering. Both oxygen- and hydrogen- terminated nanodiamond exhibited potential for increasing chondrogenic as well as osteogenic differentiation. This was the fist time human adipose-derived stem cells and CSPCs were grown on H- and O-terminated NDs as well as boron doped diamond. It was also the first time CSPCs were successfully differentiated in a 3D culture that contained NDs of any kind. Both 2D and 3D experiments verified the potential of H–NDs as a material suitable for skeletal tissue engineering.

In Chapter 4, we investigated the potential of oxygen-functionalised boron doped nanodiamonds and detonation nanodiamonds as a substrate that can sustain growth of hADSCs. It was the first time that cells of any kind were grown on the BDD-PPy scaffolds as well as the 2D substrates that were coated with PDDAC before being seeded with NDs. All substrate morphologies were characterised by means of either SEM or AFM. SEM images indicate that hADSCs grown on BDD-PPy scaffolds attach not only on the surface, put also grow protrusions in order to reach further in the pores of the material. Furthermore, imaging of fluorescent cells on the BDD-PPy scaffold indicate uniform growth of the hADSCs at the material surface. Imaging of the hADSCs on the 2D nanodiamond surface and cell counting results after 14 days of cells in culture indicated that both types of substrates are biocompatible. Furthermore, it was shown that cells can be grown to confluency on the

2D substrates, which deemed them suitable for differentiation assays, as confluency is a key for initiation of differentiation in mesenchymal stem cells (MSCs).

In Chapter 5, hADSC chondrocyte differentiation was carried out for the first time on H–NDs and O–NDs. Chondrogenic differentiation assays on hADSCs indicated that both H–ND and O–ND 2D substrates can sustain chondrogenic differentiation. CSPCs underwent trilineage (chondrogenic, osteogenic and adipogenic) differentiation on these substrates. Results demonstrated that all 3 types of differentiation can be sustained on these 2D substrates. It was furthermore shown that cells undergoing osteogenic differentiation showed statistically significant deposition of calcium deposit when grown on H–NDs, indicating stronger osteogenic differentiation.

In Chapter 6 it was demonstrated that inclusion of H–NDs in fibrin scaffolds affects the polymerisation on the scaffold and as such does not enhance stiffness at concentrations up to 0.02 g/l. On the other hand, it was demonstrated for the first time that the concentration of functionalised NDs has an impact on chondrocyte differentiation activity of CSPCs within fibrin scaffolds. CSPCs undergoing chondrogenic differentiation in scaffolds containing 0.2g/l concentration of H–NDs demonstrated increased gene expression of late-stage differentiation markers, as well as indicators of endochondral ossification. Overall, it was demonstrated that not only the presence, but increased amounts of H–NDs in the scaffolds had an accelerating effect on the chondrocyte differentiation process.

In Chapter 6, fibrin–H–ND composites were also explored as a novel platform for osteocyte differentiation. While CSPCs undergoing osteogenic differentiation in H–ND–fibrin scaffolds did not display significant differentiation markers, mesenchymal stem cells like hADSCs have demonstrated sufficient levels of differentiation in fibrin scaffolds fabricated with different protocols [306]. Since Chapter 5 demonstrated that H–NDs sustain osteogenic differentiation, it can be argued that the H–NDs in the 3D experiment did not play an inhibitory role in osteogenic differentiation in 3D.

This work represents a comprehensive study of the interaction of two different types of mesenchymal stem cells with functionalised NDs. A combination of a novel fabrication method of 3D biomaterial scaffolds that include H–NDs and the subsequent demonstration of influence of H–ND concentration on chondrogenic differentiation promote diamond as a valuable material for skeletal tissue engineering.

Chapter 8

Future work

The research of this thesis presents how functionalised NDs can promote differentiation of mesenchymal stem cells into chondrocyte and osteocyte fates.

The work in Chapter 4 demonstrated that cell proliferation can be sustained on functionalised BDDs and DNDs. Despite characterisation of the substrate by microscopy (AFM and SEM), the precise adhesion mechanism and how it is affected by different topographies has not been tested. This can be further tested with immunohistochemistry assays such as focal adhesion kinase migration (FAK) assay and vinculin immunofluorescence assay.

During the process of this thesis, optical microscopy of fluorescent nanodiamonds (FNDs) was attempted in order to visualise them in 3–dimensional scaffolds. Due to their high zeta potential and affinity to glass, the equipment was not deemed appropriate for such experiments. Transmission electron microscopy (TEM) of the H–ND–fibrin scaffolds can give a further insight into the dispersion of H–NDs within the scaffolds, as it can demonstrate the structure of fibrin at the fibril level and the topology of the H–NDs within the structure, therefore driving further the hypothesis that arises in this thesis that the polymerisation of fibrin is affected by the presence of H–NDs.

In order to further investigate the suitability of the H–ND–fibrin scaffold as a platform for chondrogenic differentiation as explored in Chapter 6, the use of

hADSCs as a potential stem cell type is suggested. This is due to the fact that extraction of hADSCs from the human body, especially that of children, is less invasive compared to CSPCs.

The results from Chapter 6 indicate that after 3 weeks in culture, H–ND–fibrin scaffolds undergoing chondrogenic differentiation show markers of endochondral ossification. Further extension of the time of incubation of these constructs could be utilised in order to examine potential expression of Osteocalcin, a gene marker associated with osteogenic differentiation, as well as Alizarin red staining for detection of calcium deposits.

Furthermore, further optimisation for 3D scaffolds for osteogenic differentiation should be explored. As demonstrated in [306], fibrin as a standalone biomaterial can sustain osteogenic differentiation of hADSCs. Composites of fibrin of lower concentration with H–NDs can be used in order to further investigate chondrogenic differentiation in 3D with the use of H–NDs.

A scaffold free method for chondrogenic tissue differentiation in 3D involves the creation of micromass pellets from MSCs and has been practiced successfully on both hADSCs [307] and CSPCs [308]. Integration of H–NDs in micromasses could potentially create new, scaffold free 3D platforms for cartilage tissue engineering.

Further experiments that can exploit the superior mechanical properties of NDs in 3D scaffolds can be explored. Studies have shown the integration of NDs in biomaterials for bone tissue engineering such as the biodegredable composite Polycaprolactone (PCL) [281] and poly(L-lactide)-co-(ε-caprolactone) [(poly(LLA-co-CL)] [309] can enhance the mechanical properties of such materials and promote bone growth. Further experiments validating the integration of hADSCs in scaffolds with similar properties can confirm the compatibility of NDs with a stem cell type that is easier to isolate and therefore more attractive for real–life applications.

The reported success of H–ND integration in 3D scaffolds for chondrocyte differentiation should also be explored *in vivo*. Chorioallantoic Membrane (CAM) grafts can be used in order to explore the biointegration and potential vascularisation

of the H–ND–fibrin scaffolds in chicks.

As NDs have been confirmed to enhance the mechanical properties of PCL [281], potential composites of ND+fibrin+PCL scaffolds could be examined in order to create scaffolds with increased mechanical properties that can maintain their stiffness while translating the positive effects of H–NDs on chondrogenic differentiation discovered in this thesis *in vivo*.

An important part of the appeal of NDs for tissue engineering is their functionalisation potential. Studies have shown successful ND functionalisation with dexamethasone [310], one of the differentiation factors utilised throughout this thesis. Further investigation of functionalisation of NDs with differentiation factors could potentially eliminate the use of differentiation media during skeletal tissue differentiation.

Overall, the future work stemming from this thesis is particularly complex and challenging, requiring interdisciplinary skills. However, potential results can create breakthroughs in tissue engineering.

Appendix A

Supplementary information to Chapter 4

SEM images of hADSCs grown on BDD–ppy6 and BDD–ppy8 samples are demonstrated below. Cells were grown for 7 days on those substrates and were subsequently fixed and dehydrated as described in 4.

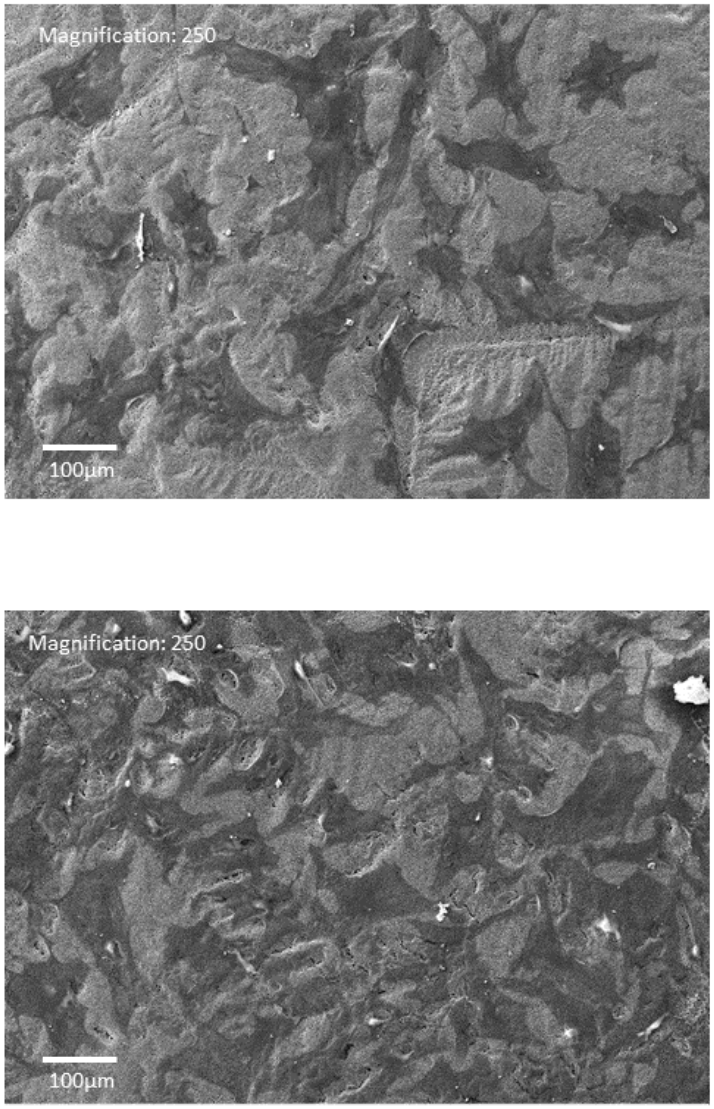

Figure A.1: SEM imaging of hADSCs grown on BDD–ppy6 and BDD–ppy8 samples after 7 days in culture. Both images show uniform growth of the cells on the substrate.

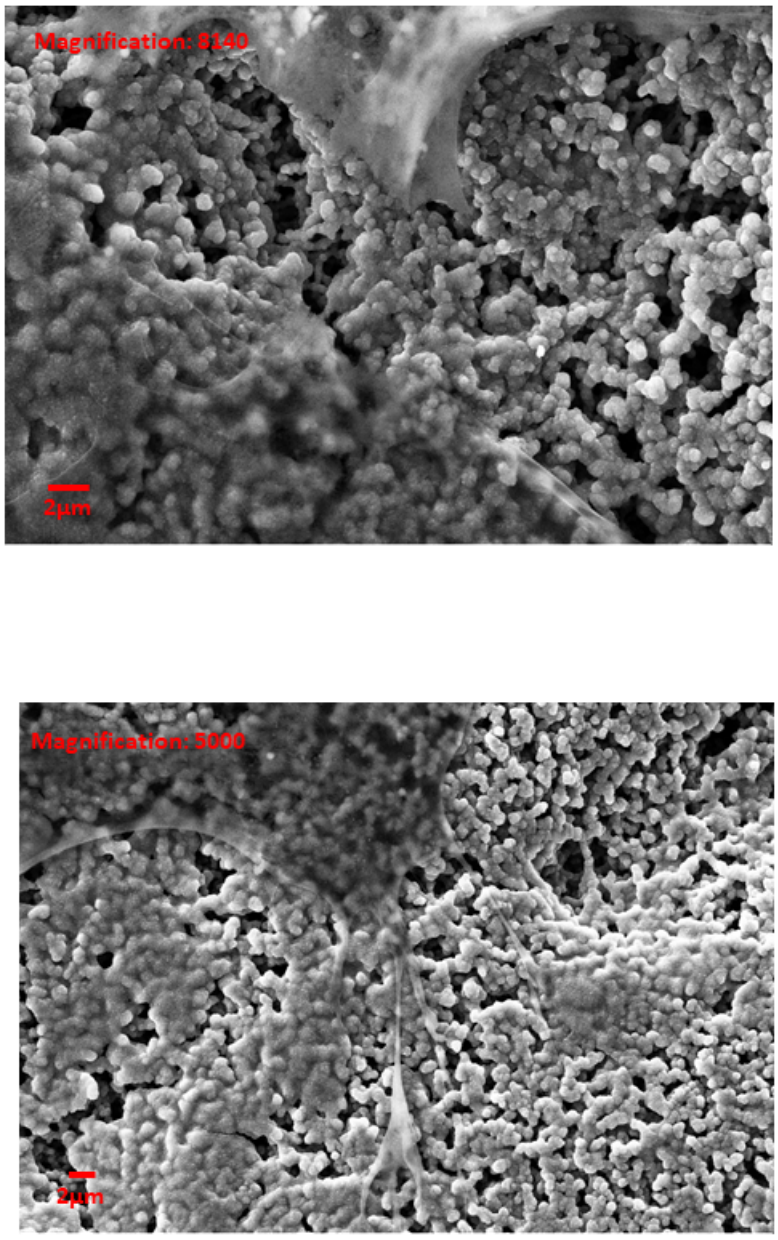

Figure A.2: SEM imaging of hADSCs grown on a BDD–ppy8 sample after 7 days in culture. Both images show protrusions grown by the main cell bodies towards the pores of the porus diamond structures.

Appendix A

Supplementary information to Chapter 6

In Chapter 6, ultimately H–ND–fibrin constructs were examined. However, efforts were made to create different types of scaffolds. Preliminary results derived from these experiments are presented in this appendix. Experiments were performed by the author and Ijeoma Patrick, MSc Nanotechnology who was supervised by the author at the time these results were obtained.

A.1 Materials and Methods

A.1.1 Chemicals

Fibrinogen from bovine plasma, thrombin from bovine plasma and collagen type I from rat tail tendons were purchased from Sigma-Aldrich, UK. 20-25 nm average Fluorescent nanodiamonds (FNDs) were purchased from Adamas Nanotechnologies, NC, USA and are stated by the supplier as "high brightness" FNDs containing up to 3ppm NV-minus centres.

A.1.2 Fluorescent nanodiamond characterisation

To characterise the fluorescence signal, 10 μl of FNDs (0.01 mg/ml) suspended in distilled water was pipetted onto a glass coverslip placed in a culture dish then left

to evaporate for 4 hours. A plain class coverslip was placed into a culture dish for the control. Size characterisation was done by dynamic light scattering (DLS) using a Brookhaven Instruments DLS system, 1 ml of FNDs (0.01 mg/ml) suspended in distilled water was pipetted into a cuvette and placed in the device.

A.1.3 Preparation of fibrin–fluorescent nanodiamond scaffolds

Firstly, 50 μl of fibrinogen (10–20 mg/ml) was added to a 96 well plate. FNDs suspended in distilled water (0.01 mg/ml) ranging in volumes from 1 - 3 µl were added to the wells and mixed with the fibrinogen. The crosslinked fibrin gel was generated by adding 50 µl of thrombin to (20-100 IU/ml) the wells and then mixing. The well plate was then placed on a plate shaker at 200 RPM for 30 minutes before being incubated at 37^{o}C for 1 hour and 15 minutes. The scaffolds were then transferred to a culture dish then 400 μl of PBS was poured over the scaffolds and in the surrounding wells to keep them hydrated before they were stored in a 4°C fridge. Controls without FNDs incorporated were also made in a separate well plate to minimise contamination.

A.1.4 Preparation of collagen–FND scaffolds

The protocol for creating the collagen scaffolds was adapted from one provided by the Ferretti lab. 8 scaffolds were prepared - 6 with FND (0.01 mg/ml) incorporation and 2 controls. The collagen stock solution was diluted with PBS and DMEM to achieve a final concentration of 2.7 mg/ml. 16 μl of FNDs were then added to the mix to achieve a final volume per scaffold of 2 μl. The pH of the solution was then adjusted to 7.4 by adding sterile 1M NaOH solution. Overall collagen hydrogels of volumes 100 µl and 150 µl were added to the 35 mm $\times$ 10 mm cell culture dishes before being incubated at 37 °C for 45 minutes. Halfway through the incubation time PBS was added on top of the scaffolds for hydration.

A.1.5 Confocal imaging of the fluorescent nanodiamonds

Multiphoton microscopy was carried out using a Mai Tai laser at a wavelength of 800 nm; after testing both higher and lower wavelengths this was shown to provide the best signal.

A.2 Results

Table A.1: Young's moduli values retrieved from the Nanoindenter for the fibrin-FND samples

Sample	**Young's modulus (Pa)**
Fibrin 1 control	0.84 ± 0.063
Fibrin 1–FND	1.22 ± 0.470
Fibrin 2 control	0.98 ± 0.053
Fibrin 2–FND	2.48 ± 1.309

The values for the Young's moduli indicate that the incorporation of the FNDs resulted in a 45-153% increase in the stiffness of Fibrin hydrogels. However, the corresponding Young's modulus values were at least three orders of magnitude lower. Furthermore, there are relatively high errors associated with the fibrin 1-FND and fibrin 2-FND scaffolds in comparison to the controls which is most likely due to higher level of heterogeneity in the material which indicates that the FNDs are not equally distributed to a high standard. This is most likely due to the experimental method which did not include any sonication of the ND with the fibrinogen to fully disperse them before polymerisation.

The collagen scaffolds were very sensitive to external environmental conditions and therefore it was difficult to perform mechanical characterisation on them with the equipment available.

A.3 Conclusions

Overall, while the fibrin scaffolds tested with the nanoindenter showed positive results in terms of enhancement of Young's Modulus with the inclusion of NDs, this method of fabrication was not considered further, as the resulting scaf-

folds, despite low content of FNDs within them, displayed low structural integrity and results were not repeatable. However, the process of incorporating FNDs in fibrin scaffolds informed the development of the protocols followed in Chapter 6. Furthermore, FNDs of this size were not detectable by the confocal microscope, and therefore were deemed not suitable for tracing dispersion within scaffolds by imaging methods.

Appendix B

AFM characterisation of hADSCs

As part of the work done in the time period of this thesis, the characterisation of the mechanical properties of hADSCs and CSPCs using AFM was attempted. The purpose of these experiments was to understand the mechanical properties of these cells and subsequently inform the exerimental design of the 3D scaffolds based on this results. Ultimately, the effort was not completed due to complicated experimental design. Nevertheless, these attempts led us to optimisations used for the nanoindentation results of Chapter 6.

In order to obtain more appropriate results, AFM measurements were obtained using a JPK Nanowizard II with a glass bead at the edge of the measurement tip. This method allows for not only more accurate topography of the cells, but also for better demonstration of the mechanical properties of the cells. In the figures below, both of these attributes are demonstrated.

Through these AFM measurements, some preliminary results on the Young's Modulus of hADSCs and CSPCs were obtained. They are shown below, in Table B.1.

Table B.1: Young's modulus values for hADSCs and CSPCs (n=3), 4 measurements per sample.

Sample	**Young's modulus (kPa)**
ADSCs	3.01 ± 1.05
CSPCs	2.78 ± 1.14

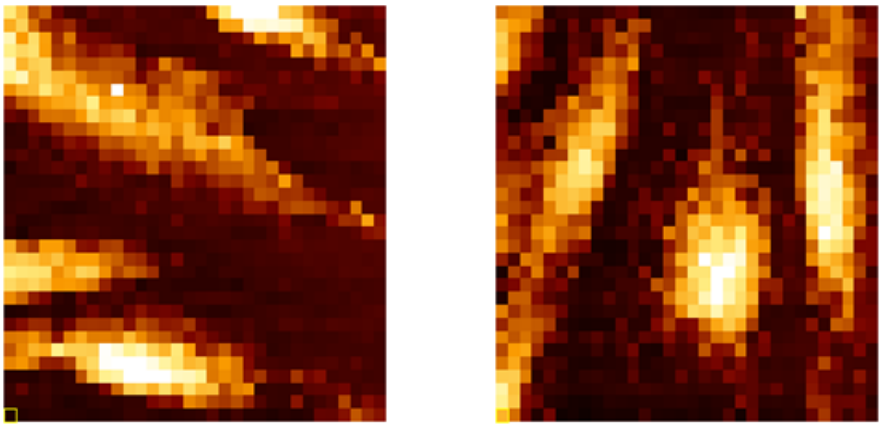

Figure B.1: Topological maps of CSPCs, derived using Atomic Force Microscopy (AFM). The map indicates the difference in the mechanical properties of the different parts of the cells, with 'softer' parts indicated in lighter colours and harder parts indicated in darker colours. The maps give a rough outline of the way the cells would look if we observed them under a microscope.

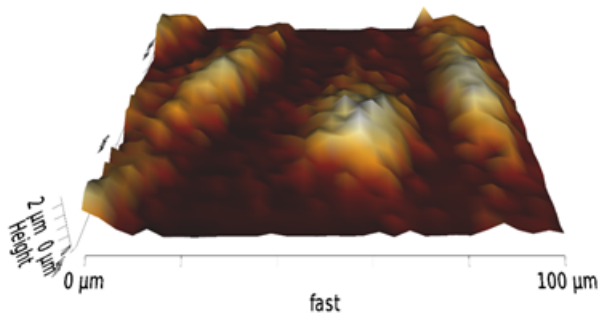

Figure B.2: 3D rendering of the AFM topography of chondroblasts seeded with density of 10000 cells/ cm^2. The x,y-axes indicate the scanning area, whereas the z-axis indicates the height of the scanned cells.

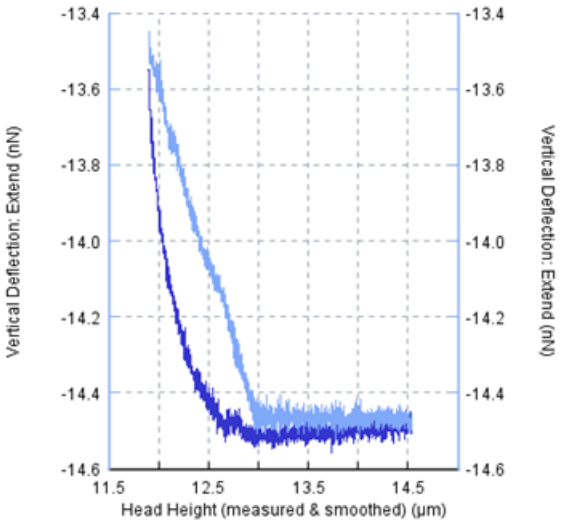

Figure B.3: The force demonstrates the vertical deflection that results from the contact of the conical AFM tip with the surface of the cell. The dark blue curve indicates the vertical deflection upon extension of the cantilever towards the substrate and the light blue curve indicates retraction of the cantilever.

These results give an interesting insight in the Young's Modulus of both cell times and imply similarities. However, further examination of these properties is required.

Bibliography

[1] C Vinatier, D Mrugala, C Jorgensen, J Guicheux, and D Noël. Cartilage engineering: a crucial combination of cells, biomaterials and biofactors. *Trends in biotechnology*, 27(5):307–314, 2009.

[2] Y Li, H Meng, Y Liu, and B Lee. Fibrin gel as an injectable biodegradable scaffold and cell carrier for tissue engineering. *The Scientific World Journal*, 2015, 2015.

[3] J Zazula. On graphite transformations at high temperature and pressure induced by absorption of the LHC beam. Technical report, CERN-LHC-Project-Note-78, 1997.

[4] C Hébert, E Scorsone, M Mermoux, and P Bergonzo. Porous diamond with high electrochemical performance. *Carbon*, 90:102–109, 2015.

[5] J Schindelin, I Arganda-Carreras, E Frise, V Kaynig, M Longair, T Pietzsch, S Preibisch, C Rueden, S Saalfeld, B Schmid, et al. Fiji: an open-source platform for biological-image analysis. *Nature methods*, 9(7):676, 2012.

[6] DK Reinhard, TA Grotjohn, M Becker, MK Yaran, T Schuelke, and J Asmussen. Fabrication and properties of ultranano, nano, and microcrystalline diamond membranes and sheets. *Journal of Vacuum Science & Technology B: Microelectronics and Nanometer Structures Processing, Measurement, and Phenomena*, 22(6):2811–2817, 2004.

[7] J Hunt and P Hobar. Common craniofacial anomalies: the facial dysostoses. *Plastic and reconstructive surgery*, 110(7):1714–25, 2002.

[8] J Vacanti and R Langer. Tissue engineering: the design and fabrication of living replacement devices for surgical reconstruction and transplantation. *The lancet*, 354:S32–S34, 1999.

[9] P Bianco and P G Robey. Stem cells in tissue engineering. *Nature*, 414 (6859):118, 2001.

[10] F J O'Brien. Biomaterials & scaffolds for tissue engineering. *Materials today*, 14(3):88–95, 2011.

[11] N De Isla, C Huseltein, N Jessel, A Pinzano, V Decot, J Magdalou, D Bensoussan, and J-F Stoltz. Introduction to tissue engineering and application for cartilage engineering. *Bio-medical materials and engineering*, 20(3-4): 127–133, 2010.

[12] U Meyer, T Meyer, J Handschel, and HP Wiesmann. *Fundamentals of tissue engineering and regenerative medicine*. Springer, Belin Germany, 2009.

[13] R Langer. Tissue engineering: perspectives, challenges, and future directions. *Tissue engineering*, 13(1):1–2, 2007.

[14] CA Chung, CW Yang, and CW Chen. Analysis of cell growth and diffusion in a scaffold for cartilage tissue engineering. *Biotechnology and bioengineering*, 94(6):1138–1146, 2006.

[15] N Isogai, H Kusuhara, Y Ikada, H Ohtani, R Jacquet, J Hillyer, E Lowder, and W J Landis. Comparison of different chondrocytes for use in tissue engineering of cartilage model structures. *Tissue engineering*, 12(4):691–703, 2006.

[16] R Sodian, P Fu, C Lueders, D Szymanski, C Fritsche, M Gutberlet, SP Hoerstrup, H Hausmann, T Lueth, and R Hetzer. Tissue engineering of vascular conduits: fabrication of custom-made scaffolds using rapid prototyping techniques. *The Thoracic and cardiovascular surgeon*, 53(03):144–149, 2005.

[17] H Muir. The chondrocyte, architect of cartilage. biomechanics, structure, function and molecular biology of cartilage matrix macromolecules. *Bioessays*, 17(12):1039–1048, 1995.

[18] WA Horton, JG Hall, and JT Hecht. Achondroplasia. *The Lancet*, 370(9582): 162–172, 2007.

[19] JT Hecht, CA Francomano, WA Horton, and JF Annegers. Mortality in achondroplasia. *American journal of human genetics*, 41(3):454, 1987.

[20] MD Irving, LS Chitty, S Mansour, and CM Hall. Chondrodysplasia punctata: a clinical diagnostic and radiological review. *Clinical dysmorphology*, 17(4): 229–241, 2008.

[21] Y Krishnan and AJ Grodzinsky. Cartilage diseases. *Matrix Biology*, 71: 51–69, 2018.

[22] TF Moyad. Cartilage injuries in the adult knee: evaluation and management. *Cartilage*, 2(3):226–236, 2011.

[23] J Jaroszewicz, A Kosowska, D Hutmacher, W Swieszkowski, and S Moskalewski. Insight into characteristic features of cartilage growth plate as a physiological template for bone formation. *Journal of Biomedical Materials Research Part A*, 104(2):357–366, 2016.

[24] AR Poole, T Kojima, T Yasuda, F Mwale, M Kobayashi, and S Laverty. Composition and structure of articular cartilage: a template for tissue repair. *Clinical Orthopaedics and Related Research*, 391:S26–S33, 2001.

[25] JA Buckwalter and HJ Mankin. Articular cartilage: part ii. *Journal of bone and joint surgery*, 79(4):612, 1997.

[26] AI Caplan. Cartilage. *Scientific American*, 251(4):84–97, 1984.

[27] VC Mow, MH Holmes, and WM Lai. Fluid transport and mechanical properties of articular cartilage: a review. *Journal of biomechanics*, 17(5):377–394, 1984.

[28] E Kheir and D Shaw. Hyaline articular cartilage. *Orthopaedics and Trauma*, 23(6):450–455, 2009.

[29] HJ Mankin, L Lippiello, et al. The glycosaminoglycans of normal and arthritic cartilage. *The Journal of clinical investigation*, 50(8):1712–1719, 1971.

[30] VH Pomin and B Mulloy. Glycosaminoglycans and proteoglycans, 2018.

[31] AJ Sophia Fox, A Bedi, and SA Rodeo. The basic science of articular cartilage: structure, composition, and function. *Sports health*, 1(6):461–468, 2009.

[32] G Quintarelli, BC Starcher, A Vocaturo, FD Gianfilippo, L Gotte, and RP Mecham. Fibrogenesis and biosynthesis of elastin in cartilage. *Connective tissue research*, 7(1):1–19, 1979.

[33] O Franke, K Durst, V Maier, M Göken, T Birkholz, H Schneider, F Hennig, and K Gelse. Mechanical properties of hyaline and repair cartilage studied by nanoindentation. *Acta Biomaterialia*, 3(6):873–881, 2007.

[34] ML Oyen, TAV Shean, DGT Strange, and M Galli. Size effects in indentation of hydrated biological tissues. *Journal of materials research*, 27(1):245–255, 2012.

[35] E Borchi, U Biggeri, F Lemeilleur, C Furetta, and Mara Bruzzi. Elastic moduli of polycrystalline diamond. Technical report, 1994.

[36] Engineering Toolbox. Embryology education and research website. `https://www.engineeringtoolbox.com/modulus-rigidity-d_946.html`, 2005.

[37] H-Ch Spatz and JFV Vincent. Young's moduli and shear moduli in cortical bone. *Proceedings of the Royal Society of London. Series B: Biological Sciences*, 263(1368):287–294, 1996.

[38] RA Stockwell. *Biology of cartilage cells*, volume 7. CUP Archive, Cambridge United Kingdom, 1979.

[39] CW Archer and P Francis-West. The chondrocyte. *The international journal of biochemistry & cell biology*, 35(4):401–404, 2003.

[40] JW Milgram. The classification of loose bodies in human joints. *Clinical orthopaedics and related research*, (124):282–291, 1977.

[41] ML Duynstee, HL Verwoerd-Verhoef, CD Verwoerd, and GJ Van Osch. The dual role of perichondrium in cartilage wound healing. *Plastic and reconstructive surgery*, 110(4):1073–1079, 2002.

[42] R St Gilmore and AJ Palfrey. Chondrocyte distribution in the articular cartilage of human femoral condyles. *Journal of anatomy*, 157:23, 1988.

[43] RA Stockwell. Chondrocytes. *Journal of Clinical Pathology. Supplement (Royal College of Pathologists).*, 12:7, 1978.

[44] NZ Zambrano, GS Montes, KM Shigihara, EM Sanchez, and LCU Junqueira. Collagen arrangement in cartilages. *Cells Tissues Organs*, 113(1):26–38, 1982.

[45] A Maroudas, P Bullough, SAV Swanson, and MAR Freeman. The permeability of articular cartilage. *The Journal of bone and joint surgery. British volume*, 50(1):166–177, 1968.

[46] M Benjamin and EJ Evans. Fibrocartilage. *Journal of anatomy*, 171:1, 1990.

[47] M Benjamin, RN Tyers, and JR Ralphs. Age-related changes in tendon fibrocartilage. *Journal of anatomy*, 179:127, 1991.

[48] RF MacBarb, AL Chen, JC Hu, and KA Athanasiou. Engineering functional anisotropy in fibrocartilage neotissues. *Biomaterials*, 34(38):9980–9989, 2013.

[49] H Liu. *Nanocomposites for musculoskeletal tissue regeneration*. Woodhead Publishing, Cambridge MA, 2016.

[50] J Watkins. *Pocket Podiatry: Functional Anatomy*. Elsevier Health Sciences, Cambridge MA, 2009.

[51] C Kiecker, T Bates, and E Bell. Molecular specification of germ layers in vertebrate embryos. *Cellular and Molecular Life Sciences*, 73(5):923–947, 2016.

[52] MB Goldring, K Tsuchimochi, and K Ijiri. The control of chondrogenesis. *Journal of cellular biochemistry*, 97(1):33–44, 2006.

[53] S Foppiano, D Hu, and RS Marcucio. Signaling by bone morphogenetic proteins directs formation of an ectodermal signaling center that regulates craniofacial development. *Developmental biology*, 312(1):103–114, 2007.

[54] TW Glenister. An embryological view of cartilage. *Journal of anatomy*, 122 (Pt 2):323, 1976.

[55] EF Wagner and G Karsenty. Genetic control of skeletal development. *Current opinion in genetics & development*, 11(5):527–532, 2001.

[56] EJ Mackie, YA Ahmed, L Tatarczuch, K-S Chen, and M Mirams. Endochondral ossification: how cartilage is converted into bone in the developing skeleton. *The international journal of biochemistry & cell biology*, 40(1): 46–62, 2008.

[57] BS Yoon and KM Lyons. Multiple functions of bmps in chondrogenesis. *Journal of cellular biochemistry*, 93(1):93–103, 2004.

[58] T Wagner, J Wirth, J Meyer, B Zabel, M Held, J Zimmer, J Pasantes, FD Bricarelli, J Keutel, E Hustert, et al. Autosomal sex reversal and campomelic dysplasia are caused by mutations in and around the sry-related gene sox9. *Cell*, 79(6):1111–1120, 1994.

[59] C Kwok, PA Weller, S Guioli, JW Foster, S Mansour, O Zuffardi, HH Punnett, MA Dominguez-Steglich, JD Brook, ID Young, et al. Mutations in sox9, the gene responsible for campomelic dysplasia and autosomal sex reversal. *American journal of human genetics*, 57(5):1028, 1995.

[60] V Lefebvre, P Li, and B De Crombrugghe. A new long form of sox5 (l-sox5), sox6 and sox9 are coexpressed in chondrogenesis and cooperatively activate the type ii collagen gene. *The EMBO journal*, 17(19):5718–5733, 1998.

[61] LC Murtaugh, JH Chyung, and AB Lassar. Sonic hedgehog promotes somitic chondrogenesis by altering the cellular response to bmp signaling. *Genes & development*, 13(2):225–237, 1999.

[62] F Yano, F Kugimiya, S Ohba, T Ikeda, H Chikuda, T Ogasawara, N Ogata, T Takato, K Nakamura, H Kawaguchi, et al. The canonical wnt signaling pathway promotes chondrocyte differentiation in a sox9-dependent manner. *Biochemical and biophysical research communications*, 333(4):1300–1308, 2005.

[63] D Correa, RA Somoza, P Lin, S Greenberg, E Rom, L Duesler, JF Welter, A Yayon, and AI Caplan. Sequential exposure to fibroblast growth factors (fgf) 2, 9 and 18 enhances hmsc chondrogenic differentiation. *Osteoarthritis and Cartilage*, 23(3):443–453, 2015.

[64] D Yu, J Han, and B Kim. Stimulation of chondrogenic differentiation of mesenchymal stem cells. *International journal of stem cells*, 5(1):16, 2012.

[65] CM Leonard, HM Fuld, DA Frenz, SA Downie, J Massague, and SA Newman. Role of transforming growth factor-β in chondrogenic pattern formation in the embryonic limb: stimulation of mesenchymal condensation and fibronectin gene expression by exogenenous tgf-β and evidence for endogenous tgf-β-like activity. *Developmental biology*, 145(1):99–109, 1991.

[66] T Hattori, C Müller, S Gebhard, E Bauer, F Pausch, B Schlund, MR Bösl, A Hess, C Surmann-Schmitt, H Von Der Mark, et al. Sox9 is a major negative

regulator of cartilage vascularization, bone marrow formation and endochondral ossification. *Development*, 137(6):901–911, 2010.

[67] F Shapiro, S Koide, and MJ Glimcher. Cell origin and differentiation in the repair of full-thickness defects of articular cartilage. *The Journal of bone and joint surgery. American volume*, 75(4):532–553, 1993.

[68] Y Gao, S Liu, J Huang, W Guo, J Chen, L Zhang, B Zhao, J Peng, A Wang, Y Wang, et al. The ecm-cell interaction of cartilage extracellular matrix on chondrocytes. *BioMed research international*, 2014, 2014.

[69] MA Hill. Embryology education and research website. `https://embryology.med.unsw.edu.au`, 1997.

[70] JT Hancock. *Cell signalling*. Oxford University Press, Oxford United Kingdom, 2017.

[71] DE Ingber. Cellular mechanotransduction: putting all the pieces together again. *The FASEB journal*, 20(7):811–827, 2006.

[72] RO Hynes. Integrins: versatility, modulation, and signaling in cell adhesion. *Cell*, 69(1):11–25, 1992.

[73] M Rumpler, A Woesz, JWC Dunlop, JT Van Dongen, and P Fratzl. The effect of geometry on three-dimensional tissue growth. *Journal of the Royal Society Interface*, 5(27):1173–1180, 2008.

[74] A Nusrat, JR Turner, JL Madara, et al. Molecular physiology and pathophysiology of tight junctions. iv. regulation of tight junctions by extracellular stimuli: nutrients, cytokines, and immune cells. *American Journal of Physiology*, 279(1):G851–G857, 2000.

[75] R Rajaraman, DE Rounds, SPS Yen, and ANDA Rembaum. A scanning electron microscope study of cell adhesion and spreading in vitro. *Experimental Cell Research*, 88(2):327–339, 1974.

[76] SK Mitra, DA Hanson, and DD Schlaepfer. Focal adhesion kinase: in command and control of cell motility. *Nature reviews Molecular cell biology*, 6 (1):56–68, 2005.

[77] ND Gallant, KE Michael, and AJ García. Cell adhesion strengthening: contributions of adhesive area, integrin binding, and focal adhesion assembly. *Molecular biology of the cell*, 16(9):4329–4340, 2005.

[78] KE Michael, DW Dumbauld, KL Burns, SK Hanks, and AJ García. Focal adhesion kinase modulates cell adhesion strengthening via integrin activation. *Molecular biology of the cell*, 20(9):2508–2519, 2009.

[79] CH Golias, A Charalabopoulos, and K Charalabopoulos. Cell proliferation and cell cycle control: a mini review. *International journal of clinical practice*, 58(12):1134–1141, 2004.

[80] T Nouspikel and PC Hanawalt. DNA repair in terminally differentiated cells. *DNA repair*, 1(1):59–75, 2002.

[81] HA Coller, L Sang, and JM Roberts. A new description of cellular quiescence. *PLoS Biol*, 4(3):e83, 2006.

[82] R Poulsom, MR Alison, SJ Forbes, and NA Wright. Adult stem cell plasticity. *The Journal of Pathology: A Journal of the Pathological Society of Great Britain and Ireland*, 197(4):441–456, 2002.

[83] AW Seifert and K Muneoka. The blastema and epimorphic regeneration in mammals. *Developmental biology*, 433(2):190–199, 2018.

[84] N Barker, S Bartfeld, and H Clevers. Tissue-resident adult stem cell populations of rapidly self-renewing organs. *Cell stem cell*, 7(6):656–670, 2010.

[85] S Hemmat, DM Lieberman, and SP Most. An introduction to stem cell biology. *Facial plastic surgery*, 26(05):343–349, 2010.

[86] S Mitalipov and D Wolf. Totipotency, pluripotency and nuclear reprogramming. In *Engineering of stem cells*, pages 185–199. Springer, Berlin Germany, 2009.

[87] Y Jiang, BN Jahagirdar, R Reinhardt, RE Schwartz, CD Keene, XR Ortiz-Gonzalez, M Reyes, T Lenvik, T Lund, M Blackstad, et al. Pluripotency of mesenchymal stem cells derived from adult marrow. *Nature*, 418(6893): 41–49, 2002.

[88] MF Pittenger, AM Mackay, SC Beck, RK Jaiswal, R Douglas, JD Mosca, MA Moorman, DW Simonetti, S Craig, and DR Marshak. Multilineage potential of adult human mesenchymal stem cells. *science*, 284(5411):143–147, 1999.

[89] S Kern, H Eichler, J Stoeve, H Klüter, and K Bieback. Comparative analysis of mesenchymal stem cells from bone marrow, umbilical cord blood, or adipose tissue. *Stem cells*, 24(5):1294–1301, 2006.

[90] D Noël, D Caton, S Roche, C Bony, S Lehmann, L Casteilla, C Jorgensen, and B Cousin. Cell specific differences between human adipose-derived and mesenchymal–stromal cells despite similar differentiation potentials. *Experimental cell research*, 314(7):1575–1584, 2008.

[91] PA Zuk, M Zhu, H Mizuno, J Huang, JW Futrell, AJ Katz, P Benhaim, HP Lorenz, and MH Hedrick. Multilineage cells from human adipose tissue: implications for cell-based therapies. *Tissue engineering*, 7(2):211–228, 2001.

[92] W Tsuji, JP Rubin, and KG Marra. Adipose-derived stem cells: Implications in tissue regeneration. *World journal of stem cells*, 6(3):312, 2014.

[93] H Mizuno, M Tobita, and AC Uysal. Concise review: adipose-derived stem cells as a novel tool for future regenerative medicine. *Stem cells*, 30(5):804–810, 2012.

[94] SEP New, C Alvarez-Gonzalez, B Vagaska, SG Gomez, NW Bulstrode, A Madrigal, and P Ferretti. A matter of identity—phenotype and differentiation potential of human somatic stem cells. *Stem cell research*, 15(1):1–13, 2015.

[95] L Guasti, B Vagaska, NW Bulstrode, AM Seifalian, and P Ferretti. Chondrogenic differentiation of adipose tissue-derived stem cells within nanocaged poss-pcu scaffolds: a new tool for nanomedicine. *Nanomedicine: Nanotechnology, Biology and Medicine*, 10(2):279–289, 2014.

[96] JB Richardson, B Caterson, EH Evans, BA Ashton, and S Roberts. Repair of human articular cartilage after implantation of autologous chondrocytes. *The Journal of bone and joint surgery. British volume*, 81(6):1064–1068, 1999.

[97] Y Jiang and RS Tuan. Origin and function of cartilage stem/progenitor cells in osteoarthritis. *Nature Reviews Rheumatology*, 11(4):206, 2015.

[98] D Seol, DJ McCabe, H Choe, H Zheng, Y Yu, K Jang, MW Walter, AD Lehman, L Ding, JA Buckwalter, et al. Chondrogenic progenitor cells respond to cartilage injury. *Arthritis & Rheumatism*, 64(11):3626–3637, 2012.

[99] S Koelling, J Kruegel, M Irmer, JR Path, B Sadowski, X Miro, and N Miosge. Migratory chondrogenic progenitor cells from repair tissue during the later stages of human osteoarthritis. *Cell stem cell*, 4(4):324–335, 2009.

[100] AG Tay, J Farhadi, R Suetterlin, G Pierer, M Heberer, and I Martin. Cell yield, proliferation, and postexpansion differentiation capacity of human ear, nasal, and rib chondrocytes. *Tissue engineering*, 10(5-6):762–770, 2004.

[101] GJ Van Osch, SW van der Veen, and HL Verwoerd-Verhoef. In vitro redifferentiation of culture-expanded rabbit and human auricular chondrocytes for cartilage reconstruction. *Plastic and reconstructive surgery*, 107(2):433–440, 2001.

[102] T Togo, A Utani, M Naitoh, M Ohta, Y Tsuji, N Morikawa, M Nakamura, and S Suzuki. Identification of cartilage progenitor cells in the adult ear perichondrium: utilization for cartilage reconstruction. *Laboratory Investigation*, 86(5):445–457, 2006.

[103] A Rodriguez, YL Cao, C Ibarra, S Pap, M Vacanti, RD Eavey, and CA Vacanti. Characteristics of cartilage engineered from human pediatric auricular cartilage. *Plastic and reconstructive surgery*, 103(4):1111–1119, 1999.

[104] J Park and RS Lakes. *Biomaterials: an introduction*. Springer Science & Business Media, Berlin Germany, 2007.

[105] JO Hollinger. *An introduction to biomaterials*. CRC press, Boca Raton FL, 2011.

[106] V Migonney. History of biomaterials. *Biomaterials*, pages 1–10, 2014.

[107] N Huebsch and DJ Mooney. Inspiration and application in the evolution of biomaterials. *Nature*, 462(7272):426, 2009.

[108] M Vallet-Regí. Evolution of bioceramics within the field of biomaterials. *Comptes Rendus Chimie*, 13(1-2):174–185, 2010.

[109] I Kulinets. Biomaterials and their applications in medicine. In *Regulatory affairs for biomaterials and medical devices*, pages 1–10. Woodhead Publishing, Sawston UK, 2015.

[110] C Frantz, KM Stewart, and VM Weaver. The extracellular matrix at a glance. *Journal of cell science*, 123(24):4195–4200, 2010.

[111] LS Nair and CT Laurencin. Biodegradable polymers as biomaterials. *Progress in polymer science*, 32(8-9):762–798, 2007.

[112] DF Williams. On the mechanisms of biocompatibility. *Biomaterials*, 29(20): 2941–2953, 2008.

[113] M d'Angelo, E Benedetti, MG Tupone, M Catanesi, V Castelli, A Antonosante, and A Cimini. The role of stiffness in cell reprogramming: A potential role for biomaterials in inducing tissue regeneration. *Cells*, 8(9): 1036, 2019.

[114] AK Gaharwar, I Singh, and A Khademhosseini. Engineered biomaterials for in situ tissue regeneration. *Nature Reviews Materials*, 5(9):686–705, 2020.

[115] MC van Turnhout. *Postnatal development of articular cartilage*. Wageningen University, Wageningen Netherlands, 2010.

[116] R Khan and MH Khan. Use of collagen as a biomaterial: An update. *Journal of Indian Society of Periodontology*, 17(4):539, 2013.

[117] R Parenteau-Bareil, R Gauvin, and F Berthod. Collagen-based biomaterials for tissue engineering applications. *Materials*, 3(3):1863–1887, 2010.

[118] Z Pan and J Ding. Poly (lactide-co-glycolide) porous scaffolds for tissue engineering and regenerative medicine. *Interface focus*, 2(3):366–377, 2012.

[119] JO Akindoyo, MdDH Beg, S Ghazali, MR Islam, N Jeyaratnam, and AR Yuvaraj. Polyurethane types, synthesis and applications–a review. *RSC Advances*, 6(115):114453–114482, 2016.

[120] MF Akhtar, M Hanif, and NM Ranjha. Methods of synthesis of hydrogels… a review. *Saudi Pharmaceutical Journal*, 24(5):554–559, 2016.

[121] M Bernard, E Jubeli, MD Pungente, and N Yagoubi. Biocompatibility of polymer-based biomaterials and medical devices–regulations, in vitro screening and risk-management. *Biomaterials science*, 6(8):2025–2053, 2018.

[122] JW Weisel and RI Litvinov. Fibrin formation, structure and properties. In *Fibrous Proteins: Structures and Mechanisms*, pages 405–456. Springer International Publishing, Cham, 2017.

[123] MW Mosesson. Fibrinogen and fibrin structure and functions. *Journal of thrombosis and haemostasis*, 3(8):1894–1904, 2005.

[124] L Le Guéhennec, P Layrolle, G Daculsi, et al. A review of bioceramics and fibrin sealant. *European Cells and Materials*, 8(13):1–11, 2004.

[125] M Pieters and AS Wolberg. Fibrinogen and fibrin: An illustrated review. *Research and practice in thrombosis and haemostasis*, 3(2):161–172, 2019.

[126] P de la Puente and D Ludeña. Cell culture in autologous fibrin scaffolds for applications in tissue engineering. *Experimental cell research*, 322(1):1–11, 2014.

[127] A Noori, SJ Ashrafi, R Vaez-Ghaemi, A Hatamian-Zaremi, and TJ Webster. A review of fibrin and fibrin composites for bone tissue engineering. *International journal of nanomedicine*, 12:4937, 2017.

[128] I Dion, X Roques, H Baquey, E Baudet, B Basse Cathalinat, and N More. Hemocompatibility of diamond-like carbon coating. *Bio-medical materials and engineering*, 3(1):51–55, 1993.

[129] X Gao, S Wang, Y Xu, H Li, H Zhao, and X Pan. Ferulic acid and pdms modified medical carbon materials for artificial joint prosthesis. *Plos one*, 13 (9):e0203542, 2018.

[130] JC Bokros, VL Gott, LD La Grange, AM Fadall, KD Vos, and MD Ramos. Correlations between blood compatibility and heparin adsorptivity for an impermeable isotropic pyrolytic carbon. *Journal of biomedical materials research*, 3(3):497–528, 1969.

[131] T Shirzadian, S Bagheri, H SaeidiBorojeni, P Ghaffari, F Foroughi, and M Mahboubi. The role of biocompatible coatings of biomaterials for creation of direct and appropriate chemical bounding between bioimplant and bone tissue. *Journal of Injury and Violence Research*, 4(3):S41, 2012.

[132] A Nouri and C Wen. Introduction to surface coating and modification for metallic biomaterials. *Surface Coating and Modification of Metallic Biomaterials*, pages 3–60, 2015.

[133] M Amaral, PS Gomes, MA Lopes, JD Santos, RF Silva, and MH Fernandes. Nanocrystalline diamond as a coating for joint implants: cytotoxicity and biocompatibility assessment. *Journal of Nanomaterials*, 2008:27, 2008.

[134] M Alcaide, A Taylor, M Fjorback, V Zachar, and CP Pennisi. Boron-doped nanocrystalline diamond electrodes for neural interfaces: in vivo biocompatibility evaluation. *Frontiers in neuroscience*, 10:87, 2016.

[135] CP Pennisi and M Alcaide. Nanocrystalline diamond films for biomedical applications. In *Design, Synthetic Strategies and Biocompatibility of Polymer Scaffolds for Biomedical Application*, pages 70–100. Bentham Science Publishers, Sharjah UAE, 2014.

[136] L Fusco, E Avitabile, V Armuzza, M Orecchioni, A Istif, D Bedognetti, T Da Ros, and LG Delogu. Impact of the surface functionalization on nanodiamond biocompatibility: a comprehensive view on human blood immune cells. *Carbon*, 160:390–404, 2020.

[137] Y Zhu, J Li, W Li, Y Zhang, X Yang, N Chen, Y Sun, Y Zhao, C Fan, and Q Huang. The biocompatibility of nanodiamonds and their application in drug delivery systems. *Theranostics*, 2(3):302, 2012.

[138] S Chauhan, N Jain, and U Nagaich. Nanodiamonds with powerful ability for drug delivery and biomedical applications: Recent updates on in vivo study and patents. *Journal of pharmaceutical analysis*, 10(1):1–12, 2020.

[139] CA Brookes and EJ Brookes. Diamond in perspective: a review of mechanical properties of natural diamond. *Diamond and related materials*, 1(1): 13–17, 1991.

[140] LS Pan and DR Kania. *Diamond: electronic properties and applications*. Springer Science & Business Media, Berlin Germany, 2013.

[141] RP Mildren et al. Intrinsic optical properties of diamond. *Optical Engineering of Diamond*, 1:1–34, 2013.

[142] W Grochala. Diamond: electronic ground state of carbon at temperatures approaching 0 k. *Angewandte Chemie International Edition*, 53(14):3680–3683, 2014.

[143] AC Taylor, B Vagaska, R Edgington, C Hébert, P Ferretti, P Bergonzo, and RB Jackman. Biocompatibility of nanostructured boron doped diamond for the attachment and proliferation of human neural stem cells. *Journal of neural engineering*, 12(6):066016, 2015.

[144] L Pauling. The nature of the chemical bond. application of results obtained from the quantum mechanics and from a theory of paramagnetic susceptibility to the structure of molecules. *Journal of the American Chemical Society*, 53(4):1367–1400, 1931.

[145] AJ Domb, J Kost, and D Wiseman. *Handbook of biodegradable polymers*, volume 7. CRC press, Boca Raton FL, 1998.

[146] CA Weitz. *Human Biology*, 59(5):862–864, 1987.

[147] NV Bhagavan. *Medical biochemistry*. Academic press, Cambridge MA, 2002.

[148] JR Porter, TT Ruckh, and KC Popat. Bone tissue engineering: a review in bone biomimetics and drug delivery strategies. *Biotechnology progress*, 25 (6):1539–1560, 2009.

[149] WH Bragg and WL Bragg. The structure of the diamond. *Proceedings of the Royal Society of London. Series A, Containing Papers of a Mathematical and Physical Character*, 89(610):277–291, 1913.

[150] J Singh. *Physics of Semiconductors and Their Heterostructures*. McGraw-Hill, New York NY, 1993.

[151] T Hom, W Kiszenik, and B Post. Accurate lattice constants from multiple reflection measurements. ii. lattice constants of germanium silicon, and diamond. *Journal of Applied Crystallography*, 8(4):457–458, 1975.

[152] RS Sussmann. *CVD diamond for electronic devices and sensors*, volume 26. John Wiley & Sons, Hoboken NJ, 2009.

[153] GP Bulanova. The formation of diamond. *Journal of Geochemical Exploration*, 53(1-3):1–23, 1995.

[154] HO Pierson. *Handbook of carbon, graphite, diamonds and fullerenes: processing, properties and applications*. William Andrew, Norwich NY, 2012.

[155] JR Hannay. Vi. on the artificial formation of the diamond. *Proceedings of the Royal Society of London*, 30(200-205):450–461, 1880.

[156] FP Bundy, H Tracy Hall, HM Strong, and RH Wentorfjun. Man-made diamonds. *Nature*, 176(4471):51–55, 1955.

[157] HP Bovenkerk, FP Bundy, HM Strong, RH Wentorf, and HT Hall. Preparation of diamond. *Nature*, 184, 1959.

[158] JC Angus, Y Wang, and M Sunkara. Metastable growth of diamond and diamond-like phases. *Annual Review of Materials Science*, 21(1):221–248, 1991.

[159] M Naamoun, A Tallaire, F Silva, J Achard, P Doppelt, and A Gicquel. Etch-pit formation mechanism induced on HPHT and CVD diamond single crystals by H2/O2 plasma etching treatment: Part of topical section on fundamentals and applications of diamond. *physica status solidi (a)*, 209(9):1715–1720, 2012.

[160] W Eversole. Synthesis of diamond, November 1961. US patent 3030187 and 3003188.

[161] JC Angus, A Argoitia, R Gat, Z Li, M Sunkara, L Wang, and Y Wang. Chemical vapour deposition of diamond. *Philosophical Transactions of the Royal Society of London. Series A: Physical and Engineering Sciences*, 342(1664): 195–208, 1993.

[162] S Matsumoto, Y Sato, M Kamo, and N Setaka. Vapor deposition of diamond particles from methane. *Japanese Journal of applied physics*, 21(4A):L183, 1982.

[163] H Liu and DS Dandy. 3 - diamond CVD techniques. In H Liu and DS Dandy, editors, *Diamond Chemical Vapor Deposition*, pages 14–45. William Andrew Publishing, Park Ridge, NJ, 1995.

[164] M Kamo, Y Sato, S Matsumoto, and N Setaka. Diamond synthesis from gas phase in microwave plasma. *Journal of crystal growth*, 62(3):642–644, 1983.

[165] A Krueger. The structure and reactivity of nanoscale diamond. *Journal of Materials Chemistry*, 18(13):1485–1492, 2008.

[166] VN Mochalin, O Shenderova, D Ho, and Y Gogotsi. The properties and applications of nanodiamonds. *Nature nanotechnology*, 7(1):11–23, 2012.

[167] M Ibrahim, Y Xue, M Ostermann, A Sauter, D Steinmueller-Nethl, S Schweeberg, A Krueger, MR Cimpan, and K Mustafa. In vitro cytotoxicity assessment of nanodiamond particles and their osteogenic potential. *Journal of Biomedical Materials Research Part A*, 106(6):1697–1707, 2018.

[168] CC Fu, HY Lee, K Chen, TS Lim, HY Wu, PK Lin, PK Wei, PH Tsao, HC Chang, and W Fann. Characterization and application of single fluorescent nanodiamonds as cellular biomarkers. *Proceedings of the National Academy of Sciences*, 104(3):727–732, 2007.

[169] G Laporte and D Psaltis. Sted imaging of green fluorescent nanodiamonds containing nitrogen-vacancy-nitrogen centers. *Biomedical optics express*, 7 (1):34–44, 2016.

[170] T-C Hsu, K-K Liu, H-C Chang, E Hwang, and J-I Chao. Labeling of neuronal differentiation and neuron cells with biocompatible fluorescent nanodiamonds. *Scientific reports*, 4:5004, 2014.

[171] D Delabouglise, B Marcus, M Mermoux, P Bouvier, J Chane-Tune, JP Petit, P Mailley, and T Livache. Biotin grafting on boron-doped diamond. *Chemical Communications*, (21):2698–2699, 2003.

[172] R Ohta, N Saito, Y Inoue, H Sugimura, and O Takai. Organosilane self-assembled monolayers directly linked to the diamond surfaces. *Journal of Vacuum Science & Technology A: Vacuum, Surfaces, and Films*, 22(5):2005–2009, 2004.

[173] R Boukherroub, X Wallart, S Szunerits, B Marcus, P Bouvier, and M Mermoux. Photochemical oxidation of hydrogenated boron-doped diamond surfaces. *Electrochemistry Communications*, 7(9):937–940, 2005.

[174] H Kanazawa, KS Song, T Sakai, Y Nakamura, H Umezawa, M Tachiki, and H Kawarada. Effect of iodide ions on the hydrogen-terminated and partially oxygen-terminated diamond surface. *Diamond and related materials*, 12(3-7):618–622, 2003.

[175] M Riedel, J Ristein, and L Ley. The impact of ozone on the surface conductivity of single crystal diamond. *Diamond and related materials*, 13(4-8): 746–750, 2004.

[176] S Szunerits and R Boukherroub. Different strategies for functionalization of diamond surfaces. *Journal of Solid State Electrochemistry*, 12(10):1205–1218, 2008.

[177] J Robertson. Diamond-like amorphous carbon. *Materials science and engineering: R: Reports*, 37(4-6):129–281, 2002.

[178] L Tang, C Tsai, WW Gerberich, L Kruckeberg, and DR Kania. Biocompatibility of chemical-vapour-deposited diamond. *Biomaterials*, 16(6):483–488, 1995.

[179] M Parizek, TEL Douglas, K Novotna, A Kromka, MA Brady, A Renzing, E Voss, M Jarosova, L Palatinus, P Tesarek, et al. Nanofibrous poly (lactide-co-glycolide) membranes loaded with diamond nanoparticles as promising substrates for bone tissue engineering (vol 7, pg 1931, 2012). *International Journal of Nanomedicine*, 7:5873–5873, 2012.

[180] V Thomas, BA Halloran, N Ambalavanan, SA Catledge, and YK Vohra. In vitro studies on the effect of particle size on macrophage responses to nanodiamond wear debris. *Acta biomaterialia*, 8(5):1939–1947, 2012.

[181] W Yang, O Auciello, JE Butler, W Cai, JA Carlisle, JE Gerbi, DM Gruen, T Knickerbocker, TL Lasseter, JN Russell, et al. DNA-modified nanocrystalline diamond thin-films as stable, biologically active substrates. *Nature materials*, 1(4):253–257, 2002.

[182] L Nordsletten, AKM Høgåsen, YT Konttinen, S Santavirta, P Aspenberg, and AO Aasen. Human monocytes stimulation by particles of hydroxyapatite, silicon carbide and diamond: in vitro studies of new prosthesis coatings. *Biomaterials*, 17(15):1521–1527, 1996.

[183] LW Tsai, YC Lin, E Perevedentseva, A Lugovtsov, A Priezzhev, and CL Cheng. Nanodiamonds for medical applications: interaction with blood in vitro and in vivo. *International journal of molecular sciences*, 17(7):1111, 2016.

[184] A Alanazi, C Nojiri, T Noguchi, T Kido, Y Komatsu, K Hirakuri, A Funakubo, K Sakai, and Y Fukui. Improved blood compatibility of DLC coated polymeric material. *Asaio Journal*, 46(4):440–443, 2000.

[185] RJ Narayan, W Wei, C Jin, M Andara, A Agarwal, RA Gerhardt, Chun-Che Shih, Chun-Ming Shih, Shing-Jong Lin, Yea-Yang Su, et al. Microstructural and biological properties of nanocrystalline diamond coatings. *Diamond and Related Materials*, 15(11-12):1935–1940, 2006.

[186] L Marcon, F Riquet, D Vicogne, S Szunerits, JF Bodart, and R Boukherroub. Cellular and in vivo toxicity of functionalized nanodiamond in xenopus embryos. *Journal of Materials Chemistry*, 20(37):8064–8069, 2010.

[187] A Cid, A Picado, JB Correia, R Chaves, H Silva, J Caldeira, AP Alves de Matos, and MS Diniz. Oxidative stress and histological changes following exposure to diamond nanoparticles in the freshwater asian clam corbicula fluminea (müller, 1774). *Journal of hazardous materials*, 284:27–34, 2015.

[188] E Mendonça, M Diniz, L Silva, I Peres, L Castro, J Brito Correia, and A Picado. Effects of diamond nanoparticle exposure on the internal structure and reproduction of daphnia magna. *Journal of hazardous materials*, 186(1): 265–271, 2011.

[189] S Szunerits, A Barras, and R Boukherroub. Antibacterial applications of nanodiamonds. *International journal of environmental research and public health*, 13(4):413, 2016.

[190] PA Nistor and PW May. Diamond thin films: giving biomedical applications a new shine. *Journal of the royal society interface*, 14(134):20170382, 2017.

[191] P Bajaj, D Akin, A Gupta, D Sherman, B Shi, O Auciello, and R Bashir. Ultrananocrystalline diamond film as an optimal cell interface for biomedical applications. *Biomedical microdevices*, 9(6):787–794, 2007.

[192] AP Hopper, JM Dugan, AA Gill, OJL Fox, PW May, JW Haycock, and F Claeyssens. Amine functionalized nanodiamond promotes cellular adhesion, proliferation and neurite outgrowth. *Biomedical materials*, 9(4): 045009, 2014.

[193] YC Chen, DC Lee, TY Tsai, CY Hsiao, JW Liu, CY Kao, HK Lin, HC Chen, TJ Palathinkal, WF Pong, et al. Induction and regulation of differentiation in neural stem cells on ultra-nanocrystalline diamond films. *Biomaterials*, 31 (21):5575–5587, 2010.

[194] PA Nistor, PW May, F Tamagnini, AD Randall, and MA Caldwell. Long-term culture of pluripotent stem-cell-derived human neurons on diamond–a substrate for neurodegeneration research and therapy. *Biomaterials*, 61:139–149, 2015.

[195] T Lechleitner, F Klauser, T Seppi, J Lechner, P Jennings, P Perco, B Mayer, D Steinmüller-Nethl, J Preiner, P Hinterdorfer, et al. The surface properties of nanocrystalline diamond and nanoparticulate diamond powder and their suitability as cell growth support surfaces. *Biomaterials*, 29(32):4275–4284, 2008.

[196] M Baidakova and A Vul. New prospects and frontiers of nanodiamond clusters. *Journal of Physics D: Applied Physics*, 40(20):6300, 2007.

[197] Y Ikada. *Tissue engineering: fundamentals and applications*. Elsevier, Cambridge MA, 2011.

[198] M Kalbacova, B Rezek, V Baresova, C Wolf-Brandstetter, and A Kromka. Nanoscale topography of nanocrystalline diamonds promotes differentiation of osteoblasts. *Acta biomaterialia*, 5(8):3076–3085, 2009.

[199] J Liskova, O Babchenko, M Varga, A Kromka, D Hadraba, Z Svindrych, Z Burdikova, and L Bacakova. Osteogenic cell differentiation on H-terminated and O-terminated nanocrystalline diamond films. *International journal of nanomedicine*, 10:869, 2015.

[200] J Liskova, O Babchenko, M Varga, A Kromka, D Hadraba, Z Svidrych, and L Bacakova. Effect of H- and O- termination of nanocrystalline diamond films on cell adhesion and osteogenic differentiation.

[201] FR Kloss, R Gassner, J Preiner, A Ebner, K Larsson, O Hächl, T Tuli, M Rasse, D Moser, K Laimer, et al. The role of oxygen termination of nanocrystalline diamond on immobilisation of bmp-2 and subsequent bone formation. *Biomaterials*, 29(16):2433–2442, 2008.

[202] B Rezek, L Michalíková, E Ukraintsev, A Kromka, and M Kalbacova. Micropattern guided adhesion of osteoblasts on diamond surfaces. *Sensors*, 9(5): 3549–3562, 2009.

[203] YC Chen, DC Lee, CY Hsiao, YF Chung, HC Chen, JP Thomas, WF Pong, NH Tai, IN Lin, and M Chiu. The effect of ultra-nanocrystalline diamond films on the proliferation and differentiation of neural stem cells. *Biomaterials*, 30(20):3428–3435, 2009.

[204] A Broz, V Baresova, A Kromka, B Rezek, and M Kalbacova. Strong influence of hierarchically structured diamond nanotopography on adhesion of human osteoblasts and mesenchymal cells. *physica status solidi (a)*, 206(9): 2038–2041, 2009.

[205] W Tong, K Fox, K Ganesan, and S Prawer. Design of a patterned diamond substrate for ordered neural cell adhesion. *Procedia Technology*, 20:206–211, 2015.

[206] MA Brady, A Renzing, TEL Douglas, Q Liu, S Wille, M Parizek, L Bacakova, A Kromka, M Jarosova, G Godier, et al. Development of composite poly (lactide-co-glycolide)-nanodiamond scaffolds for bone cell growth. *Journal of nanoscience and nanotechnology*, 15(2):1060–1069, 2015.

[207] JH Kim, SK Lee, OM Kwon, and D-S Lim. Ultra thin cvd diamond film deposition by electrostatic self-assembly seeding process with nano-diamond particles. *Journal of nanoscience and nanotechnology*, 9(7):4121–4127, 2009.

[208] R Foster Davis. *Diamond films and coatings*. Norwich NY, 1993.

[209] PW May, EM Regan, A Taylor, J Uney, AD Dick, and J McGeehan. Spatially controlling neuronal adhesion on cvd diamond. *Diamond and related materials*, 23:100–104, 2012.

[210] RJ Edgington, A Thalhammer, JO Welch, A Bongrain, P Bergonzo, E Scorsone, RB Jackman, and R Schoepfer. Patterned neuronal networks using nanodiamonds and the effect of varying nanodiamond properties on neuronal adhesion and outgrowth. *Journal of neural engineering*, 10(5):056022, 2013.

[211] SR Meyers, X Khoo, X Huang, EB Walsh, MW Grinstaff, and DJ Kenan. The development of peptide-based interfacial biomaterials for generating biological functionality on the surface of bioinert materials. *Biomaterials*, 30 (3):277–286, 2009.

[212] A Aminian, B Shirzadi, Z Azizi, K Maedler, E Volkmann, N Hildebrand, M Maas, L Treccani, and K Rezwan. Enhanced cell adhesion on bioinert ceramics mediated by the osteogenic cell membrane enzyme alkaline phosphatase. *Materials Science and Engineering: C*, 69:184–194, 2016.

[213] R Bogdanowicz, M Sobaszek, M Ficek, D Kopiec, M Moczała, K Orłowska, M Sawczak, and T Gotszalk. Fabrication and characterization of boron-doped nanocrystalline diamond-coated mems probes. *Applied Physics A*, 122(4):270, 2016.

[214] SA Skoog, G Kumar, J Zheng, AV Sumant, PL Goering, and RJ Narayan. Biological evaluation of ultrananocrystalline and nanocrystalline diamond coatings. *Journal of Materials Science: Materials in Medicine*, 27(12):187, 2016.

[215] A Rifai, N Tran, DW Lau, A Elbourne, H Zhan, AD Stacey, ELH Mayes, A Sarker, EP Ivanova, RJ Crawford, et al. Polycrystalline diamond coating of additively manufactured titanium for biomedical applications. *ACS applied materials & interfaces*, 10(10):8474–8484, 2018.

[216] SA Catledge, V Thomas, and YK Vohra. Nanostructured diamond coatings for orthopaedic applications. In *Diamond-Based Materials for Biomedical Applications*, pages 105–150. Elsevier, Cambridge MA, 2013.

[217] P Khanna, A Villagra, S Kim, E Seto, M Jaroszeski, A Kumar, and S Bhansali. Use of nanocrystalline diamond for microfluidic lab-on-a-chip. *Diamond and related materials*, 15(11-12):2073–2077, 2006.

[218] P Khanna, N Ramachandran, J Yang, J Wang, A Kumar, M Jaroszeski, and S Bhansali. Nanocrystalline diamond microspikes increase the efficiency of ultrasonic cell lysis in a microfluidic lab-on-a-chip. *Diamond and Related Materials*, 18(4):606–610, 2009.

[219] D Steinmüller-Nethl, FR Kloss, M Najam-Ul-Haq, M Rainer, K Larsson, C Linsmeier, G Köhler, C Fehrer, G Lepperdinger, X Liu, et al. Strong binding of bioactive BMP-2 to nanocrystalline diamond by physisorption. *Biomaterials*, 27(26):4547–4556, 2006.

[220] KF Chong, KP Loh, SRK Vedula, CT Lim, H Sternschulte, D Steinmüller, FS Sheu, and YL Zhong. Cell adhesion properties on photochemically functionalized diamond. *Langmuir*, 23(10):5615–5621, 2007.

[221] L Yang, BW Sheldon, and TJ Webster. The impact of diamond nanocrystallinity on osteoblast functions. *Biomaterials*, 30(20):3458–3465, 2009.

[222] Q Zhang, VN Mochalin, I Neitzel, IY Knoke, J Han, CA Klug, JG Zhou, PI Lelkes, and Y Gogotsi. Fluorescent plla-nanodiamond composites for bone tissue engineering. *Biomaterials*, 32(1):87–94, 2011.

[223] L Moore, M Gatica, H Kim, E Osawa, and D Ho. Multi-protein delivery by nanodiamonds promotes bone formation. *Journal of dental research*, 92(11): 976–981, 2013.

[224] Q Zhang, VN Mochalin, I Neitzel, K Hazeli, J Niu, A Kontsos, JG Zhou, PI Lelkes, and Y Gogotsi. Mechanical properties and biomineralization of

multifunctional nanodiamond-plla composites for bone tissue engineering. *Biomaterials*, 33(20):5067–5075, 2012.

[225] AC Taylor, C Helenes González, P Ferretti, and RB Jackman. Spontaneous differentiation of human neural stem cells on nanodiamonds. *Advanced Biosystems*, 3(4):1800299, 2019.

[226] J Raymakers, K Haenen, and W Maes. Diamond surface functionalization: from gemstone to photoelectrochemical applications. *Journal of Materials Chemistry C*, 7(33):10134–10165, 2019.

[227] SV Kontomaris. The Hertz model in AFM nanoindentation experiments: applications in biological samples and biomaterials. *Micro and Nanosystems*, 10(1):11–22, 2018.

[228] WT Welford. Advanced light microscopy. vol. 1. principles and basic properties. 36(11):1546–1547, 1989.

[229] G McNamara, MJ Difilippantonio, and T Ried. Microscopy and image analysis. *Current protocols in human genetics*, 46(1):4–4, 2005.

[230] A Nwaneshiudu, C Kuschal, FH Sakamoto, R Rox Anderson, K Schwarzenberger, and RC Young. Introduction to confocal microscopy. *Journal of Investigative Dermatology*, 132(12):1–5, 2012.

[231] R Weaver. Rediscovering polarized light microscopy. *American Laboratory*, 35(20):55–61, 2003.

[232] W Strober. Trypan blue exclusion test of cell viability. *Current protocols in immunology*, 21(1):A–3B, 1997.

[233] J Carroll, MJ Wood, and DG Whittingham. Normal fertilization and development of frozen-thawed mouse oocytes: protective action of certain macromolecules. *Biology of reproduction*, 48(3):606–612, 1993.

[234] TM Temu, KY Wu, PA Gruppuso, and C Phornphutkul. The mechanism of ascorbic acid-induced differentiation of atdc5 chondrogenic cells. *American Journal of Physiology-Endocrinology and Metabolism*, 299(2):E325–E334, 2010.

[235] AA Stewart, CR Byron, HC Pondenis, and MC Stewart. Effect of dexamethasone supplementation on chondrogenesis of equine mesenchymal stem cells. *American journal of veterinary research*, 69(8):1013–1021, 2008.

[236] F Langenbach and J Handschel. Effects of dexamethasone, ascorbic acid and β-glycerophosphate on the osteogenic differentiation of stem cells in vitro. *Stem cell research & therapy*, 4(5):117, 2013.

[237] MA Scott, VT Nguyen, B Levi, and AW James. Current methods of adipogenic differentiation of mesenchymal stem cells. *Stem cells and development*, 20(10):1793–1804, 2011.

[238] RF Doolittle. The conversion of fibrinogen to fibrin: A brief history of some key events. *Matrix Biology*, 60:5–7, 2017.

[239] C Joyce. Quantitative rt-PCR. *RT-PCR Protocols*, pages 83–92, 2002.

[240] S Maddocks and R Jenkins. *Understanding PCR: A Practical Bench-top Guide*. Academic Press, Cambridge MA, 2016.

[241] FH Stephenson. *Calculations for molecular biology and biotechnology*. Academic press, Cambridge MA, 2016.

[242] DH Cormack. *Essential histology*. Lippincott Williams & Wilkins, Philadelphia PA, 2001.

[243] K Painting and B Kirsop. A quick method for estimating the percentage of viable cells in a yeast population, using methylene blue staining. *World Journal of Microbiology and Biotechnology*, 6(3):346–347, 1990.

[244] D Ovchinnikov. Alcian blue/alizarin red staining of cartilage and bone in mouse. *Cold Spring Harbor Protocols*, 2009(3):pdb–prot5170, 2009.

[245] HF Steedman. Alcian blue 8GS: a new stain for mucin. *Journal of Cell Science*, 3(16):477–479, 1950.

[246] JE Scott and J Dorling. Differential staining of acid glycosaminoglycans (mucopolysaccharides) by alcian blue in salt solutions. *Histochemie*, 5(3): 221–233, 1965.

[247] H Puchtler, Susan N Meloan, and MS Terry. On the history and mechanism of alizarin and alizarin red s stains for calcium. *Journal of Histochemistry & Cytochemistry*, 17(2):110–124, 1969.

[248] R Lattouf, R Younes, D Lutomski, N Naaman, G Godeau, K Senni, and S Changotade. Picrosirius red staining: a useful tool to appraise collagen networks in normal and pathological tissues. *Journal of Histochemistry & Cytochemistry*, 62(10):751–758, 2014.

[249] G Sridharan and AA Shankar. Toluidine blue: A review of its chemistry and clinical utility. *Journal of oral and maxillofacial pathology: JOMFP*, 16(2): 251, 2012.

[250] AS Mao, JW Shin, and DJ Mooney. Effects of substrate stiffness and cell-cell contact on mesenchymal stem cell differentiation. *Biomaterials*, 98:184–191, 2016.

[251] A Haeger, K Wolf, MM Zegers, and P Friedl. Collective cell migration: guidance principles and hierarchies. *Trends in cell biology*, 25(9):556–566, 2015.

[252] O Chaudhuri, L Gu, M Darnell, D Klumpers, SA Bencherif, JC Weaver, N Huebsch, and DJ Mooney. Substrate stress relaxation regulates cell spreading. *Nature communications*, 6:6365, 2015.

[253] W Murphy, TC McDevitt, and AJ Engler. Materials as stem cell regulators. *Nature materials*, 13(6):547, 2014.

[254] DE Discher, P Janmey, and YL Wang. Tissue cells feel and respond to the stiffness of their substrate. *Science*, 310(5751):1139–1143, 2005.

[255] X Liu and S Wang. Three-dimensional nano-biointerface as a new platform for guiding cell fate. *Chemical Society Reviews*, 43(8):2385–2401, 2014.

[256] D Khang, J Lu, C Yao, KM Haberstroh, and TJ Webster. The role of nanometer and sub-micron surface features on vascular and bone cell adhesion on titanium. *Biomaterials*, 29(8):970–983, 2008.

[257] A Khalili and M Ahmad. A review of cell adhesion studies for biomedical and biological applications. *International journal of molecular sciences*, 16 (8):18149–18184, 2015.

[258] YI Cho, JS Choi, SY Jeong, and HS Yoo. Nerve growth factor (ngf)-conjugated electrospun nanostructures with topographical cues for neuronal differentiation of mesenchymal stem cells. *Acta biomaterialia*, 6(12):4725–4733, 2010.

[259] EKF Yim, RM Reano, SW Pang, AF Yee, CS Chen, and KW Leong. Nanopattern-induced changes in morphology and motility of smooth muscle cells. *Biomaterials*, 26(26):5405–5413, 2005.

[260] J Lu, MP Rao, NC MacDonald, D Khang, and TJ Webster. Improved endothelial cell adhesion and proliferation on patterned titanium surfaces with rationally designed, micrometer to nanometer features. *Acta biomaterialia*, 4(1):192–201, 2008.

[261] PM Mendes, CL Yeung, and JA Preece. Bio-nanopatterning of surfaces. *Nanoscale research letters*, 2(8):373, 2007.

[262] A Jaggessar, H Shahali, A Mathew, and PKDV Yarlagadda. Bio-mimicking nano and micro-structured surface fabrication for antibacterial properties in medical implants. *Journal of nanobiotechnology*, 15(1):64, 2017.

[263] E Vanhove, J De Sanoit, P Mailley, M-A Pinault, F Jomard, and P Bergonzo. High reactivity and stability of diamond electrodes: The influence of the b-doping concentration. *physica status solidi (a)*, 206(9):2063–2069, 2009.

[264] HA Girard, S Perruchas, C Gesset, M Chaigneau, L Vieille, JC Arnault, P Bergonzo, JP Boilot, and T Gacoin. Electrostatic grafting of diamond nanoparticles: a versatile route to nanocrystalline diamond thin films. *ACS applied materials & interfaces*, 1(12):2738–2746, 2009.

[265] L Guasti, W Prasongchean, G Kleftouris, S Mukherjee, AJ Thrasher, NW Bulstrode, and P Ferretti. High plasticity of pediatric adipose tissue-derived stem cells: Too much for selective skeletogenic differentiation? *Stem cells translational medicine*, 1(5):384–395, 2012.

[266] CS Yah and GS Simate. Engineered nanoparticle bio-conjugates toxicity screening: The xcelligence cells viability impact. *BioImpacts: BI*, 10(3): 195, 2020.

[267] H Hamidi, J Lilja, and J Ivaska. Using xcelligence rtca instrument to measure cell adhesion. *Bio-protocol*, 7(24), 2017.

[268] S Stehlik, T Glatzel, V Pichot, R Pawlak, E Meyer, D Spitzer, and B Rezek. Water interaction with hydrogenated and oxidized detonation nanodiamonds—microscopic and spectroscopic analyses. *Diamond and Related Materials*, 63:97–102, 2016.

[269] A Thalhammer, RJ Edgington, LA Cingolani, R Schoepfer, and RB Jackman. The use of nanodiamond monolayer coatings to promote the formation of functional neuronal networks. *Biomaterials*, 31(8):2097–2104, 2010.

[270] AM Monaco and M Giugliano. Carbon-based smart nanomaterials in biomedicine and neuroengineering. *Beilstein journal of nanotechnology*, 5 (1):1849–1863, 2014.

[271] M Aramesh, O Shimoni, K Ostrikov, S Prawer, and J Cervenka. Surface charge effects in protein adsorption on nanodiamonds. *Nanoscale*, 7(13): 5726–5736, 2015.

[272] SM Nalluri, GR Krishnan, C Cheah, A Arzumand, Y Yuan, CA Richardson, S Yang, and D Sarkar. Hydrophilic polyurethane matrix promotes chondrogenesis of mesenchymal stem cells. *Materials Science and Engineering: C*, 54:182–195, 2015.

[273] MJ Dalby, N Gadegaard, R Tare, A Andar, MO Riehle, P Herzyk, CDW Wilkinson, and ROC Oreffo. The control of human mesenchymal cell differentiation using nanoscale symmetry and disorder. *Nature materials*, 6(12): 997, 2007.

[274] DD Deligianni, ND Katsala, PG Koutsoukos, and YF Missirlis. Effect of surface roughness of hydroxyapatite on human bone marrow cell adhesion, proliferation, differentiation and detachment strength. *Biomaterials*, 22(1): 87–96, 2000.

[275] B Rezek, E Ukraintsev, M Krátká, A Taylor, F Fendrych, and V Mandys. Epithelial cell morphology and adhesion on diamond films deposited and chemically modified by plasma processes. *Biointerphases*, 9(3):031012, 2014.

[276] P Newman, A Minett, R Ellis-Behnke, and H Zreiqat. Carbon nanotubes: their potential and pitfalls for bone tissue regeneration and engineering. *Nanomedicine: Nanotechnology, biology and medicine*, 9(8):1139–1158, 2013.

[277] N Mohan, CS Chen, HH Hsieh, YC Wu, and HC Chang. In vivo imaging and toxicity assessments of fluorescent nanodiamonds in caenorhabditis elegans. *Nano letters*, 10(9):3692–3699, 2010.

[278] Y Yuan, Y Chen, JH Liu, H Wang, and Y Liu. Biodistribution and fate of nanodiamonds in vivo. *Diamond and related materials*, 18(1):95–100, 2009.

[279] LJ Su, MS Wu, YY Hui, BM Chang, L Pan, PC Hsu, YT Chen, HN Ho, YH Huang, TY Ling, et al. Fluorescent nanodiamonds enable quantitative tracking of human mesenchymal stem cells in miniature pigs. *Scientific reports*, 7:45607, 2017.

[280] F Pampaloni, E Reynaud, and EHK Stelzer. The third dimension bridges the gap between cell culture and live tissue. *Nature reviews Molecular cell biology*, 8(10):839–845, 2007.

[281] K Fox, R Ratwatte, MA Booth, HM Tran, and PA Tran. High nanodiamond content-pcl composite for tissue engineering scaffolds. *Nanomaterials*, 10 (5):948, 2020.

[282] L Wang, W Cao, X Wang, P Li, J Zhou, G Zhang, X Li, and X Xing. Biodegradable silver-loaded polycation modified nanodiamonds/polyurethane scaffold with improved antibacterial and mechanical properties for cartilage tissue repairing. *Journal of Materials Science: Materials in Medicine*, 30(4):1–12, 2019.

[283] R Williams, IM Khan, K Richardson, L Nelson, HE McCarthy, T Analbelsi, SK Singhrao, GP Dowthwaite, RE Jones, DM Baird, et al. Identification and clonal characterisation of a progenitor cell sub-population in normal human articular cartilage. *PloS one*, 5(10):e13246, 2010.

[284] MP Stuart, RAM Matsui, MFS Santos, I Côrtes, MS Azevedo, KR Silva, A Beatrici, PEC Leite, P Falagan-Lotsch, JM Granjeiro, et al. Successful low-cost scaffold-free cartilage tissue engineering using human cartilage progenitor cell spheroids formed by micromolded nonadhesive hydrogel. *Stem cells international*, 2017, 2017.

[285] EV Dare, SG Vascotto, DJ Carlsson, MT Hincke, and M Griffith. Differen-

tiation of a fibrin gel encapsulated chondrogenic cell line. *The International journal of artificial organs*, 30(7):619–627, 2007.

[286] TAE Ahmed, EV Dare, and M Hincke. Fibrin: a versatile scaffold for tissue engineering applications. *Tissue Engineering Part B: Reviews*, 14(2):199–215, 2008.

[287] VJ Bianchi, A Lee, J Anderson, J Parreno, J Theodoropoulos, D Backstein, and R Kandel. Redifferentiated chondrocytes in fibrin gel for the repair of articular cartilage lesions. *The American journal of sports medicine*, 47(10): 2348–2359, 2019.

[288] C Prante, K Bieback, C Funke, S Schön, S Kern, J Kuhn, M Gastens, K Kleesiek, and C Götting. The formation of extracellular matrix during chondrogenic differentiation of mesenchymal stem cells correlates with increased levels of xylosyltransferase i. *Stem Cells*, 24(10):2252–2261, 2006.

[289] W Bi, JM Deng, Z Zhang, RR Behringer, and B De Crombrugghe. Sox9 is required for cartilage formation. *Nature genetics*, 22(1):85–89, 1999.

[290] C Loebel, EM Czekanska, M Bruderer, G Salzmann, M Alini, and MJ Stoddart. In vitro osteogenic potential of human mesenchymal stem cells is predicted by runx2/sox9 ratio. *Tissue Engineering Part A*, 21(1-2):115–123, 2015.

[291] A Cheng and PG Genever. Sox9 determines RUNX2 transactivity by directing intracellular degradation. *Journal of Bone and Mineral Research*, 25(12): 2680–2689, 2010.

[292] M Mardani, B Hashemibeni, M Masoud Ansar, SHZ Esfahani, M Kazemi, V Goharian, N Esmaeili, and E Esfandiary. Comparison between chondrogenic markers of differentiated chondrocytes from adipose derived stem cells and articular chondrocytes in vitro. *Iranian journal of basic medical sciences*, 16(6):763, 2013.

[293] C Kiani, C Liwen, YJ Wu, JY Albert, and BY Burton. Structure and function of aggrecan. *Cell research*, 12(1):19–32, 2002.

[294] JT Rich, I Rosová, JA Nolta, TM Myckatyn, LJ Sandell, and A McAlinden. Upregulation of runx2 and osterix during in vitro chondrogenesis of human adipose-derived stromal cells. *Biochemical and biophysical research communications*, 372(1):230–235, 2008.

[295] JN Janssen, S Batschkus, S Schimmel, C Bode, B Schminke, and N Miosge. The influence of TGF-β3, EGF, and BGN on SOX9 and RUNX2 expression in human chondrogenic progenitor cells. *Journal of Histochemistry & Cytochemistry*, 67(2):117–127, 2019.

[296] LA Kaback, DY Soung, A Naik, N Smith, EM Schwarz, RJ O'Keefe, and H Drissi. Osterix/sp7 regulates mesenchymal stem cell mediated endochondral ossification. *Journal of cellular physiology*, 214(1):173–182, 2008.

[297] P Losi, E Briganti, C Errico, A Lisella, E Sanguinetti, F Chiellini, and G Soldani. Fibrin-based scaffold incorporating vegf-and bfgf-loaded nanoparticles stimulates wound healing in diabetic mice. *Acta biomaterialia*, 9(8):7814–7821, 2013.

[298] C-Y Cheng, E Perevedentseva, J-S Tu, P-H Chung, C-L Cheng, K-K Liu, J-I Chao, P-H Chen, and C-C Chang. Direct and in vitro observation of growth hormone receptor molecules in a549 human lung epithelial cells by nanodiamond labeling. *Applied physics letters*, 90(16):163903, 2007.

[299] S Pacelli, R Maloney, AR Chakravarti, J Whitlow, S Basu, S Modaresi, S Gehrke, and A Paul. Controlling adult stem cell behavior using nanodiamond-reinforced hydrogel: implication in bone regeneration therapy. *Scientific reports*, 7(1):1–15, 2017.

[300] JK Hodax, JB Quintos, PA Gruppuso, Q Chen, S Desai, and CT Jayasuriya. Aggrecan is required for chondrocyte differentiation in atdc5 chondroprogenitor cells. *PloS one*, 14(6):e0218399, 2019.

[301] CJ Brew, JG Andrew, R Boot-Handford, and TE Hardingham. Late osteoarthritic cartilage shows down regulation of sox9 and aggrecan expression but little evidence of chondrocyte hypertrophy. *Trans Orthop Res Soc*, 50: 938, 2004.

[302] SR Tew, Y Li, P Pothacharoen, LM Tweats, RE Hawkins, and TE Hardingham. Retroviral transduction with sox9 enhances re-expression of the chondrocyte phenotype in passaged osteoarthritic human articular chondrocytes. *Osteoarthritis and cartilage*, 13(1):80–89, 2005.

[303] T Kawane, X Qin, Q Jiang, T Miyazaki, H Komori, CA Yoshida, VK dos Santos Matsuura-Kawata, C Sakane, Y Matsuo, K Nagai, et al. Runx2 is required for the proliferation of osteoblast progenitors and induces proliferation by regulating fgfr2 and fgfr3. *Scientific reports*, 8(1):1–17, 2018.

[304] J-H Oh, S-Y Park, B de Crombrugghe, and J-E Kim. Chondrocyte-specific ablation of osterix leads to impaired endochondral ossification. *Biochemical and biophysical research communications*, 418(4):634–640, 2012.

[305] H Chen, FY Ghori-Javed, H Rashid, MD Adhami, R Serra, SE Gutierrez, and A Javed. Runx2 regulates endochondral ossification through control of chondrocyte proliferation and differentiation. *Journal of Bone and Mineral Research*, 29(12):2653–2665, 2014.

[306] A Ibrahim, N Rodriguez-Florez, OFW Gardner, E Zucchelli, SEP New, A Borghi, D Dunaway, NW Bulstrode, and P Ferretti. Three-dimensional environment and vascularization induce osteogenic maturation of human adipose-derived stem cells comparable to that of bone-derived progenitors. *Stem cells translational medicine*, 9(12):1651–1666, 2020.

[307] B Kleineidam, S Sielker, M Hanisch, J Kleinheinz, and S Jung. The micromass formation potential of human adipose-derived stromal cells isolated from different various origins. *Head & face medicine*, 14(1):1–11, 2018.

[308] ZM Jessop, S Manivannan, Y Zhang, CA Thornton, R Narayan, and IS Whitaker. Tissue specific stem/progenitor cells for cartilage tissue engineering: A systematic review of the literature. *Applied Physics Reviews*, 6 (3):031301, 2019.

[309] Z Xing, TO Pedersen, X Wu, Y Xue, Y Sun, A Finne-Wistrand, FR Kloss, T Waag, A Krueger, D Steinmüller-Nethl, et al. Biological effects of functionalizing copolymer scaffolds with nanodiamond particles. *Tissue engineering part A*, 19(15-16):1783–1791, 2013.

[310] KA Laptinskiy, H Kettiger, OA Shenderova, SA Burikov, JM Rosenholm, and TA Dolenko. Nanodiamond based complexes for prolonged dexamethasone release. In *Saratov Fall Meeting 2018: Computations and Data Analysis: from Nanoscale Tools to Brain Functions*, volume 11067, page 110671G. International Society for Optics and Photonics, 2019.